Study of Gangotri Glacier Dynamics using Remote Sensing and Geospatial Tools

Thesis submitted to the Andhra University, Visakhapatnam in partial fulfilment of the requirement for the award of *Master of Technology in Remote Sensing and GIS*

Submitted By:

Mr. Sanjay Manohar Bisht

Supervised By:

Dr. Praveen K. Thakur
Scientist/Engineer SE
Water Resources Department
Indian Institute of Remote Sensing
Dehradun

Dr. Arpit Chouksey
Scientist/Engineer SD
Water Resources Department
Indian Institute of Remote Sensing
Dehradun

Indian Institute of Remote Sensing, ISRO,
Dept. of Space, Govt. of India, Dehradun – 248001
Uttrakhand, India
August, 2015

Dedicated to my Brother

Acknowledgement

This thesis arose as a part of M.Tech project work carried out at Indian Institute of Remote Sensing. The thesis would not have materialized without the guidance and support of many people. Their contribution in the making of this thesis deserves a special mention. This is a humble acknowledgement to convey my gratitude to them all.

I would like to acknowledge the efforts of my supervisor Dr. Praveen Kumar Thakur Scientist SE, Water Resources Department, IIRS and Co-supervisor Mr. Arpit Chouksey Scientist SD, Water Resources Department group, IIRS. The help and guidance they provided me throughout my research duration at Indian Institute of Remote Sensing, Dehradun is deeply appreciated.

I am also thankful to Dr. Shiv Prasad Agarwal, Scientist SG, Head, Water Resources Department, for his valuable support and timely inputs refining my research work. I am also thankful to him because he has given me opportunity to carry out research work in the field of glaciology.

I am thankful to Dr. SPS Kushwaha Dean, Academics, Dr. S.K. Saha, Former Dean Academics, Ms. Shefali Agarwal, Course Director and Head PRSD, IIRS, for their valuable advices and insightful observations during the intermediate presentations which provided direction for mid-course corrections during the course of the research work.

I am also grateful to Dr. Y.V.N. Krishnamurthy, former Director, IIRS and Dr. A Senthil Kumar Director IIRS for providing an energetic and conducive research environment at IIRS.

I would also like to thank all faculty members, Dr. Bhaskar Nikam and Dr. Vaibhav Garg, of WRD, IIRS for their valuable direct and indirect support during my research work.

I submit my sincere thanks to all unknown people who helped me during my field visit required to complete my research work.

Friends are a great support system in itself. Thank you Aniket, Pratiman,Vikrant, Sukant, Sakshi, Surya, Raja, Ram, KD, Neeraj, Ram, Abhishek, Prateek, Abhishek Sir, Ponraj Sir, Raj Bhagat Sir and Ashutosh for providing me with much needed entertainment in my monotonous life.

I am also grateful to my dear friend and roommate Mr. Harjeet Singh, who has been helping me various occasions; be it problems in the field of GIS or matter of documentation or life advices.

Lastly, I offer my regards to all those who knowingly and unknowingly have supported me during the completion of this research project.

Sanjay Manohar Bisht

Declaration

I, Sanjay Manohar Bisht, hereby declare that this dissertation entitled "Study of Gangotri Glacier Dynamics using Remote Sensing and Geospatial Tools" submitted to Andhra University, Visakhapatnam in partial fulfilment of the requirements for the award of M.Tech in Remote Sensing and GIS, is my own work and that to the best of my knowledge and belief. It is a record of original research carried out be me under the guidance and supervision of Dr. Praveen Kumar Thakur, Scientist SE, Water Resources Department, and Mr. Arpit Chouksey, Scientist SD, Water Resources, IIRS. Indian Institute of Remote Sensing, ISRO, Dehradun. It contains no material previously published or written by another person nor material which to a substantial extent nor material which to a substantial extent has been accepted for the award of any other degree or diploma of the university or other institute of higher learning, except where due acknowledgement has been made in the text.

Place: Dehradun Mr. Sanjay M. Bisht

Date: 7 August, 2015

Certificate

This is to certify that the project titled "**Study of Gangotri Glacier Dynamics using Remote Sensing and Geospatial Tools**" is a bona fide record of work carried out by **Mr. Sanjay Manohar Bisht** during 01 Aug 2014 to 14 Aug 2015. The report has been submitted in partial fulfillment of requirement for the award of Master of Technology in Remote Sensing and GIS with specialization in Water Resources, conducted at Indian Institute of Remote Sensing (IIRS), Indian Space Research Organisation (ISRO), Dehradun from 19 Aug 2013 to 14 Aug 2015. The work has been carried out under the supervision of **Dr. Praveen Kumar Thakur, Scientist-SE**, and **Dr. Arpit Chouksey, Scientist-SD**, Water Resources.

No part of this report is to be published without the prior permission/intimation from/to the undersigned.

Dr. Praveen K. Thakur
Supervisor
Scientist-'SE'
Water Resources Department
IIRS, Dehradun

Dr. Arpit Chouksey
Co-Supervisor
Scientist-'SD'
Water Resources Department
IIRS, Dehradun

Dr. S.P. Agarwal
Head
Water Resources Department
IIRS, Dehradun

Dr. S.P.S. Kushwaha
Dean (Academics) & Group Director, ER&SSG
IIRS, Dehradun

Abstract

The Himalayan glaciers have been melting for the past few decades. Local climatic variation have influenced the glacier retreat or surges. But these phenomena does not appear to effect the glacier health over long terms. As such there is bound to be an underlying mechanism in the two processes. Glacial Lakes Outburst Floods have become a present and looming danger for the population in current vicinity of these retreating glacier. This calls for an informative approach toward studying the dynamics of this huge river of moving ice. Classification of glacier based on the geometry and shape and size of the glacier is available for a long time but classification of different facies of glacier is still a nascent topic from remote sensing perspective. It is important to understand the dynamism involved with that of different class of glacier and other related properties. The study aims to finds the dynamics of the glacier using geospatial tools and remote sensing. The main objective is to measure the surface glacial velocity, modelling of depth from the equation defined as Laminar flow and other models and classification of glaciers using SAR (Synthetic Aperture Radar) and Optical data. The classes found for the glacier were Debris, Ice, Snow, Lakes/Crevasses, Percolation Zone, etc. Also SAR data was found to be better equipped for classification studies. The study was able to successfully conclude the measured velocity to that of 0.2m/day for the duration of 1998-2014. Also the modelled depth was analyzed and found to be in between 20m-550m for the entire glacier. Finally the modelled depth was correlated to the Terrestrial Laser Scanner (TLS) field measurements and was found to be in having a correlation of R^2=0.799.

Keywords: *Glacier Velocity, Glacier Depth, SAR, TLS, Glacier dynamics, Glacier Classification*

Contents

List of Tables

List of Figures

1. INTRODUCTION

1.1. Background

Observations from present day indicate that a gradual change in global climatic conditions are a major cause of natural disasters. Glaciers are one among many phenomena that are directly affected by climate change. Glaciers are vast body of ice moving over landmass due to its own weight and slope of the underlying topography. These are found in polar (ice caps) and mountainous areas (alpine glaciers) of the world all over. Even small change in climate can have a well recognizable effect on glaciers. Glacier retreats and advances or changes in the amount of area under accumulations and ablations regions are different forms of glacier change. A gradual negative change (glacier retreat) in a glacier may result into its disappearance after a long time period of existence. Various studies on glacier properties recommend that if the present trend of retreat remains, most of the glaciers will disappear by a time less than a decade (Zemp et al., 2006). In addition a small change in glacier volume may have a direct impact on the local environment as these also act as heat sinks and source. These are also sensitive to climate change as small fluctuations can sometime lead to rapid retreat or surge in glacial extent. It may lead to flooding due to bursting of a moraine dammed lake which was not previously there. Such recent outbursts of flood may claim several hundreds of life and cause significant damage to infrastructure and livelihoods (Luckman et al., 2007). An accurate assessment of this mass and the snow cover which helps in reflectance of solar energy and hence reduction of local temperature is of utmost importance. The study of glacier physics and dynamics is a major motivation for this research as this will help us better understand glaciers and the underlying dynamics of it.

A start for such an analysis would be to estimate its current size, e.g. using earth observation techniques. However such an observation is affected by the presence of debris (Benn et al., 2012). This complicates estimation of its size and thickness. A major problem is thus to accurately estimate glacier volume and hence its movement, in particular in an inaccessible region. An analysis done by the geological department of India has shown that most glaciers are retreating or that they show deteriorated conditions along the glacier tongues. The average annual retreat is approximately 17.5 ma^{-1} in the period from 1971 to 2004 (Raina, 2009). Literature has shown that warming in the region has been greater than the global average, due to the high altitude of Himalayan glaciers (Jianchu et al., 2007). Thus melting in Himalayan glaciers may increase during the next decades and the frequency of various environmental risks like floods, avalanches, and failure of moraine-dammed lakes is likely to increase. This may also affect the water regimes (Ives et al., 2010). Promising results were obtained in the past on monitoring flow rates of Himalayan glaciers using remote sensing techniques (Luckman et al., 2007). No such comprehensive and inclusive study has been carried out in Gangotri glacier till date.

Satellite remote sensing allows gathering of information about objects on the ground, without having physical contact. Optical remote sensing satellites are passive earth observation system using the electromagnetic spectrum between 0.4µm to 2.1µm whereas Radar remote sensing is an active earth observation technique which uses the electromagnetic spectrum between 1 mm and 1.3 m (Lusch, 1999). The radar antenna transmits energy and receives the

backscattered signal from the object. The high penetration capability of the radar wave receives information from surface and subsurface, with penetration depth depending upon the wavelength. It differs from optical remote sensing as these systems uses reflectance from the target surface to retrieve information about its properties (no sub-surface penetration). Radar waves can penetrate through clouds, rain, and smoke with little attenuation due to their longer wavelengths from optical spectrum and thus radar serves as an all-weather remote sensing technique. Synthetic Aperture Radar (SAR) has revolutionized and expanded the use of microwave remote sensing in various geophysical studies, especially with respect to development of Interferometry. A SAR image contains both phase and amplitude information from the back scattered signal as opposed to just amplitude information in optical systems. The phase information on SAR depends upon the wave length used, the round path atmosphere between several acquisitions and the individual point scatterers on the ground. Interferometric SAR (InSAR) uses phase information from two SAR images of the same scene. It derives an image of phase difference between these two images. The resulting interferogram represents the ground topography. If the SAR images are acquired from different orbits then both atmosphere and system noise attenuates the phase signal. This calls for stereo topographic information removal to derive surface deformation or movement information.

For that purpose, digital elevation models (DEMs) are used, which are precisely aligned with the SAR images (Massonnet et al., 1993), or by using an additional independent interferogram which contains topographic information (Zebker et al., 1994). In glacier studies, only after the topographic information is removed, glacier movements can be calculated or else the images will be replete with noise due to geometry.

A radar system is called monostatic if a common antenna is used both as a transmitter and receiver. It is called bistatic if the transmitter and receiver antenna of radar system are separated by a considerable distance within a platform (Skolnik, 1961). Glacier movement using SAR interferometry can reveal centimeter motion of the surface. If glaciers have a rapid or incoherent flow or if a large time interval exists between acquisitions of two SAR images then this may result into loss of coherence. Under such conditions feature-tracking may help to estimate glacier movements (Giles et al., 2009).

This problem can be addressed from optical systems which are older of the two systems and hence historical records can be used to study movement patterns of glaciers from early on. This is an important reason as most glaciers are very slow moving and to truly understand their dynamics, we need to study them for very long time-scales (i.e. centuries). Optical feature tracking is based on the premise of phase correlation where the phase information derived from optical images are used to calculate the movement of the feature over time(Heid, 2011). This is done by taking observation of same areas for different time dates and precise registration of the two images. Typically temporal distance between the two images depend on the velocity of the glacier, such that the movement of feature is measureable in the images and the features are recognizable after the movement.

Until 1980s, all movement studies were done manually and hence sub-pixel movement was not possible. Image matching was first used by (Brecher, 1985) based on normalized cross-correlation image matching technique. Automatic movement technique were then used with different sets of operating procedure such as correct use of window. This meant that the

window size of the algorithm should be such that signal to noise ratio must be minimum and the features are distinguishable. This gave rise to Fourier based matching algorithms as these were faster and better to precisely identify features. Also these method needed larger window size to compensate for Heisenberg's uncertainty principle(Heid, 2011).

1.2. Motivation and Problem Statement

Glacier movement may depend upon the different forms of change such as accumulation and ablation. Climatic influences on glacier changes can be monitored by studying the glaciers during successive years. Such a study may give an average yearly movement value. A sudden variation in weather may also affect these forms. Such a study, however, may not give a precise movement value following a single weather phenomenon. To monitor such effects, more precise data collection during consecutive months is needed. This study will focus on deriving glacier movement for whole year so that average values can be unearthed for the glacier. Movements will be monitored using optical image matching (feature tracking), based on images of different days. To perform feature tracking, a pair of images must contain features which are identifiable. This limits the feature tracking to be used over debris covered area of the glacier or the ablation area. Also temporal separation between the two images should be such that coherence is not diminished below a certain threshold. For a fast moving glacier a small temporal separation between images may reduce such an effect. Measuring glacier movements using feature tracking is only possible if precise ortho-rectification of non-moving objects is done in both images that can be identified using fixed points. The average Gangotri glacier movement equals 4 – 6 cm day-1, corresponding to 15 – 20 m a-1 (Bhambri et al., 2011). This calls for a tracking algorithm which is able to calculate and identify sub-pixel movement of features.

Before the images are used for feature tracking, we need them to be ortho-rectified or original images without ortho-rectification cannot be used for image matching. This requires that all the information about the attitude of the satellite sensor is available. The ortho-rectification will be the single biggest factor of the algorithm error and fidelity. Incorrect values of camera position, look direction, lens distortion and atmospheric effects give horizontal shifts in the images that can be incorrectly identified as movement. Similarly vertical inaccuracy in the DEM used for ortho-rectification will also give images a sense of horizontal motion in features contained in it.

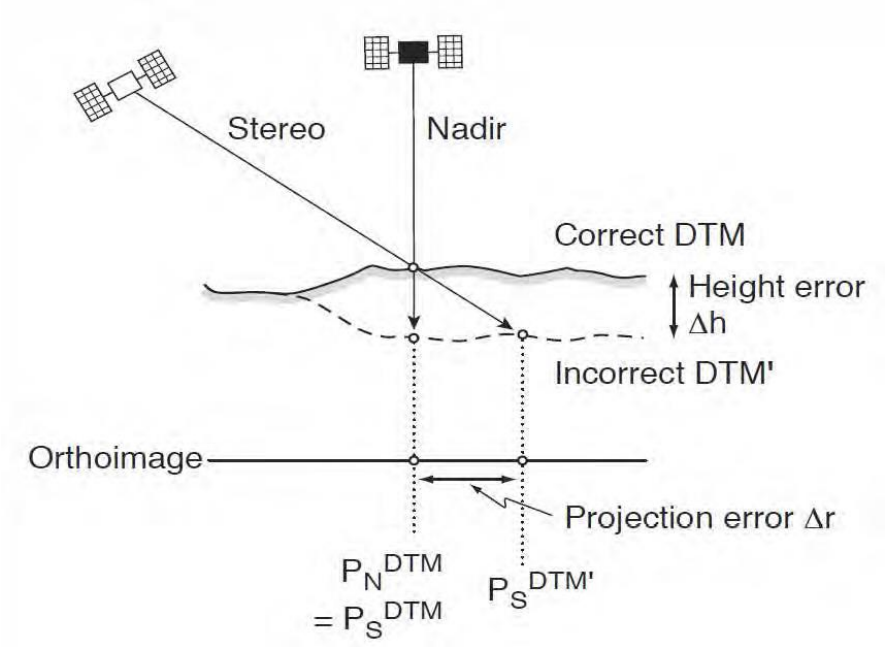

Figure 1.1 Translation of DEM error to Horizontal Motion (Kaab,2005)

A post-processing step is needed wherein the movement values which are erroneously high are removed. This is done by putting a threshold value to the SNR obtained for a particular matched pixel. This method lead to deletion of some pixel with right movement values. To overcome this problem, directional filters are employed which allow for flexibility in setting the SNR values for pixel as long as they confirm to the predefined direction of motion of the glacier. Also reverse correlation was used for some filters; the two images are correlated but with temporal reversal for the image pair, when the correlation coefficient was above a certain threshold the image pixel was returned as valid. Filters looking for varying speed for a short distance have also been used in some studies.

1.3. Research Identification

1.3.1. Research Objectives

The prime focus is to study the glacier movement over the surface using both optical techniques and infer classes of the glacier for the period of observation.

1.3.2. Sub-objectives

- To estimate the glacier movement using Optical feature-tracking method.
- To estimate subsurface depth and basal movement using modelling techniques.
- To estimate glacier classes for the observed period using SAR methods.

1.3.3. Research Questions

- Which error sources limit the quality of the movement map and how does this influence propagate in the feature tracking processing?
- What are the error propagating parameters in the depth model used?
- What are the classes obtained using SAR (Synthetic Aperture Radar) techniques?

2. LITERATURE REVIEW

2.1. Glacier

Glaciers are one of the most important constituent of a hydrological system. Around 10% of the world's land mass is covered with glacier (USGS, 2013). Glacier, ice caps and continental ice sheets are storage of fresh water, and it corresponds to three-quarter of world's total fresh water resources. Glaciers are essential elements of landscape and environment in High Mountain and Polar Regions. They are unique source of fresh water for agriculture, industry and domestic use, an important economic component, yet they constitute serious natural hazards. As glaciers are natural component, they are directly affected by small climatic fluctuations at both local as well as global level.

The accelerated changing of glacier has severe impact on human-being, vegetation patterns, natural disaster, water supplies and local climate (UNEP). Glacier length changes indicate the global climatic changes (Oerlemans, 2005). The increasing mass loss and decline in glacier size in mountain and other regions contribute to sea level rise (Larsen et al., 2007). The mass loss and change of length of glacier depends up on its geometry, and climatic variation (Oerlemans, 2005). Various meteorological experiments have shown that the primary source for melting in glaciers is solar radiation, and loss of mass balance are due to temperature and precipitation (Oerlemans, 2005; Ohmura, 2001).

Recently using various ground measurements, remote sensing and aerial photogrammetry a global scaled record of glacier is obtained (Barry, 2006; DeBEER and Sharp, 2009; Racoviteanu et al., 2008). The trend obtained in this study shows that only a few glaciers are advancing. Temperate glacier with large accumulation and mass-balance are very active than continental glacier due to want of precipitation. Hence temperate glaciers are more sensitive to the changing climate than continental glacier sheets.

Types of glaciers:

Mountain glaciers: These glaciers develop in high mountainous regions, often flowing out of ice fields that span several peaks or even a mountain range.

Valley glaciers: Commonly originating from mountain glaciers or ice fields, these glaciers spill down valleys, looking much like giant tongues. Valley glaciers may be very long, often flowing down beyond the snow line, sometimes reaching sea level.

Tidewater glaciers: As the name implies, these are valley glaciers that flow far enough to reach out into the sea.

Piedmont glaciers: Piedmont glaciers occur when steep valley glaciers spill into relatively flat plains, where they spread out into bulb-like lobes

Hanging glaciers: When a major valley glacier system retreats and thins, sometimes the tributary glaciers are left in smaller valleys high above the shrunken central glacier surface. These are called hanging glaciers.

Cirque glaciers: Cirque glaciers are named for the bowl-like hollows they occupy, which are called cirques. Typically, they are found high on mountainsides and tend to be wide rather than long.

Rock Glaciers: Rock glaciers sometimes form when slow-moving glacial ice is covered by debris. They are often found in steep-sided valleys, where rocks and soil fall from the valley walls onto the ice. Rock glaciers may also form when frozen soil creeps downslope.

2.2. Himalayan Glacier Study Overview

Himalayan glaciers are the largest glacier in central Asia. In Himalayan mountain region, glacier covers approximately 30,000 km^2 which is about 17% of mountain area (Ahmad et al., 2004). Himalayan Mountain is located near tropic of cancer and receives more heat from solar radiation over any time period than other glaciers (Ahmad et al., 2004). Therefore, Himalayan glaciers are more sensitive to climatic fluctuations than other mountain glaciers in the world (Ahmad et al., 2004). Most of the glaciers in this region are retreating and only some are advancing or are static causing long-term loss of fresh water storage. For example, Pandey et al. (2012) had referred to a loss of 20 % in surface runoff in the Hunza and Shyock Rivers in Karakoram and Hindukush mountains since 1961. The high altitude of Himalayan glacier preserves its glacial existence in these mountain areas. Variable climatic change and terrain difference resulted into different glacier responses to same climatic changes in Himalayan area. The hydro-meteorology and the contribution of precipitation due to glaciation are controlled mainly by Indian monsoon and westerly, climatic regimes.

The study conducted by Benn and Owen (1998) suggest to emphasis on the effect of Indian and westerly monsoon, which control majority of the glaciation and hydrology components in the region. The recorded glacio-chronologies are uncertain in Himalayan region with respect to timing and the extent of glacier length (Owen et al., 1998). A recent study suggests that during south west monsoon, cooling associated changes resulted in glacier advances (Owen et al., 2002). Therefore, studying regional climatic influence is essential to predicting future responses of glaciers.

In current scenario glaciation in Himalayas depends on regional climatic change and any variation in global climatic regime will have greater impact on this region. So it is necessary to understand the relationship between regional and global climatic influence to study glaciation. In addition this helps to understand the possible impact of regional climatic effect on human population, not in an averaged global climatic change. It should be considered that variation in glaciation characteristic of Himalayan glacier is a result of terrain, regional and extent of the area. Therefore, it starts to develop glacier morpho-metric characteristic across Himalayan region. Several studies have initiated to accommodate the morpho-metric characteristic of glaciers on Himalayan region. Study conducted by Naithani et al. (2001) and Ahmad et al. (2004) to identify the effect of such characteristics in Gangotri as well as in Himalayan region and try to understand the regional climatic impact and its impact on glaciation.

Various studies show that glaciers in Himalayan region have various retreat rate during last century in response to climatic warming (Bhambri and Bolch, 2009; Hansen et al., 2005; Kulkarni and Bahuguna 2002; Prasad et al., 2009). Dokrani glacier, a glacier in North-West Himalaya, has an annual average retreat rate varying of 17.4m $year^{-1}$ (Dobhal et al., 2004). During past few decades variable retreat rates are observed in different time domains. In

central glacier recently a higher retreat rate is recorded in the southern slope part. One of the main glaciers in central Himalaya is Gangotri glacier, Gharwal. Bhambri et al. (2012) reported an average retreat rate of 5.9±4.2 m year^{-1} from 1965 to 1968 and 26.9±1.8m year^{-1} from 1968 to 1980, and it retreated 21.0±1.2m year^{-1} between 1980 and 2000. During 2001-2006 the retreat rate of Gangotri has declined to 7.0±4.0 m year^{-1}.

2.3. Glacier Components

Accumulation:

Accumulation zone in glacier is a place where precipitation of snow occurs during entire season. Appearance of snow precipitation is seasonal dependent, in which snow accumulation varies with different seasons. Hence accumulation of snow is also directly related to glacier movement during the melting season. Accumulation zone is the adding of snow fall or ice, avalanches snow, drift snow and rain that freezes. Usually accumulation zone is a zone over the glacier, it may be the starting point of a glacier, or resulted from previous years' snow deposition. Accumulation area can be easily identifiable as it appears as a clear white snow or ice, which does not have any track of surface moraines.

Study conducted by (Pelto, 2010) discussed about survival of temperate glacier from accumulation zone observation, in which recent climatic changes can be identified from terminus changes; however, terminus change does not identify the ability of glacier to survive. A glacier can retreat fast and also reestablish the equilibrium line with respect to accumulation. Hence a temperate glacier can only be survived by the steady accumulation. Pelto (2010) suggests that glacier survival assessment study should focus on the accumulation zone and not on terminus.

Ablation:

Ablation in a glacier is the loss of ice from the glacier. Ablation is a process of loss of ice mass from the glacier by melting, evaporation and calving etc. Ablation zone is the zone above the glacier surface where, the loss of ice happened is higher than previous year. The ablation zone is dirty, covered with rubble, with presence of glacier ponds, or even presence of supra glacier lakes. This helps to easily identify the ablation zone on the glacier.

During ablation period loss of ice or snow melt depends mostly on the duration of ablation period, slope and wind effects (Olefs and Fischer, 2008). In glacier these areas are located either near the snout or along ice divides in the upper part of the glacier. The study conducted by Olefs and Fischer (2008) on glacier Schaufelferner in stubai Alps, Austria at an altitude of 2900 m a.s.l. and 3100 m a.s.l. shows that for a period of 105 days, a total amount of 3.8 m snow and ice (1760 kgm^{-2}) melted.

Snout:

Snout or Terminus is a point at which a glacier terminates (Figure_3A). The advance and retreat of glacier from different seasons are identified from the current position of snout. Glacier length change can be identified from the snout position (Vieli and Gudmundsson, 2010). Snout can represent the changes in glacier which indicate recent climate changes

(Pelto, 2010). Different retreat rate for Gangotri glacier has been discussed by different authors from 1962-2000(Bahuguna et al., 2007). An annual retreat of 18m of the snout was observed using PAN data of 2000-2001(Bahuguna et al., 2007). Bhambri et al. (2011) has reported a retreat of Gangotri glacier from 1965-2006 with a retreat up to 819+-14m. These retreat rates of snout depend on different climatic conditions i.e., progressive temperature rise (1890 - 1949), cooler and wetter conditions (1950-1975), and warmer condition, present (Pelto, 2010).

Equilibrium Line Altitude (ELA):

Equilibrium line is the line which separates the accumulation and ablation zone over the glacier surface. Usually mass balance governs the equilibrium line altitude. Equilibrium line is considered as a permanent snow line, which is used by glaciologists to identify two zones of a glacier on satellite imageries (Raina, 2009).

Formation of Glacier and Glacier Flow:

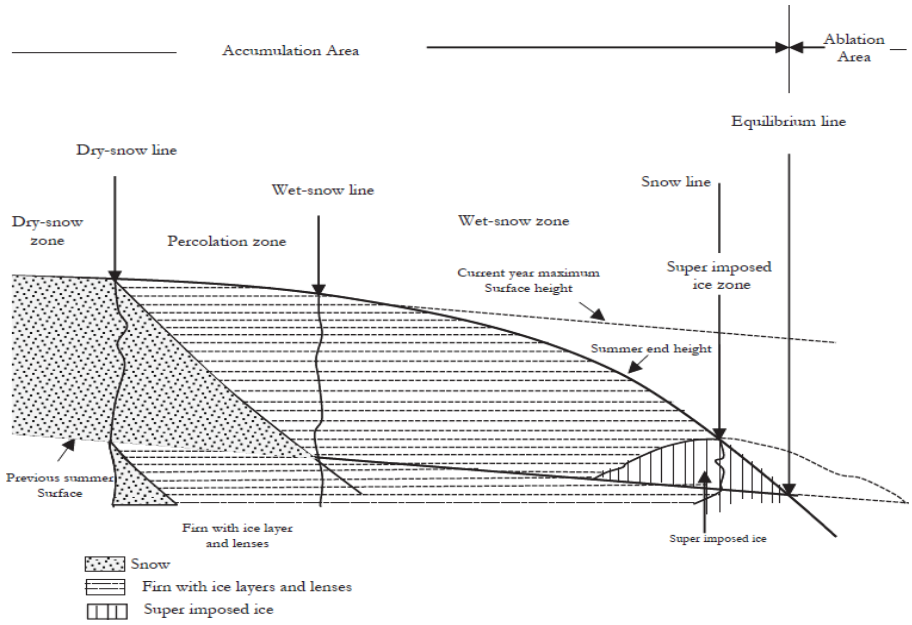

Figure 2.1 Cross-sectional structure of glacier (Cuffey and Paterson, 2010)

A high altitude region favors glaciation due to small ablation rate. Glaciers in mountain area are formed from continuous accumulation, but the rate of ablation also decreases with altitude. The high accumulation of snow forms a layer of dry snow which is mostly seen in upper region of the glacier. The snow metamorphosis in dry glacier region is due to compression, and snow remains similar except where the density increases with height. A glacier is formed when ablation fails to remove the accumulated snow, and the size depends on accumulation, ablation and flow. A slow movement occurs from accumulation towards ablation to balance the overall mass balance.

Glaciers are formed from snow accumulation, flake of layers one after other, which gradually turns into firn and in due course ice. The transformation of snow to ice is driven by gravity and temperature variations. The result is a sealed deposit, which grades from snow at the surface to ice. Air bubbles terrestrial materials transported by wind and other substances

brought by precipitation and by erosion due to glacier flow are present in these laminated deposits of ice. Initially these materials are hidden underneath the accumulation zone and later on it is brought to glacier surface in ablation zone.

Due to its own weight and weight of the snow, glacier pressure increases with depth. Because of the rheological characteristic dependence of the ice, pressure causes compression. Hence the lower layers of glacier are capable of deformation and movement. Thus one of the main characteristic to the growth of glacier is its deformation and movement. Various glaciers have recorded different annual flow velocity varying from 10 - 1000 m per year, with maximum at the surface and center of valley glaciers (Pellika, 2009). The three main mechanisms by which an ice flows are internal deformation inside the ice itself through the process of basal sliding and deformation of water-saturated weak sections. Internal deformation occurs in almost all moving ice and usually accounts for a few meters per year. When ice bed is at pressure melting point basal motion occurs due to the presence of water (Siegert, 2008). Internal deformation occurs in all situation of glacier flow. Some of such conditions are (a).if the ice is warm and rests on bedrock then basal sliding occurs (Figure 2-2 A), (b). Deformation will take place when bedrock is frozen (Figure 2.2 B) and (c). An internal deformation can add to ice deformation when ice is warm and unconsolidated and basal sliding as a contribution to ice flow (Figure 2.2 C).

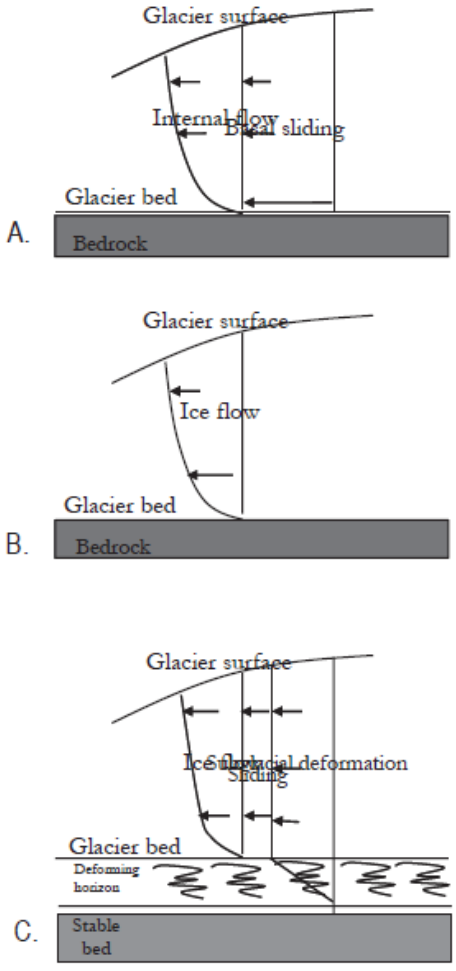

Figure 2.2 Flow controlling processes (Siegert, 2008)

Flow of a glacier is relatively organized as follows. At the center of an ice the flow speed is very low (Siegert, 2008). Particles present on the ice sheet surface were buried by subsequent snowfall and gradually a vertical velocity component develops downward into the ice. These ice sheets are divided into margins of ice drainage basins. When ice sheets are drained by ice streams, such process transports ice from the interior to the ice margins (Bennett, 2003). The presence of water at the bases of ice stream reduces the sub glacial friction thus allows it to move quickly.

2.4. Glacier Study Using Remote Sensing

A growing demand for studying glacier characteristics during current and coming days plays a vital role in monitoring global as well as local climatic changes. Climatic change continues to cause various physical changes on glaciers mainly in mountainous regions (Scherler et al., 2008).This has an important role for areas characterized under water stress regions, such as central and south Asia which, to a large degree depend on glacier and snow melt water(Scherler et al., 2008; Winiger et al., 2005). Successful quantification of the climate-related hydrological changes and their impact on society is demanding challenge. Hence a large scale monitoring of glaciers and a better understanding of their physical characteristic needs to be observed. Due to their large area and difficult accessibility of mountain topography, especially in Himalayan regions, remote sensing technique offers a decisive way to collect data. Remote sensing techniques have been used to track glacier geometry (Khalsa et al., 2004), study the formation of supra glacial lake, determine equilibrium line altitude, monitor annual mass balance change and estimate various movement rate(Berthier et al., 2007; Mathieu et al., 2009; Wessels et al., 2002).

Remote sensing can also be used to monitor velocity of different glacier, it is crucial because it determines ice discharge (Scherler et al., 2008; Strozzi et al., 2002b). Even though glacier velocity can be monitored directly from a glacier with high accuracy, observation for long periods involves frequent revisit of the same inspection area, which should only be located on accessible parts of a glacier. Therefore, sight measurement usually results in scant spatial coverage (Scherler et al., 2008). In addition to that, remotes sensing characteristic like wide area coverage, frequent repetivity of data collection on same area and cost effectiveness of satellite data compared with field measurement, have led to the increasing application of them on glaciology (Karimi et al., 2012).Satellite glacier monitoring using both optical and radar images are widely used during these days. Monitoring glacier characteristics using remote sensing has been well recognized since the middle of 1980s (Aizen et al., 2007). Both World Glacier Monitoring Service (WGMS) and Global Land-Ice Measurements from Space (GLIMS) are global initiative to monitor glacier inventory all over the world (Aizen et al., 2007; Kargel et al., 2005; Raup et al., 2007). In contrast, glacier monitoring by satellite remote sensing data provides an opportunity to study large spatial coverage, even in inaccessible areas. Optical and radar images are used to monitor glacier velocity and the most common methods used are SAR interferometry, SAR feature tracking, and cross-correlation of optical satellite images.

Kumar et al. (2011) has studied Siachen glacier utilizing ERS- 1/2 tandem mission data to resolve the three velocity components. Assuming that glacier flow is parallel to its surface, and the interferometric pair retains excellent coherence return SAR mages with one day

interval, observed a velocity of 43 cm day-1 in the upper middle potion of the glacier. A comparison study by Luckman et al. (2007) using SAR interferometry and feature tracking for monitoring the Kumbu glacier appears relatively high flow rate up to 10 cm day-1.

(Bhambri et al., 2012) monitored the frontal recession of the Gangotri group of glacier from 1965- 2006 using high resolution remote sensing data. Declassified images of CORONA were used to map for the year 1965 and 1968, Hexagon for year 1968, IRS Pan for 2001 and Cartosat-1 for year 2006. The reported recession for the time period was 819±14 m. rate of retreat varied from 5.9±4.2 m/year (1965-68) to 21.0±1.2 m/year (1980-2001).(Gardelle et al., 2011) presented a regional assessment of glacial lake distribution and evolution in the Hindu Kush Himalaya (HKH) area. Glacial lakes were mapped out for the region. In the East (India, Nepal and Bhutan), glacial lakes are bigger and more numerous than in the West (Pakistan, Afghanistan), and have grown continuously between 1990 and 2009 by 20% to 65%. On the other hand, during the same period, the glacial lake coverage has shrunk in the Hindu Kush (−50%) and the Karakorum (−30%).

(Naithani et al., 2001) studied the geomorphological features of Gangotri glacier to access the retreat of the glacier. Various geomorphological features and morphometric parameters were studied. The presence of supra-glacial lakes points to subsidence fast degenerating nature of the glacier. Also comparative studies of retreat rate was deduced and concurred that the rates was faster after 1971 and continue to be so.(Berthier et al., 2010) documented the rise of sea level due to shrinking of Alaskan glaciers derived from satellite imageries. A comprehensive glacier inventory with elevation changes were derived from sequential DEMs. It is reported that between 1962 and 2006, Alaskan glaciers lost 41.9±8.6 km^3 yr^{-1} of water, and contributed $0.12 \pm 0.02 mmyr^{-1}$ to sea-level rise.

(Shukla et al., 2010) tried to map glacier boundary over supra-glacial and peri-glacial debris over Chenab basin. The mapping of glacier is impeded due to presence of debris over both the glacier and the boundary adjoining the area which has almost similar spectral signature leaving them mutually indistinguishable. As there is a significant difference in the temperature between the two classes, inclusion of Thermal Infrared (TIR) in optical data processing provides a viable approach. The results obtained correlate to earlier studies and 87.98% user accuracy in peri-glacial debris and 76.87% in supra-glacial debris is achieved.

(Malinverni et al., 2008) reported the contribution of open source environment for glacier studies. Three multi-temporal optical data (MSS, TM and ETM+) were combined with other spatial data was used to extrapolate meaningful parameters of glacier dynamics. Finally ELA and AAR were calculated by integrating DTM and presented into a visual outlay.

(Barry, 2006) reviewed various mapping techniques and other physical factors required to understand glacier physics better. These included computing annual mass balance, equilibrium line altitude, accumulation area ratio, glacier response time, response time of glaciers, scaling relationships, modelling techniques, glacier sensitivity indices, glacier change and glacier monitoring. (Wagnon et al., 2007) measured mass-balance of Chota-Shigri glacier for four year (2002-06). Overall specific mass balances were mostly negative during the study period and varied from a minimum value of –1.4mw.e. in 2002-03 and 2005-06 (equilibrium-line altitude (ELA) 5180ma.s.l.) to a maximum value of +0.1mw.e. in 2004/05 (ELA 4855ma.s.l.).

(Zemp et al., 2009) reviewed the six decades of worldwide glacial monitoring network and concluded that most of the studies were being conducted in the northern hemisphere. Also monitoring of 30 reference glacier since 1976 revealed a mean annual ice loss of 0.14 m.w.e. (1976–85), 0.25 m.w.e. (1986–95) and 0.58 m.w.e. (1996–2005). This in turn suggest a strong mass losses in early 1940's and 50's followed by moderate mass loss in 1970's and a subsequent acceleration until now.(Bhambri and Bolch, 2009) reviewed the status of glacier mapping in Indian Himalayas. The development of glacier mapping and glacier fluctuations since the mid-nineteenth century, with special reference to the Indian Himalayas, and the contributions of the Survey of India and the Geological Survey of India were taken into account.

(Bamber and Rivera, 2007) reviewed the remote sensing approach for glacier mass balance determination. Wherein different approaches such as component approach, photogrammetry, altimetry and Interferometric SAR were discussed. Data sets such SRTM, IKONOS, CORONA, ICESAT, CRYOsat II, TerraSAR-X, TerraSAR-L, etc. their respective biases were discussed. Also future studies in the area and the GLIMS project was appreciated for providing a baseline dataset for both extent and elevation for Andean glacier.

(Hubbard et al., 2000) presented an approach to calculate the mass balance of a glacier using remote sensing and ice flow modelling. Using the mass-continuity equation with mass-flux divergence field and spatial distribution of elevation change, the model was used to calculate mass balance distribution for the year '92-'93. Elevation change for the study area is calculated from analytical photogrammetry for the time frame and mass-flux divergence from the numerical modelling constrained from surface velocity measurement. This was then correlated with the ground measurement giving R^2=0.91 using ground stakes over the central flow line of the glacier.

(Berthier et al., 2007) approached the problem of mass balance using SPOT5 and SRTM digital elevation model (DEM). The SPOT5 DEM was analyzed for any error in elevation calculation and a long wavelength bias corresponding to satellite roll anomaly was detected. SRTM bias regarding altitude was also modelled and both biases were removed over the whole study area. A clear thinning was reported even over debris covered tongues of some glaciers. A specific mass balance of -0.7 to -0.85m/a (water equivalent) was noted and the rate of ice loss was twice than the long term (1977-1999) mass balance record of Himalayan region.

(Berthier et al., 2012; Shuman et al., 2011) investigated the mass-balance and elevation response of the Larsen A & B embayment of the Antarctic peninsula from 2001-11. They used temporal DEM derived from SPOT & ASTER and laser altimetry data from ICESat and ATM. This was then used to elevation changes in conjunction with MODIS data to track ice events. The measurement accuracy of the DEM was determined using the "null test" where DEM changes are measured within few weeks of each other. This enabled them to resolve large residual uncertainties in Larsen sector B. A continued thinning of ≥ 3 m a^{-1} was reported for the time period which was then correlated with GRACE data.

Biases in DEM are a major sources of error in monitoring glacier volume changes. As global coverage is provided by SRTM (Shuttle Radar Topography Mission), the biases in high-mountain areas are to be noted for monitoring volume changes (Berthier et al., 2006). The

study finds an error of up to 10m in underestimation at high altitudes and volume loss is overestimated if SRTM is recent of the two compared topographies.(Casey et al., 2011) characterized the glacier debris of the Khumbu-Himalayan region via in-situ & optical remote sensing methods. Supraglacial mineral components were identified and mineral abundances were estimated on Khumbu-Himalayan glaciers. This study identified significant variability in the debris cover in the Khumbu-Himalayan region glaciers.

(Huang and Li, 2011) compared SAR and optical based feature tracking technique to calculate glacier flow. Feature tracking is based on a cross-correlation algorithm that seeks offsets of the maximal correlation windows on repeated satellite images. It was noted that optical images require terrain corrections before co-registration, but this is not necessary for SAR images. Ortho-rectification is difficult for SAR images in mountainous areas. It is suggested that single-look SAR intensity images be first co-registered without terrain correction to better maintain the raw glacier surface features.

(Anthwal et al., 2006) studied the interaction between climate and glacier. Although global air temperature was directly related to glacier retreat over the polar ice sheet, the correlation was not evident for alpine glaciers. Mass balance loss from mountainous glacier leading to sea level rise was reported to be 0.2 -0.4 mm/yr. (Haq et al., 2011) used repeat satellite optical imagery to deduce the Gangotri glacier extent change for the year 1972-2010. The overall deglaciation was reported at 7%, accumulation area decrease of 25%, ablation area increase at 7% and mass balance for the year 1972 at -10.808 and -31.87166 for 2010.

(Negi et al., 2012) used IRS LISS-III sensor data in conjunction with the field collected snow-meteorological data for seven year (2001-08). A declining trend in SCA (Snow Cover Area) and an upward trend for snow line was observed. A deglaciation of 6% was detected for the whole of the glacier. Low snowfall in winter season and more rainfall in monsoon season are attributed for fast melting of the glacier and affecting its health.

(Karimi et al., 2012) reported the elevation changes for the Alamkoukh glacier in Iran using multi-temporal remote sensing images. DEM were adjusted for their respective biases and morphometric changes were assessed for different dates. Thinning rates (-0.5 ± 0.06 m/year for tongue areas and -4.5 ± 0.32 m/year for high altitude areas) were calculated for the time period (1955-2010) and hence volume loss was reported at 0.29 ± 0.03 km^3.

(Ahmad et al., 2004) analyzed the morphometric characteristics of glacier in Indian Himalayas. Health of the glaciers were inferred using the AAR method with the results categorizing the glacier into zones with 0 AAR (34%) and 100 AAR (9%). Also AAR was reported to be closely related to length, mean elevation and area of the glacier. (Kulkarni, 1992) investigated the effect of global warming on the Himalayan glaciers reporting on glacial extent, glacial mass balance and seasonal snow cover. The study covered retreat on 466 glacier in Chenab, Pārbati and Bapsa Basin since 1962. It reported a deglaciation of 21% and a loss of 0.2347 km^2 of glacial ice.

(Engeset, 2002) studied the capabilities of SAR (Synthetic Aperture Radar) sensors to detect changes in mass balance and glacier facies. Two distinct zones, namely firn accumulation zone and low backscatter zone were easily identified. Firn Edge Altitude were readily retrieved for 31 of the 40 glacier under study which did not change significantly over time. Also the low scatter zone was further divided into two sub-zones which also did not change frequently over time and was detectable only on 20 of the 40 glaciers.(Eineder et al., 2011)

used TERRASAR-X and TANDEM-X imageries to derive surface velocity for Drygalski glacier, Antarctica Peninsula. A velocity accuracy of 2cm/day was achieved without any GCP, a slowdown of $0.34md^{-1}a^{-1}$ was detected at the tongue during 2007-08. Also TERRASAR-X was used to compute a DEM for accurate assignment of height and position values to velocity measurement.

(Berthier et al., 2005) considered the alternative to SAR interferometry for mountain glacier velocity measurement: optical feature tracking. Also the methodology discussed does not need GCP's (Ground Control Point) for accurate assessment of surface velocity as precise relative orientation was used to derive the movement in the order of $1/5^{th}$ of pixel resolution for well correlated areas. (Budillon et al., 2008) used Along Track interferometric SAR (AT-InSAR) to estimate radial velocity of ground moving targets. Two models for target response were used to analyze radial velocity maximum likelihood estimation accuracy. The paper concluded that AT-InSAR exhibited better estimation accuracy for slow moving targets.

(Fallourd et al., 2011) combined GPS measurements and Multi-Temporal TerraSAR-X images to derive movement of temperate glacier. The test glacier at Chamonix Mont-Blanc was used for the study and results derived using 4 time series images over the site for one year exhibited phase information getting lost after 11 days on such sites. The results also suggested a high coherence values for ablation areas with debris cover.(Fallourd et al., 2009) used HR SAR images for monitoring of temperate glaciers over the Mount Blanc area. The study concluded that on snow covered glaciers, surface changes are important to obtain coherence and phase information which is readily high in ablation areas or black glacier (covered by snow).

(Trouvé et al., 2008) experimented with corner reflector adjusted for TerraSAR-X acquisitions and GPS (Global Positioning System) measurements providing atmospheric delay information. The error reported for GPS measurement was 2-4 mm and 7-24 mm for horizontal and vertical components. Also heavy snowfall was noted to cause error in gradients such as Zenith Total delay and Horizontal Tropospheric Gradients. This can then be further developed to extract velocity using natural vertical reflectors such as rocks and crevasses. (Strozzi et al., 2002) measured glacier velocity using Offset-Tracking procedure wherein Intensity tracking based on patch intensity cross-correlation optimization was used. Also the limits of the technique was discussed using the case of surge of Monaco Breen in the Northern Svalbard in 1992-1996.

3. STUDY AREA, DATA SETS AND DATA DESCRIPTION

3.1. Study Area

The study area concerns the Gangotri glacier of the Gharwal Himalayas in India. The Gangotri glacier is one of the largest glaciers in the Himalayas, being approximately 30 km long with a width varying between 0.5 and 2.5 km. It has a height varying between 4120 and 7000 m.a.s.l. The Gangotri glacier is a valley type glacier, flowing into the NW direction. The glacier is confined between 30º43'22''-30º55'49'' (latitude) and 79º04'41''-79º16'34'' (longitude). Of the Gangotri glacier, approximately 29% of the total area is affected by debris. The glacier is affected by aspects of the valley, elevation and weather conditions.

Climate in the study area is influenced by the south west monsoon.

The three main tributaries of Raktvarn (15.90 km), Chaturangi (22.45 km) and Kirti (11.05 km) and eighteen other tributaries contribute to the retreat of the Gangotri glacier (Naithani et al., 2001). The present land forms are the result of erosion and deposition processes of glacial-periglacial features.

Examples of erosion features are cirques, glacial troughs, smooth rock walls, steep head walls, rock steps, waterfalls, rock basins, pyramidal and conical peaks, U-shaped valley, glacial lakes, serrated crust of ridges and arêtes. Some Important deposition features are dead ice mounds, deposited debris, moraines, snow avalanche, talus cones and snow-bridges. Along the Gangotri glacier, several transverse and longitudinal crevasses were formed where the ice has broken down. The ablation zone of Gangotri glacier is covered by thick piles of moraines, due to which supra glacier lakes were formed around that area (Naithani et al., 2001).

In the Gangotri glacier area, various land forms and geomorphology of glaciated terrain such as accumulation zone, ablation zone, equilibrium line, supra glacier lakes, glacial moraines and snout have been identified. Between 2005 and 2007, the Gangotri glacier has retreated at a much lower rate than between 1971 and 2004(Raina, 2009). Several studies of frontal recession of Gangotri glacier by different authors are summarized in Table 3.1.

Table 3.1 Retreat rate of Gangotri glacier measured by various authors (Bhambri et al., 2011)

Year	**Total m**	**Mean retreat year^{-1} (m)**
1935 – 1996	1220	20
1962 – 1999	1250	34
1935 – 1997	2500	40
1962 – 2000	1600	42
1986-2001	368	23
1962-2000	1510	40
1962-2006	1651	38

The unique erosion and deposition land forms around the Gangotri glacier, made this glacier interesting to serve as a key indicator for local climatic variation in Himalayan region. Seasonal variation of aspects show large behavioural and physical changes of Gangotri glacier. The high elevation and a valley like structure as present here not only depend upon

climatic variation but also on other physical parameters like slope, aspect and equilibrium line altitude.

Due to the large spatial variability of the Gangotri glacier it is impossible to study the entire glacier using ground measurements. It is also important to monitor glacier behaviour in an area covering different slopes and aspects particularly in inaccessible regions. These prominent geomorphological characteristics in the upper layers of Gangotri glacier develop changes in its physical behaviour such as movement. Hence, these behavioural changes have to be monitored from time to time for understanding glacier behaviour in different seasons. Such a study, using radar and optical remote sensing techniques is carried out in this thesis.

The different retreat rates of the Gangotri glacier recorded in different time periods emphasize to focus on accommodating various physical parameters which affects Gangotri glacier. These parameters address whether the glacier is retreating or advancing or remains balanced following either accumulation or ablation. As per Auden report, that once the Gangotri glacier was extended up to Jahala, that is 47 km down the present position (Raina, 2009). This shows the importance of monitoring the current changes in this glacier during different time periods. Such a study is further important for understanding the contributions from different tributary glaciers on its geomorphological changes.

Figure 3.1 Snout position of Gangotri (Date of Capture: 16-09-2014) (Source: WRD, IIRS)

Figure 3.2 Crevasses near Snout Position of Gangotri (Date of Capture: 16-09-2014) (Source: WRD, IIRS)

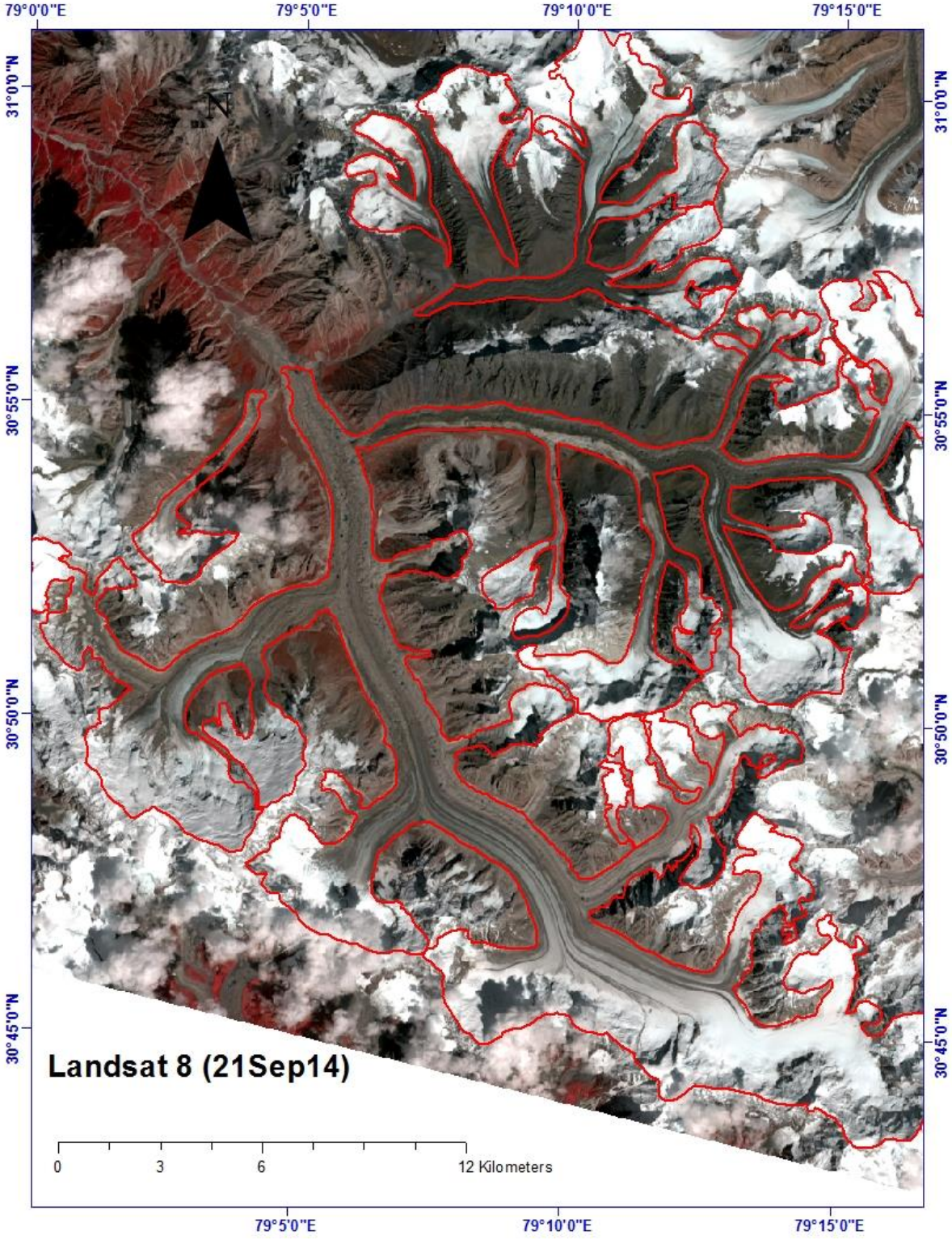

Figure 3.3 Gangotri Glacier Area Landsat 7, 20-09-2014

3.2. Data Description

1. Landsat 5, 7, 8 were used for temporal change in glacier extent.
2. Landsat 7 ETM+ and Landsat 8 was used for optical feature tracking.
3. IRS 1C/1D data was used for optical feature tracking.
4. RISAT-1 Circular polarimetry data is used for Polarimetric decomposition.
5. RADARSAT 2 fully Polarimetric data was used for glacier classification.
6. ALOS-PRISM and CARTOSAT 1 optical stereo pairs was used for DEM generation.

Table 3.2 List of Datasets used in Study

S. no.	Satellite	Sensor	Date of Pass	Resolution(m)
1	Landsat 2	MSS	01-11-1976	60
2	Landsat 2	MSS	22-09-1977	60
3	Landsat 5	TM	29-09-1993	30
4	Landsat 5	TM	17-11-1994	30
5	Landsat 5	TM	09-09-1998	30
6	Landsat 5	TM	21-04-1999	30
7	Landsat 5	TM	16-04-2000	30
8	Landsat 7	ETM+	22-10-1999	15
9	Landsat 7	ETM+	08-10-2000	15
10	Landsat 7	ETM+	20-10-2001	15
11	Landsat 7	ETM+	22-08-2002	15
12	Landsat 7	ETM+	22-10-2005	15
13	Landsat 8	OLI	01-08-2013	15
14	Landsat 8	OLI	26-08-2013	15
15	Landsat 8	OLI	21-09-2014	15
16	Cartosat 1	PAF	09-11-2008	2.5
17	ALOS	PRISM	12-08-2009	2.5
18	RISAT 1		01-04-2014	25
19	RISAT 1		29-08-2014	25
20	RISAT 1		26-01-2015	25
21	RISAT 1		18-02-2014	5
22	RadarSat 2		05-11-2010	8

4. RESEARCH METHODOLOGY

This chapter explains the methodology adopted to achieve the objectives using both SAR interferometry and Feature tracking technique. Section 4.1 explains how movement map can obtained optical feature tracking using COSI-CORR software. A set by set execution both in terms of software and science behind it to derive movement has been discussed in detail. Section 4.2 give the back ground details of Feature tracking technique using SAR images.

4.1. SAR Decomposition

A polarized wave gets change when it interacts with a target in terms of its polarization state. There are many ways in which the state of a polarized electromagnetic wave can be represented mathematically. The way in which it is represented should contain all of the information associated with the polarized wave. One such method of representation is by using Stokes parameters, developed by Gabriel Stokes. The Stokes parameters are sufficient to describe the polarization state and other information like phase, intensity, degree of polarization, etc. associated with the wave. These parameters can be collectively represented by Stokes vector. In other terms it can be stated that a partially polarized wave can also be characterized by the four time-averaged Stokes parameters, since they are simply related to the elements of the coherency matrix and can be represented as

$$S_1 = |E_H|^2 + |E_V|^2 = \langle E_H E_H^* \rangle + \langle E_H E_V^* \rangle = J_{HH} + J_{VV} \quad (4.1)$$

$$S_1 = |E_H|^2 + |E_V|^2 = \langle E_H E_H^* \rangle + \langle E_H E_V^* \rangle = J_{HH} + J_{VV} \quad (4.2)$$

$$S_2 = |E_H|^2 - |E_V|^2 = \langle E_H E_H^* \rangle - \langle E_H E_V^* \rangle = J_{HH} - J_{VV} \quad (4.3)$$

$$S_3 = 2|E_H||E_V| \cos \phi_{HV} = \langle E_H E_V^* \rangle + \langle E_V E_H^* \rangle = J_{HV} + J_{VH} \quad (4.4)$$

$$S_4 = 2|E_H||E_V| \sin \phi_{HV} = j\langle E_H E_V^* \rangle - j\langle E_V E_H^* \rangle = jJ_{HV} - jJ_{VH} \quad (4.5)$$

Where, $E_{H \text{ or } V}$ is the horizontal or vertical value of electric field of the microwave, J is the coherency matrix and S is the Stokes parameter.

The one-to-one correspondence between the coherency matrix and the Stokes vector allowed to extend to the Stokes parameters and the results obtained regarding the uniqueness of the coherency matrix associated with a wave, and a unique set of Stokes parameters was shown to characterize a partially polarized wave. The non-negative condition satisfied for the determinant of the coherency matrix $[J]$ expressed in term of the Stokes parameters, S, implies;

$$S_1^2 \geq S_2^2 + S_3^2 + S_4^2 \quad (4.6)$$

The degree of polarization, m, using the Stokes parameters can be described as

$$m = \frac{\sqrt{S_2^2 + S_3^2 + S_4^2}}{S_1} \qquad 0 \leq m \leq 1 \qquad (4.7)$$

The value of degree of polarization lies between 0 and 1(both values are included). The degree of polarization value becomes 0 when unpolarised wave is transmitted and if fully polarized wave is transmitted then its value becomes 1. Another Stokes child parameter is chi (χ) i.e. the ellipticity parameter and it enters as

$$\sin(2\chi) = -\frac{S_4}{mS_1} \qquad -45° \leq \chi \leq 45° \qquad (4.8)$$

The ellipticity parameter or degree of circularity (χ) is in range between -45 to $+45$ (both values are included) which preserves the sense of rotation.

Raney decomposition basically developed for the hybrid polarization mode of SAR architecture. The hybrid-polarity architecture is one of several alternative approaches to compact polarimetry. A hybrid-polarity SAR is one in which the transmitted field is circularly polarized, and the resulting backscatter is received in two mutually coherent linear polarizations. As long as the relative phase between the received polarizations is retained, the specific choice of linear orientation does not matter. The generation of Stokes parameters for describing the polarization states of EM waves helps in generating those parameters which is required in Raney decomposition. The four Stokes parameters lead to child products that are used individually, of which the degree of linear polarization (m) and ellipticity parameter (χ) taken for this study to perform Raney decomposition. The degree of polarization (m) has long been recognized as the single most important parameter characteristic of a partially-polarized EM field, and is given in Equation (4.7).

The close relationship between entropy and degree of depolarization (1-m) has been verified experimentally. The degree of depolarization (1- m) is indicative of randomly-polarized backscatter, typically arising from radar-quasi-transparent volumetric materials, such as lunar regolith or forest canopy and glaciers. The degree of polarization (m) is a natural choice for the first decomposition variable for hybrid dual-polarimetric data. The Poincaré ellipticity parameter χ is an obvious and the most robust choice for the second decomposition variable. It is one of the three classical principal components (m, χ, ψ) that are necessary and sufficient to describe the polarized portion of a partially-polarized quasi-monochromatic EM field of average strength S_1. Further, the sign of χ is an unambiguous indicator of even versus odd proven to be an excellent analysis tool for Mini-RF hybrid-polarimetric data. In this formulation the key inputs are m, and the degree of circularity.

The m−chi decomposition under Raney decomposition may be expressed through a color-coded image. This color-coded image helps in making visual interpretation easier. This will generate RGB image and can be expressed as

$$R = \sqrt{s_1 \times m \times \frac{1 - \sin(2\chi)}{2}} \tag{4.9}$$

$$B = \sqrt{s_1 \times m \times \frac{1 + \sin(2\chi)}{2}} \tag{4.10}$$

$$G = \sqrt{s_1 \times (1 - m)} \tag{4.11}$$

In this formulation of RGB image, B stands for Blue color which indicates fraction of single-bounce backscattering under the law of Bragg's scattering, R stands for Red color which indicates double-bounce or even bounce backscattering and G represents Green color which indicates volume scattering due to the randomly polarized constituent. These colors can be represented in color wheel in Figure 4.1.

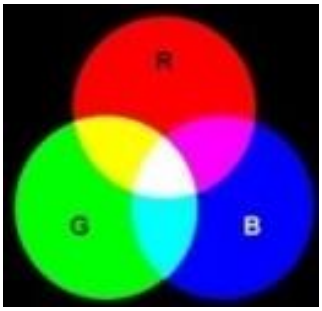

Figure 4.1 Color Wheel Used For Sar Decomposition Representation

4.2. Optical Feature Tracking

Optical feature tracking uses a pair of co-registered images, one pre-event image and other one post-event image. Usually in glacier studies images with higher temporal resolution is considered for feature tracking technique. Also minimum snow cover is a must so that features are visible in the images which is not possible in snow covered area of the glacier. It is assumed that both the images share the same resolution. Let p_1 and p_2 be two overlying areas extracted from these images i_1 and i_2 respectively. Let p_1 and p_2 be of size 2M $\times$ 2M pixels with M such that 2M is larger than twice the largest movement to be estimated. The SNR, thus the correlation accuracy, is higher when the overlapping area of patches to correlate is maximum. Patches to be correlated are then iteratively moved to compensate for the relative movement between the two. These iterations (usually at most two) are done from the peak correlation method to lower the computational cost. A Fourier transform is carried over both the images (window), each searching for maximum SNR. The point for equal value of transform in a search window corresponds to feature match. The difference in the positional value between the two features provides the idea for translational motion for the images.This is provided in three files, namely E-W file, N-S file and SNR file.

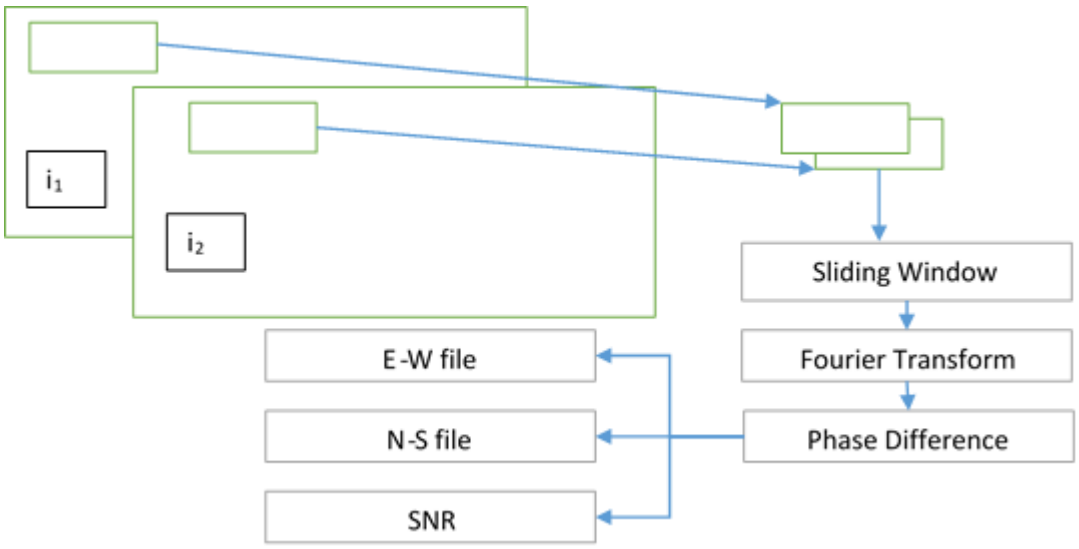

Figure 4.2 COSI-CORR Methodology

COSI-CORR relies on phase correlation methods which have shown good results for similar problems. These methods rely on the Fourier shift theorem wherein the relative movement between a pair of images with similar features is retrieved from the phase difference of their Fourier transform.

Let i_1 and i_2 be two images in which features differ only by a movement (Δx, Δy) such that

$$i_2(x.y) = i_1(x - \Delta_x, y - \Delta_y) \tag{4.12}$$

By denoting by I_1 and I_2 their Fourier transform, from the Fourier shift theorem, we have the relation

$$I_2(\omega_x, \omega_y) = I_1(\omega_x, \omega_y)e^{-j(\omega_x\Delta_x + \omega_y\Delta_y)} \tag{4.13}$$

Here ω_x and ω_y are the frequency variables in column and row. The normalized cross-spectrum of the images i_1 and i_2 is then

$$C_{i_1,i_2} = \frac{I_1(\omega_x, \omega_y)I_2^*(\omega_x, \omega_y)}{\left|I_1(\omega_x, \omega_y)I_2^*(\omega_x, \omega_y)\right|} = e^{j(\omega_x\Delta_x + \omega_y\Delta_y)} \tag{4.14}$$

Where *denotes the complex conjugate. The images' relative movement can thus be estimated from the 2-D slope of the cross-spectrum's phase. By applying the inverse Fourier transform F^{-1} to (21), we have the correlation function

$$F^{-1} = \left\{e^{j(w_x\Delta_x + w_y\Delta_y)}\right\} = \delta(x + \Delta_x, y + \Delta_y) \tag{4.15}$$

The images' relative movement can then be estimated from the coordinates of the correlation peak achieved from the inverse Fourier transform. In case of sub pixel movements, this peak is a down-sampled version of a Dirichlet kernel. Further processing is then required to recover the image shift.

4.3. Movement and Velocity Calculation

Files produced from phase difference in the matched feature can then be used for movement conversion. Using the formula,

$$D_{s=\sqrt{(E-S^2)+(N-S^2)}} \quad (4.16)$$

Where D_s represent the translation movement detected, E-S represent the movement values for the E-S direction and N-S represent the movement values for the N-S direction. Although care has to be taken to disregard all pixel having SNR less than 0.9, hence leaving patches of area with no movement values. This is then rectified by interpolating nearby values. Velocity calculation is then a simple matter of movement divided by the time interval between the two scenes. This is done using vector addition of the two fields of movement with the angle between them always at 90°. This is used to get the magnitude of the movement of the feature over the search window. Also local averaging is done to filter out rouge pixel showing movement values very high which are obviously termed as noise.

4.4. Ice Thickness Calculation from Velocity Measurement

Ice thickness calculation are done using velocity values derived from the COSI-CORR software. The basic premise behind the model for thickness estimation follows the logic of Basal Shear stress and Velocities in "Laminar flow" as described in (Patterson, 1994). Here the model of a glacier is a parallel-sided slab of ice of thickness H on a rough plane of slope α. No sliding of the slab is assumed on the plane and the thickness of the slab is much less than its length and width. The slab is perpendicular to the plane and of unit cross section. The weight of the slab is ρgH. Where ρ is density of ice, g is acceleration due to gravity and H is the height of the slab. The weight of the slab along the surface will be countered by basal stress which will be equal to:

$$\tau_b = \rho g H sin\alpha \quad (4.17)$$

This is a very simple model for glacier movement when the layers of ice do not move over each other. But in real world scenarios, ice moves over each layer and hence velocity varies with depth. This is shown in figure

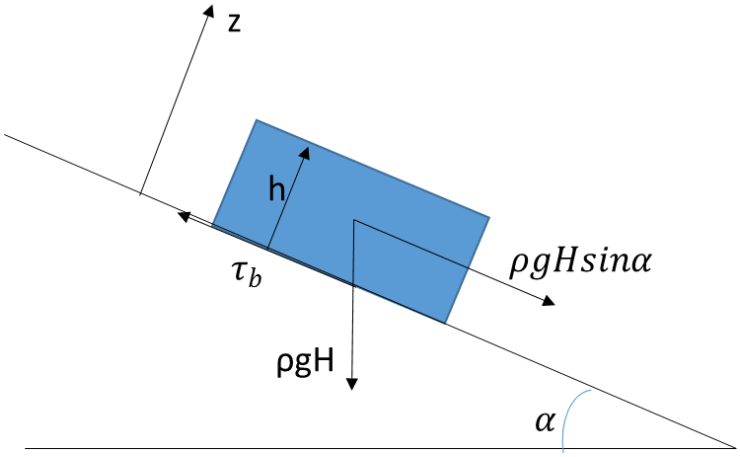

Figure 4.3 Simplified Model for Glacier Ice Movement

Let u be the x component of the velocity. Assuming the slab deforms in a simple shear, the flow lines are parallel to surface. This is Laminar flow of ice. It follows that the z component of the velocity is zero and so shear strain rate is ½(du/dz).

$$\frac{1}{2}\frac{du}{dz} = A\tau_b^n \tag{4.18}$$

Using equation (4.17) and adding a scale/shape factor, f, for temperate glaciers we get

$$\tau_b = f\rho g(h-z)sin\alpha \tag{4.19}$$

Integrating equation (4.18) into (4.17) we get

$$u_s - u(z) = \frac{2A}{n+1}(f\rho g sin\alpha)^n (h-z)^{n+1} \tag{4.20}$$

This equation can then be used to determine the depth/height of the ice over any glacier where our assumption holds true. Changing the equation into the final form by replacing (f-z) with H we get.

$$u_s - u_b = \frac{2A}{n+1}(f\rho g sin\alpha)^n (H)^{n+1} \tag{4.1}$$

Rearranging to get depth information of a particular velocity pair, we get:

$$H = \sqrt[n+1]{\frac{(n+1)(u_s - u_b)}{2A(f\rho g sin\alpha)^n}} \tag{4.2}$$

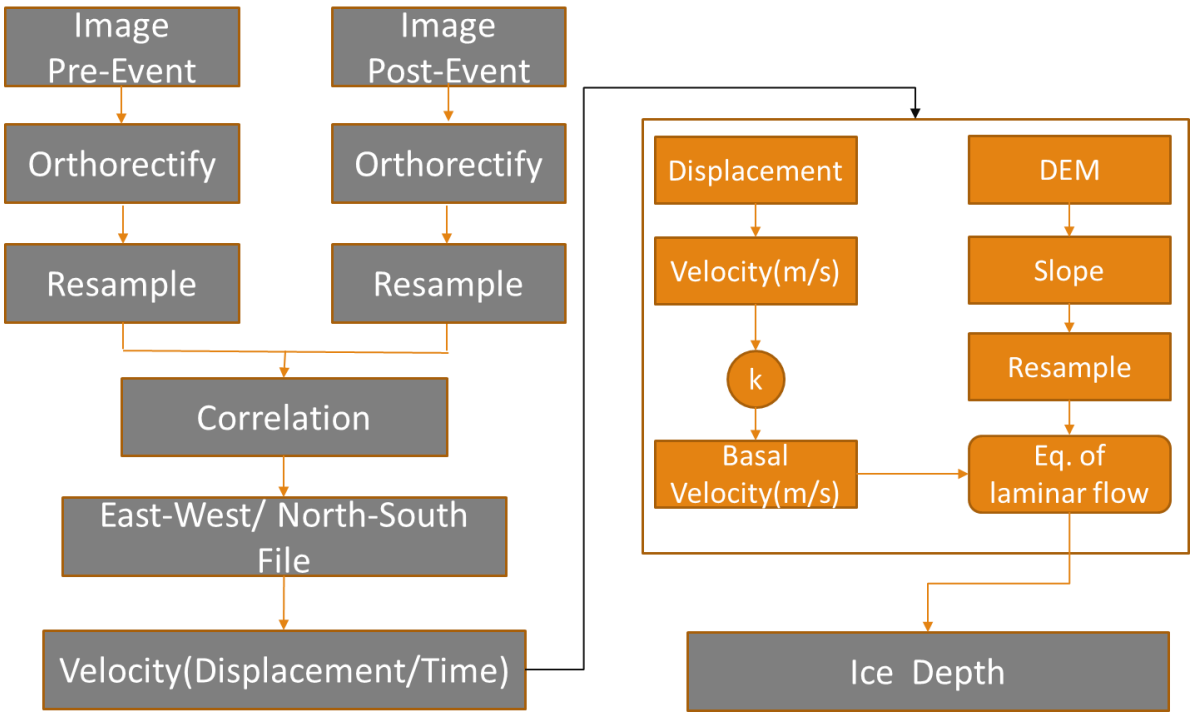

Figure 4.4 Ice Thickness Estimation using Surface Velocity

4.5. Ice Thickness Estimation Using Slope and GlabTop

(Haeberli and Hoelzle, 1995) presented a way to estimate glacier volume using average surface slope and vertical glacier extent. As this parameterization scheme has been extensively used over Himalayan range, an application of this approach can be used for depth estimation over the study area.

Here the equation governing the depth at center flow line of the glacier can be written as:

$$h_{centre} = \frac{\tau}{f\sigma g sin\alpha} \tag{4.33}$$

The shape factor, f, is determined from (Cuffey and Paterson, 2010)

Table 4.1 Shape Factor for different glacier geometries

W	F		
	Parabola	Semi-ellipse	Rectangle
1	0.445	0.5	0.558
2	0.646	0.709	0.789
3	0.746	0.799	0.884
4	0.806	0.849	
∞	1	1	1

Which is typically chose at 0.8 for valley glaciers. To interpolate the value at centre flow line over the whole of glacier taking the edges of the glacier to be at 0 depth, a multiplication of π/4 is applied.

$$h_G = h_{centre}\left(\frac{\pi}{4}\right) \tag{4.4}$$

The change in basal stress in accordance with elevation range is based on reconstructed latePleistocene glaciers of European Alps(Paul and Linsbauer, 2012). Where,

$$\tau = \begin{cases} 0.5 + 159.81\mathrm{H} - 43.5(\Delta H)^2, & \Delta H \leq 1.6km \\ 150 , & \Delta H > 1.6km \end{cases} \tag{4.5}$$

When applied over remotely sensed data, these parameters need to be considered for accurate determination. Hence ΔH (difference in height from snout to peak of glacier involved) and glacier length l is used to determine slope of the glacier using the equation:

$$\alpha_l = arctan\left(\frac{\Delta H}{l}\right) \tag{4.6}$$

This is then used to calculate the stress for the main glacier branch and consecutively centre flow line depth. This flow line depth is then interpolated to the glacier boundary which is fixed at zero depth using equation (4.24).

(Paul and Linsbauer, 2012)used an approach of that between (Clarke et al., 2009) and (Li et al., 2011) which considers just the flow dynamics and enables the bed estimation to be computationally very fast. The DEM used for the study is converted into a contour line with

50 m elevation difference. This is then converted into slope map and equation (4.25) is applied to calculate the value of τ. This is then used to calculate the ice depth distribution along the flow lines which are digitized earlier following the contour lines. The TopoToRaster tool is used from the ArcGIS to interpolate the values of the ice depth over the entire glacier from the flow line to the entire glacier.

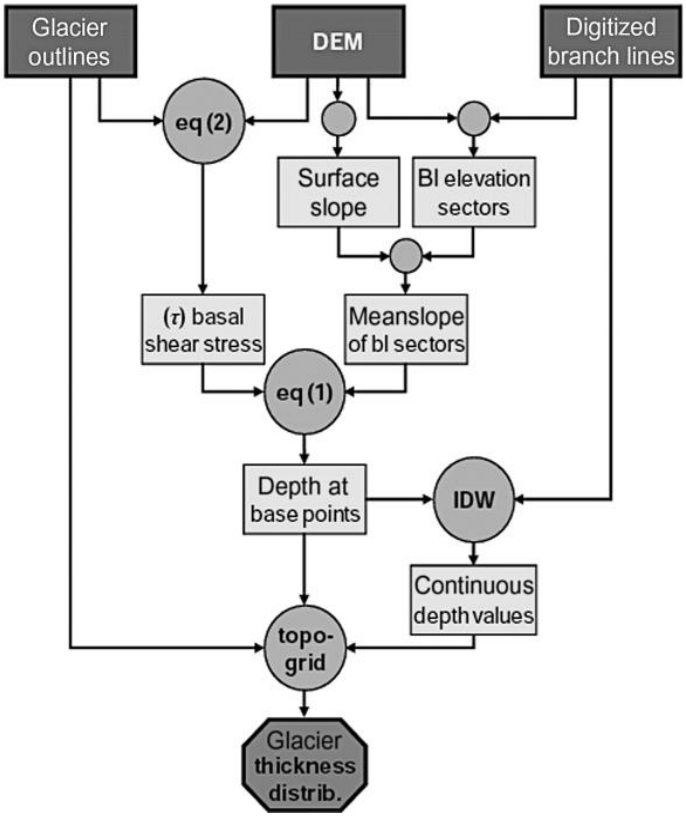

Figure 4.5 GlabTop Methodology (Linsbauer et al., 2012)

5. RESULTS AND DISCUSSIONS

This chapter explains various results obtained from the proposed method for this research work. It starts with Polarimetric Decomposition of SAR data using POLSAR Pro from RADARSAT 2 and RISAT 1; SVM classifier used for classification followed by feature tracking results of optical data from Landsat and IRS Satellite. Various product needed for laminar flow equation is then reported and the results derived by parameterizing the Laminar flow equation for ice depth and the GlabTop approach is then presented finally.

5.1. Glacier Classification

5.1.1 RISAT 1

Polarimetric Decomposition of RISAT 1 was carried out using the Raney Decomposition Technique using PolSar Pro Software. Firstly using PolSARpro software RISAT-1 data was extracted in full resolution mode. The available data was in SLC format which was multi-looked using required number of looks. The number of looks taken in azimuth direction was 3 and in the range direction, the same number of looks were taken to convert SLC data into multilook data. Stokes parameters were generated by using this multilook image. Stokes parameters are parameters required and sufficient to fully characterize the observed backscattered EM field and to describe its polarization state. These are four in number namely S_1, S_2, S_3 and S_4. With the help of these parameters, Stokes child parameters were generated; in this case degree of polarization (m) and ellipticity (chi). The m and chi parameters are then used to perform Raney decomposition. The degree of polarization is the indicator of volume scattering occur from randomly oriented features. The ellipticity parameter is an unambiguous indicator of even bounce versus odd bounce backscattering. Here in this study m-chi decomposition of Raney decomposition technique was used. The scattering elements were calculated using Stokes and its child parameters. The RGB color coded image was generated according to the backscattering aspect (BSA) convention as it is a useful analysis tool for investigating classification of scaterrers based on the type of major scattering component received to the sensor. The single bounce (odd bounce) scattering which occurs due to Bragg's law of reflection is shown by blue color in the RGB image. The red color represents double bounce scattering, green signifies volume scattering from a randomly polarized constituent.

In the case of glacier classification, the scaterrers will form different hue of the primary colors used in the decomposed image. This help us identify different features on the glacier surface. The absence of green tinge in the image suggest that either there is no snow through which volume scattering will happen or that the wavelength used is not able to penetrate through the snow. As the time of image suggest (25 Feb 2014), the wavelength is not able to penetrate in the snow. This suggest that melting has occurred in the glacier area hence forming reflective layer over the whole glacier for microwave. The problem is mitigated through using this very knowledge. The area with violet color is the one with both with surface and double bounce. This suggest that the area has a reflective surface with obstruction ahead meaning a glacial ice wall or clean ice with intermittent reflective layer (melted snow). Debris is easily identified in the image due to cyan color representing both volume and surface scattering meaning snow covered debris. Areas showing whitish reflectance are associated with all scattering

components in one. This is associated in turn with a scatter where a snow cover is over an ice wall or just plain simple ice. This gives rise to an area with lots of ice and debris. Area with plain blue color are the one associated with surface bounce, meaning presence of lots of debris.

Percolation zones are generally closely associated with ice, snow and some melting snow. This gives it a characteristic with that of ice with snow over it or something close to it. Hence area with light blue tinge with a hint of green forms this area. Finally area with dark patches which are generally associated with shadow area in SAR images will be crevasses from which no scattering is received. This can be easily seen with eyes and the ablation area is peppered with crevasses/lakes.

Figure 5.1 Circular Polarimetric Decomposition using Raney Decomposition

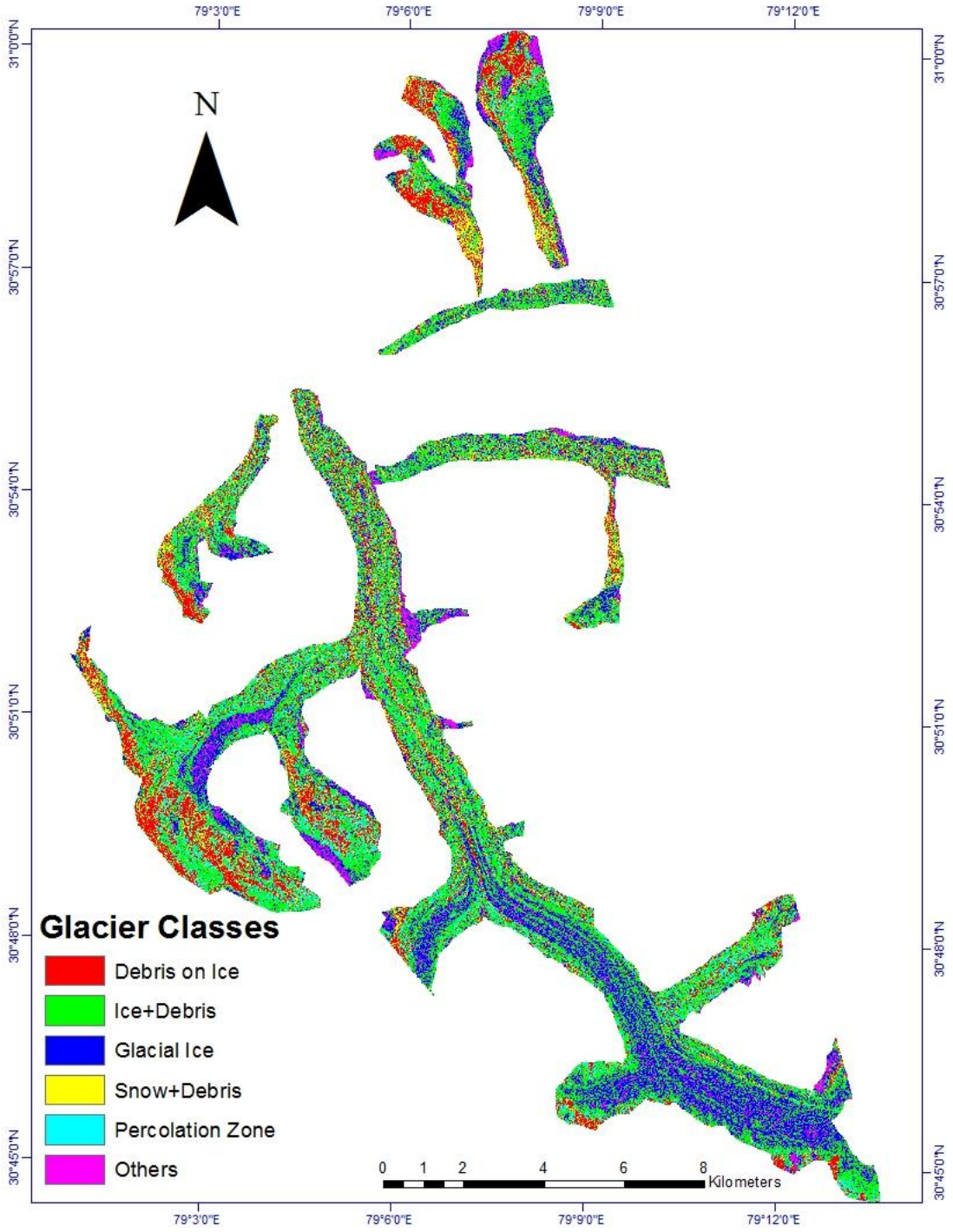

Figure 5.2 Classified Glacier Map using SAR

5.1.2 RADARSAT 2

Polarimetric Decomposition and subsequent classification of the RADARSAT 2 data was done using SARscape 5.0 and ENVI respectively. The SLC images were imported; a cartographic grid size of 10 m for the high resolution C-band data were set for further processing. Multilooking was done with a factor of azimuth looks 1 and range looks 1 for C-band data. Georefrencing and terrain correction was done using ASTER DEM; pixels with

layover and shadow were masked out. The georeferenced images were then filtered using lee filter.

A scattering matrix [*S*] is represented as the complex sum of the Pauli matrices which were calculated from the backscatter images of various polarizations using the band math tool in ENVI. Finally Span was calculated by layer stacking the Pauli matrices to display the image in a single RGB format; where red color represents single or odd bounce scatters, blue color determines the targets characterized by double or even bounce and green color represents volume scattering.

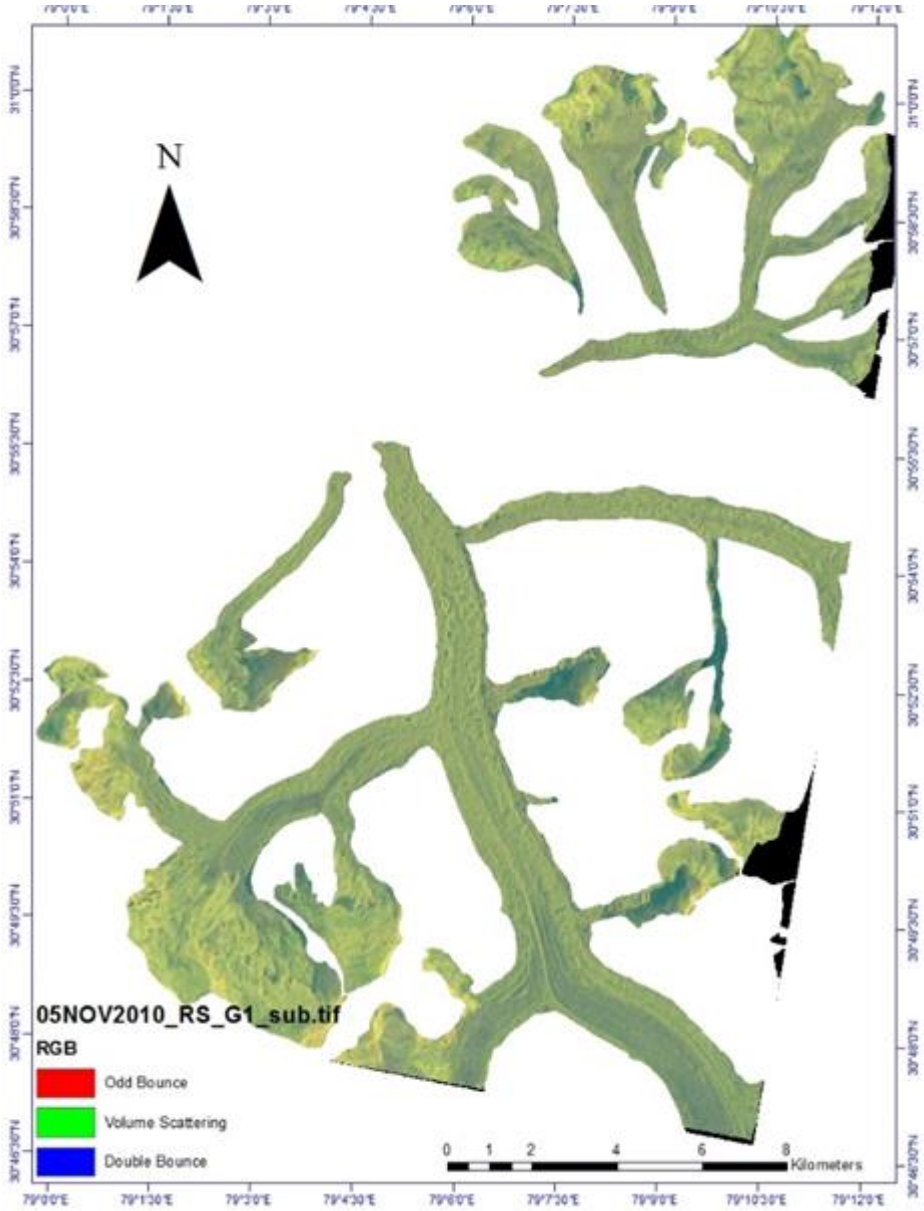

Figure 5.3 Fully Polarimetric Decomposition using Pauli's Decomposition

Figure 5.3 shows the result of Pauli decomposition of RADARSAT 2 data; different shades of RGB can be seen in the image. From figure 5.3 large patches of yellow color are seen, as yellow color is the mixture of two primary colors red and green we can say that these areas represent both scattering mechanisms i.e. surface and volume. As the date of image (18 Feb

2014) suggest, there is a blanket of snow over whole of the study area. The microwave radiations are able to penetrate the dry snow up to a certain depth and scattering is due to the presence of volume non-homogeneities. This give rise to the yellowish tinge over the whole of the glacier. Figure shows some areas with bluish color which indicates odd bounce or surface scattering and the areas can be identified as clean ice. Also the tinge of yellow suggest a layer of snow over the permanent glacial ice.

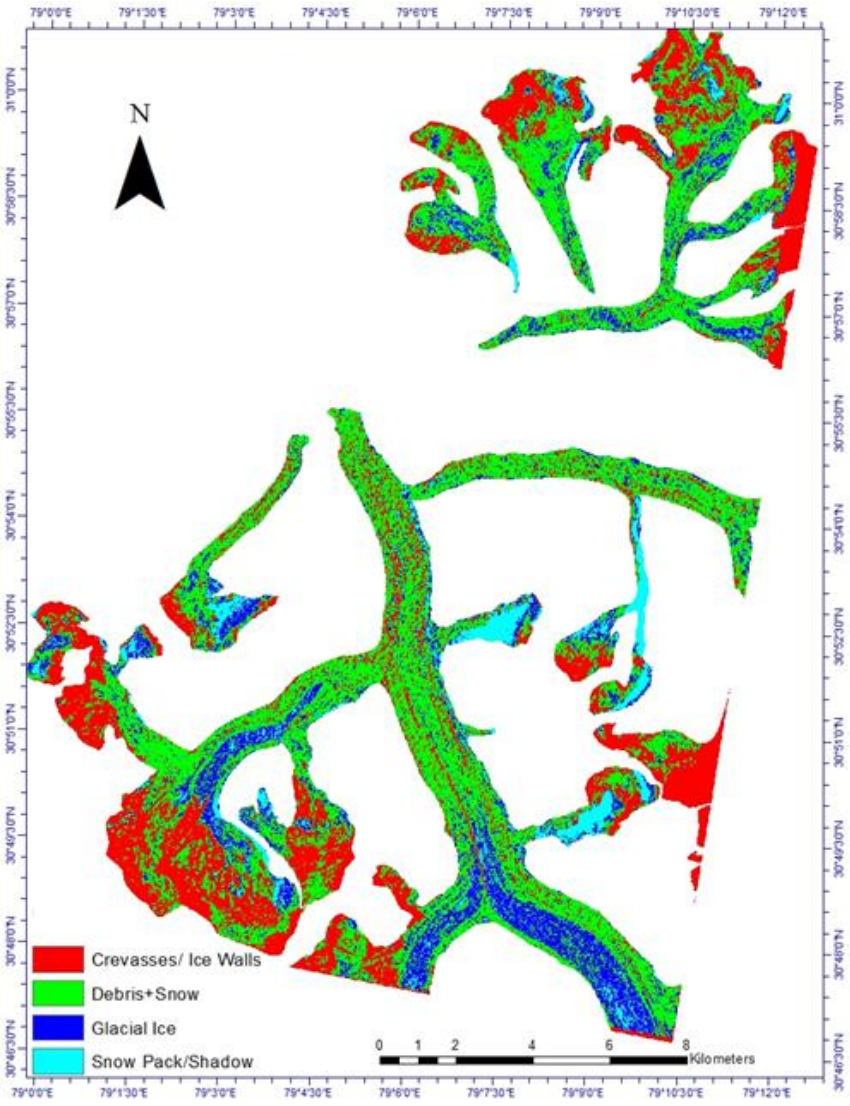

Figure 5.4 Classified Glacier Map using Fully Polarimetric Data

Also in the figure we can see bright patches of purple color these are the areas which were identified as crevasses, they also have component of double bounce scattering mechanism but less in comparison to ice. The shape and orientation of crevasses play a very important role in its identification; generally crevasses facing the look direction with its broad side will be easily identified. This follows the logic that double bounce will be registered more for a feature shaped like a wall than that like a hole as the latter will absorb all signals and will appear as a black patch.

5.1.3 Multi Temporal SAR Images

RISAT-1 Medium Resolution ScanSAR (MRS) datasets are used in this approach. The method uses datasets from different seasons; winter, late summer and early summer for discrimination of different glacier facies or zones.

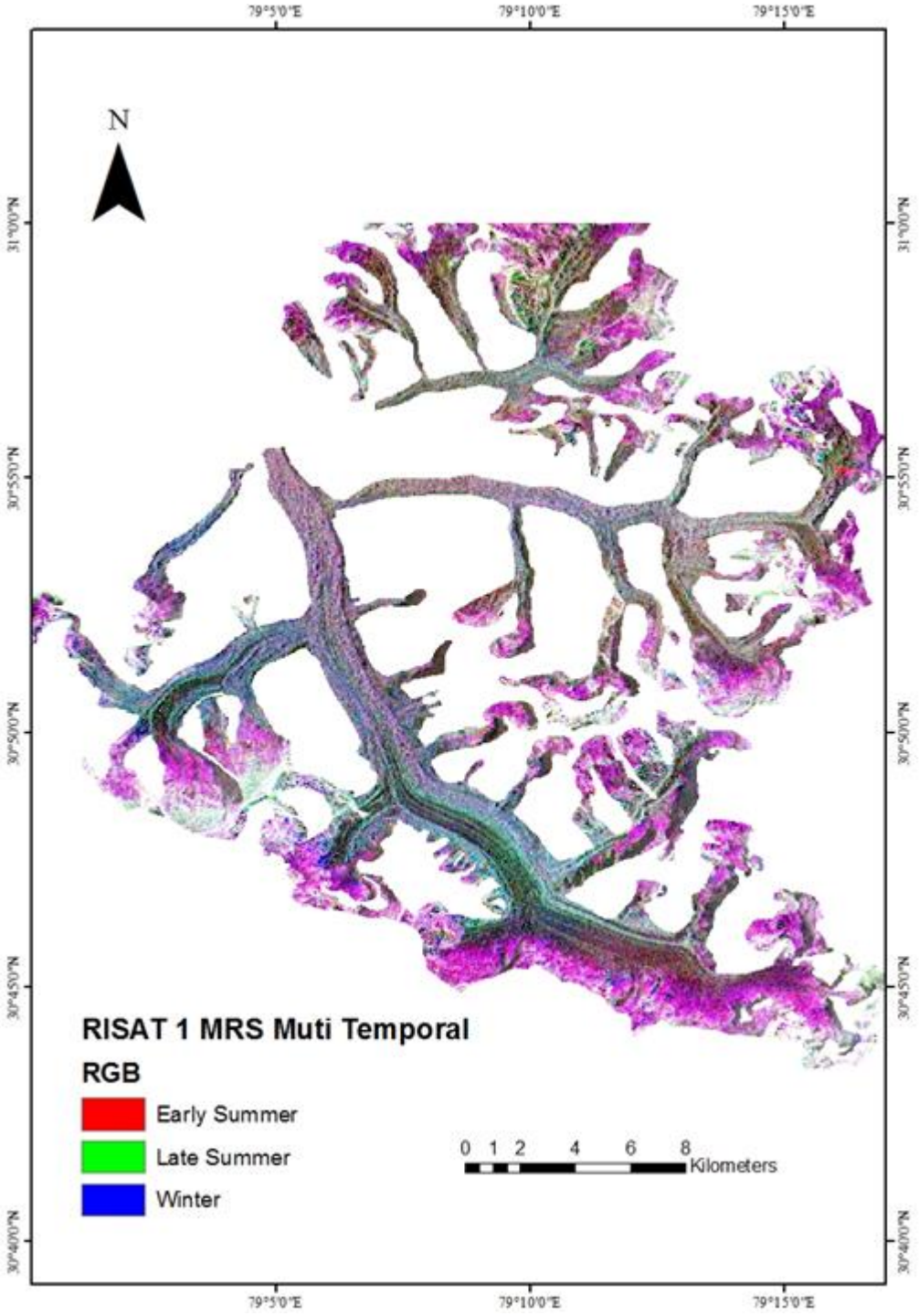

Figure 5.5 RGB stack using HV MRS Multi temporal Risat Data (Early Summer: 1Apr14, Late Summer: 29Aug14 and Winter: 26Jan15)

Percolation zone exists at high elevations where no melting in winters and late summer, so high backscatter values are observed. But in late summer the region appears dark in color due to the melting of snow leading to low backscatter values this zone appears purple in color in the Figure 5.5. Ice Facies are just found below the percolation zone where there is melt observed in late summer and early summer but no melt is observed in the winters; low backscatter values were observed in all the seasons but due to different reasons. In winters the whole glacier is covered by dry snow, the microwave radiations are transparent to dry snow and the backscatter comes from the glacial ice a smooth surface; acts as a specular reflector causing low returns back to the radar antenna. In early summer little melting occurs in the winter snow, so due to the presence of moisture low backscatter values are observed. Almost all of the seasonal snow has melted away in late summer and the backscatter is coming from the wet firn which melts in the day time and refreezes in the night and compacts into a rough solid leading to higher returns in this season. Figure 5.5 shows glacial ice with a tint of green color. The regions of debris can be clearly seen further down the glacier near the snout and also as moraines which are moving along the glacial ice. Using multi-temporal SAR image generalized results were obtained with only two distinctive colors i.e. green and purple but using this approach we were able to evaluate the extent of percolation zone, glacial ice and debris so we have to use polarimetric decompositions for a detailed discrimination of glacier facies.

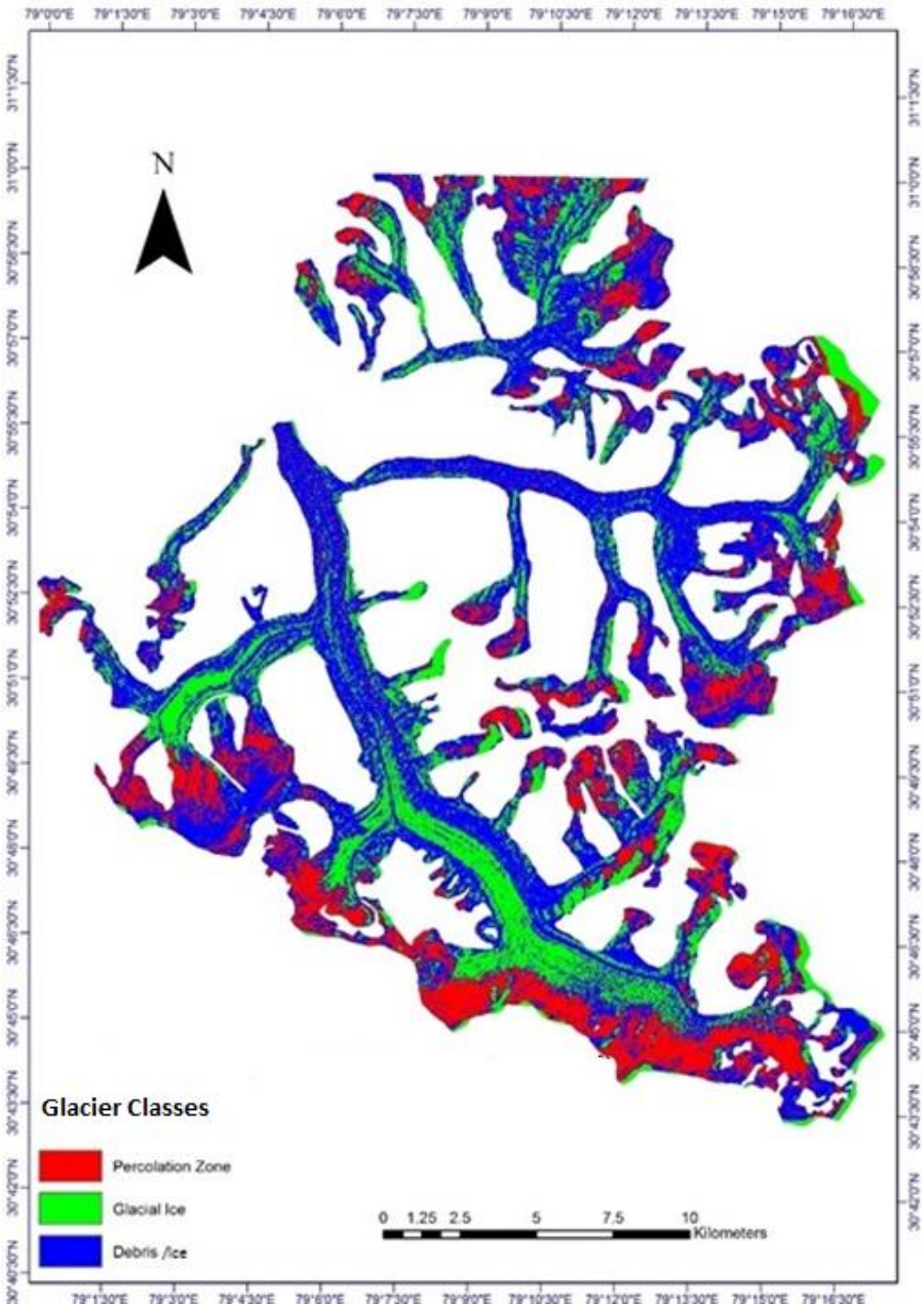

Figure 5.6 Classified Glacier Map using MRS Multitemporal Data

As can be clearly seen in the classified map of the MRS data of glacier, the classification of debris, snow and ice is highly accurate from visual inspection. This follows the logic that the scattering by the entities mentioned above are by and large unique and easily distinguishable. Debris Classification is ambiguous due to mixed scattering from a lot of adjacent features and the local geometry.

5.2. Optical Feature Tracking

All the available images used for this study should be co-registered and ortho-rectified. Images from IRS 1C/1D are manually co-registered using AutoSync tool provided in Erdas Imagine. Landsat images used in this study were already ortho-rectified. Images for further processing are selected on the basis that both images are having same coverage, high SNR (Signal to Noise Ratio) and minimal snow cover area. All the bands in the selected images are layer stacked using the ERDAS software. The study area is extracted by sub-setting using Gangotri glacier boundary to reduce the computation time.

Once all the above steps has been successfully done the actual implementation to find glacier movement using feature tracking is carried out. A cross correlation technique in the COSI-CORR, an ENVI module has been used for feature tracking. For this, the pre-event image has been considered as the image temporally taken before the post-event image. Once the images has been selected, this can be directly implemented in the correlation extension in COSI-CORR. In this correlation can be done by two methods, Frequency and Statistics. Frequency correlator is Fourier based and is preferable if the optical image is of good quality. In this study Frequency method is used for correlation.

In Frequency correlator several predefined parameters such as initial and final window size, step, robustness iteration and mask threshold has to be carefully selected to obtain an optimal movement value. This generally is a hit and trial method if prior information of the movement of feature is unknown. Hence we selected a set of parameters to conduct the studies as shown in Table 5.1

Table 5.1 Parameter combination used for optical feature tracking

Window Size		Resolution	Step	Robustness Iteration	Mask Threshold
Initial	Final				
64	32	15	2	4	0.9
128	64	15	2	4	0.9
256	64	5	2	4	0.9
256	128	5	2	4	0.9
512	256	5	2	4	0.9

For imageries with spatial resolution 15m (Landsat), window size of 64 and 32 for initial and final run is taken. High resolution imageries of 5m spatial resolution (IRS1C/1D) had window size of 256 and 64 each for initial and final run. This was then changed to 256 and 128 for longer temporal distance image pairs. The step of 2 and a mask value of 0.9 is taken to detect smallest possible movement and make the field homogenous while keeping the fidelity of the results intact.

The choice for the band with which to infer movement is determined by the spatial resolution of the band, not by its radiometric resolution as was suggested in a previous study. This follows from the fact that feature movement will only be determined if the feature moves more than half of the window size chosen for the feature tracking. The theoretical limit of this function is one-fifth (1/5) of that of window size, but is rarely achievable in practice. Also

care has to be taken that window size does not exceed the glacial width in one step; as such higher resolution band (panchromatic) will be the final choice for such kind of studies.

Movement values recorded for different years using optical feature tracking are given in Table 5.2 and 5.3. A long term movement measurement gives the idea for the current trend of physical behaviour of any glacier. To identify local climatic influence, different movement with respect to slope, aspect and ELA has been studied. Thus it gives a way to analyse various physical parameters of glacier, which have been utilized in this study using optical images starting from 1998 to 2014.

Table 5.2 Final Result for Feature Tracking using Medium Resolution Band

Satellite	Date Pair	Window Size		Resolution (m)	Movement		SNR	Time Interval	Velocity (m/day)
		Initial	Final		E-W	N-S			
Landsat 7	9Sep98-22Oct99	64	32	15	9.974	6.220	0.9	408	0.0288
Landsat 7	8Oct00-20Oct01	64	32	15	8.890	6.812	0.9	377	0.0297
Landsat 7	22Oct99-8Oct00	64	32	15	4.893	3.590	0.9	352	0.0172
Landsat 7	20Oct01-8Jun02	64	32	15	6.172	7.040	0.9	231	0.0405
Landsat 7	22Oct99-20Oct01	128	64	15	14.183	10.188	0.9	729	0.0239
Landsat 7	8Oct00-28Aug02	128	64	15	8.511	10.638	0.9	689	0.0197
Landsat 7	9Sep98-8Oct00	128	64	15	10.389	8.460	0.9	760	0.0176
Landsat 8	26Aug13-21Sep14	64	32	15	5.396	6.509	0.9	391	0.0216

Table 5.3 Final Result for Feature Tracking using High Resolution Band

Satellite	Date Pair	Window Size		Resolution (m)	Movement		SNR	Time Interval	Velocity (m/day)
		Initial	Final		E-W	N-S			
IRS	22Oct00-08Jul02	256	64	5	6.889	7.323	0.9	624	0.0161
IRS	22Oct00-05Oct03	256	64	5	7.554	8.215	0.9	1078	0.0103
IRS	8Jul02-20Oct05	256	64	5	5.968	5.609	0.9	1200	0.0068
IRS	8Jul02-5Oct03	128	32	5	7.902	7.281	0.9	454	0.0236
IRS	5Oct03-20Oct05	256	64	5	5.553	5.491	0.9	746	0.0104

Yearly data for movement is depicted in Figure 5.7- 5.9 to better analyse the trend of the movement of feature over the surface of the glacier. This is then compared with AAR of the glacier over the years to relate with the movement values.

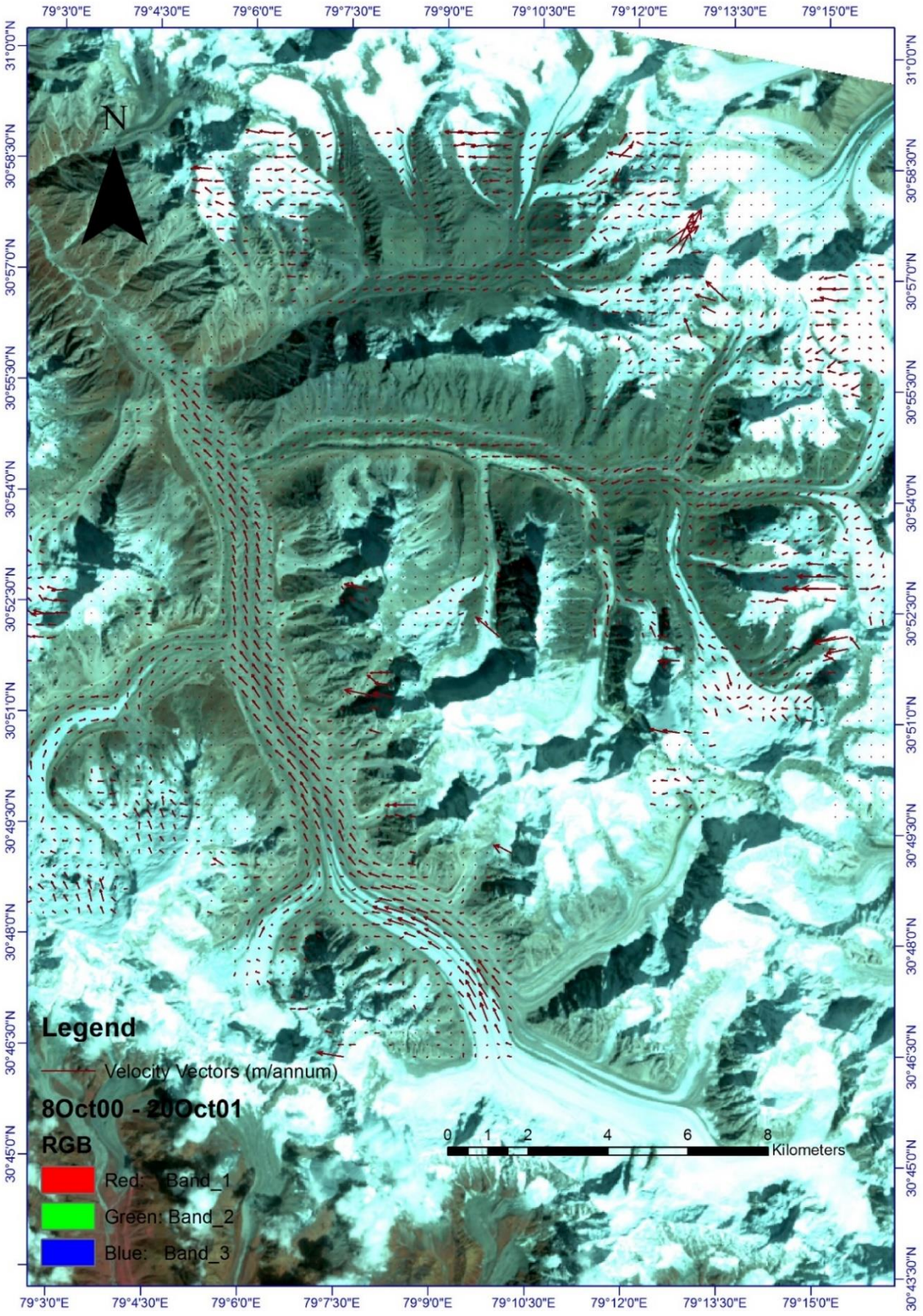

Figure 5.7 Velocity Vectors for Year2000-01

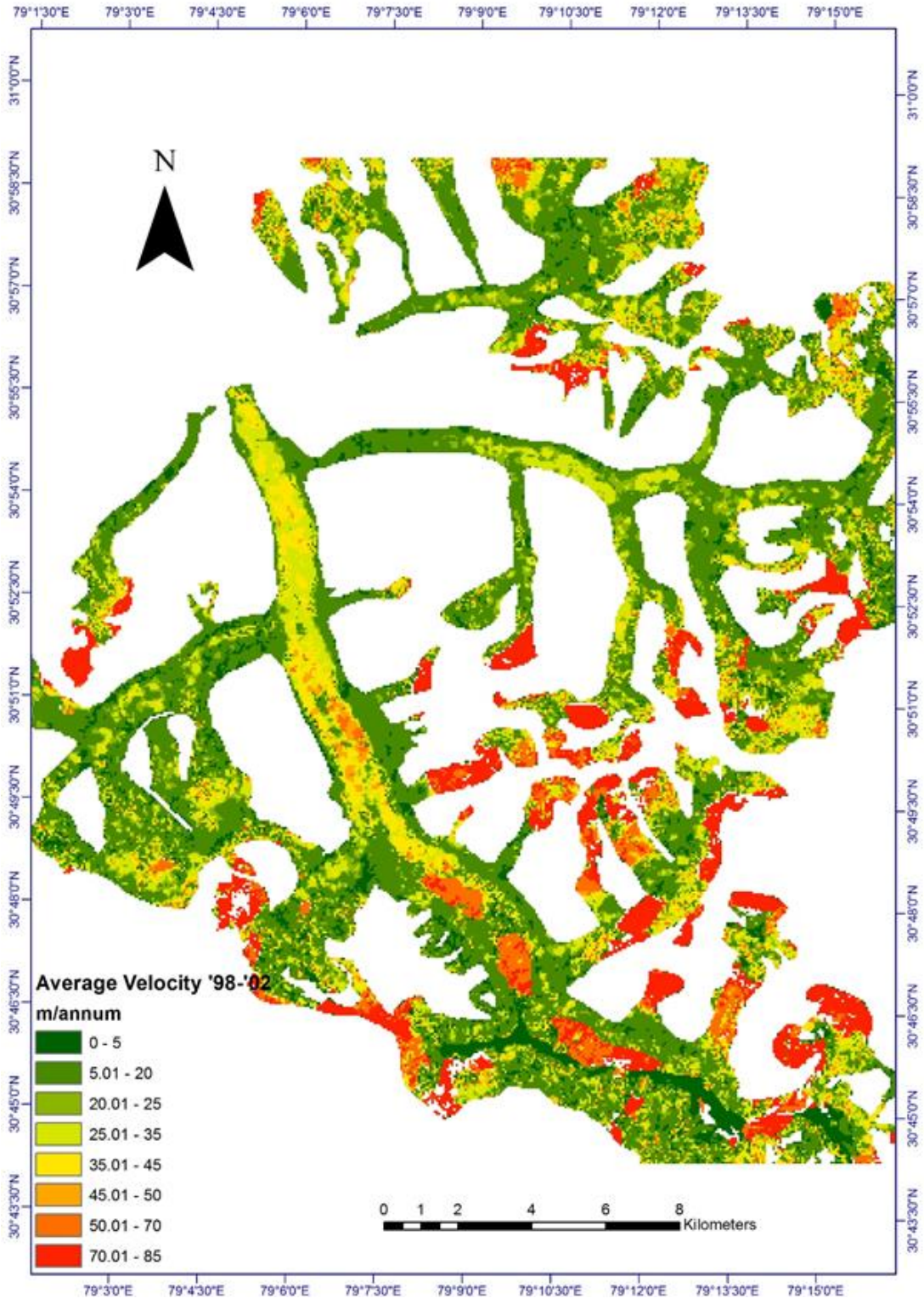

Figure 5.8 Average Magnitude of velocity for the Years 1998-2002

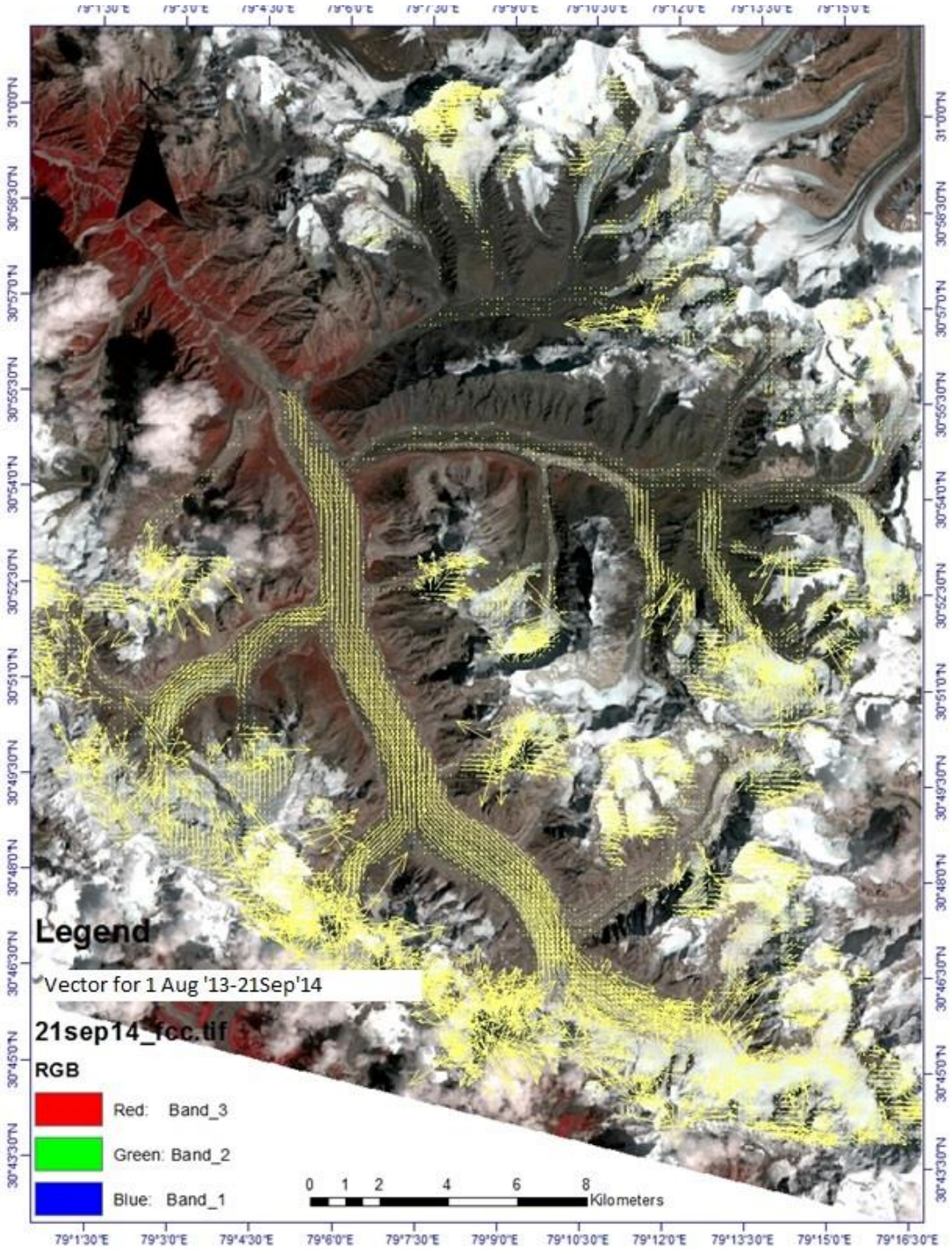

Figure 5.9 Velocity Vectors for Year 2013-14

The above maps depicts the different movement vectors and intensity for different years. During the period 2000-03 and 200-02 a very less movement was found compared to other time intervals (Table 5.3). This is due to the fact that high resolution images need high radiometric content to accurately identify features. This leads to calculation of error in the map.

Table 5.4 Error Calculation In Velocity Mearurement

Satellite	Band Resolution (m)	SNR	SNR achieved	Accuracy (m)	Error	Error in velocity (cm/day)
Landsat	15	0.9	0.99	14.85	0.15	0.04109
IRS	5	0.9	0.89	4.45	0.55	0.15068

5.3. Glacier Ice Thickness Estimation using Velocity measurements

The movement maps generated with the help of COSI-CORR contains raster based information of the local movement measured for a feature over the time period. All the dataset are then exported to ArcGIS 10.1 for further processing and map generation. These are then converted to velocity information for the same time period using the raster calculator in ArcGIS 10.1. The reason for using ArcGIS over ENVI is that ArcGIS gives the option of snapping the raster pixel to other raster datasets. A slope map was generated from the DEM which was generated from the ALOS-PRISM stereo pair. The slope values was also interpolated to 100m resolution to weed out local undulations. The velocity map is then interpolated to convert the 30m resolution Landsat data and 10m resolution IRS data into 100m resolution for further processing. The maps are stacked over for the year 1998-2002 for Landsat data. These datasets are then applied to the Equation (4.11) to get an averaged out value of ice depth over the same period. Individual year movement values are also used to derive the thickness values which are then parameterized to establish local parameters for the study area.

Table 5.5 Parameterization for basal velocity and ice depth

$\mathbf{U_s}$	30%	25%	10%	5%
	3/10	1/4	1/10	1/20
$\mathbf{(U_s - U_b)}$	7/10	3/4	9/10	19/20
	0.7	0.75	0.9	0.95
$\mathbf{2(U_s - U_b)}$	1.4	1.5	1.8	1.9

As can be seen the Figure 5.11 (A-F), the variation in the depth is higher when the velocity and the depth itself is very high. When lower depth or velocity are encountered, the variation in basal are of not much consequence. This is apparent in cases where the depth is less than 50m. However depth is in excess of 250m, we see a large variation in the resultant depth due to change in basal velocity. Consecutively the variation in basal velocity will alter the depth found in the region. Also we can safely say that the basal velocity and the depth calculated have an inverse relationship to each other. This is apparent from the increase in depth of the cross-section over all the graphs when the basal velocity is lowered. This is first tested for the main glacier trunk and validated with TLS ground points and then worked out for whole group of glacier.

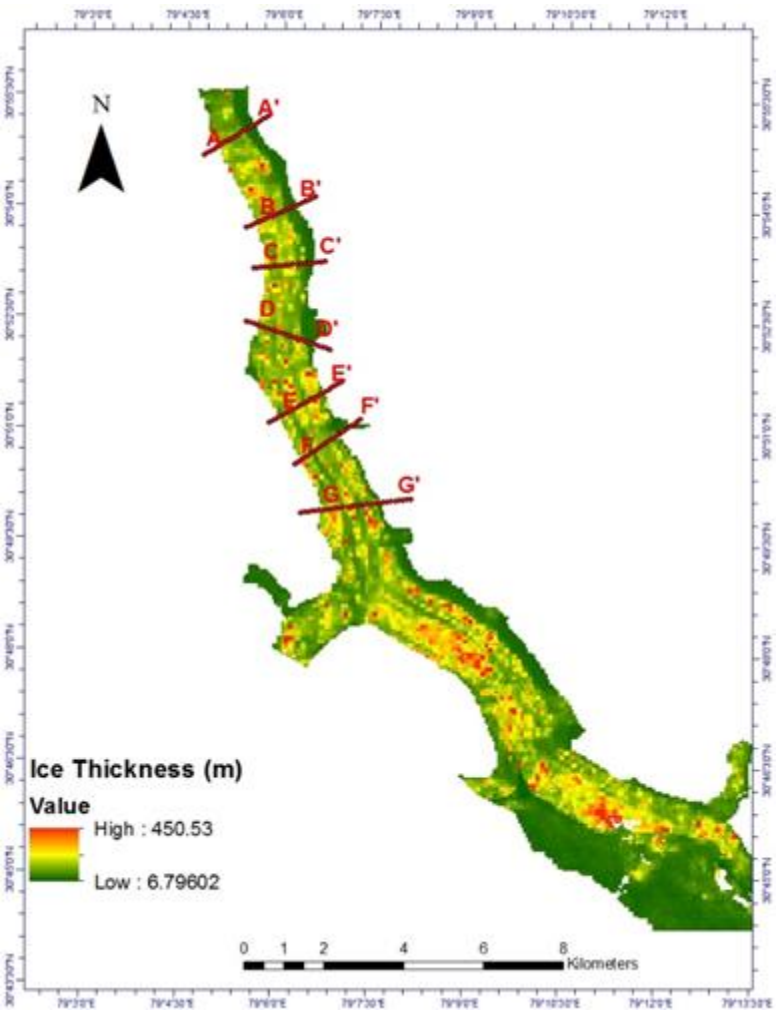

Figure 5.10 Cross-sectional Profile along the main trunk of Gangotri Glacier

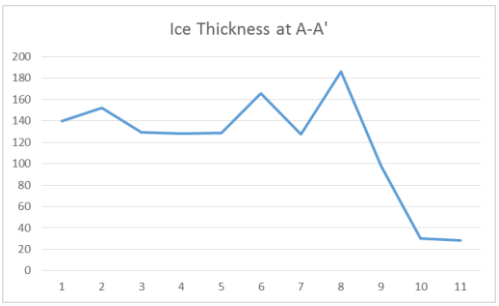

A-A’

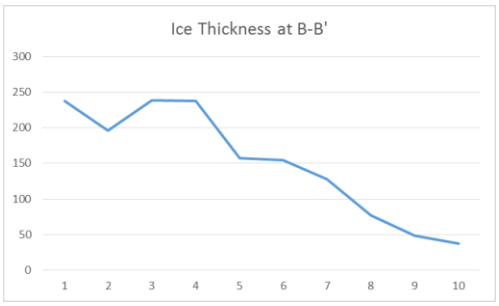

B-B’

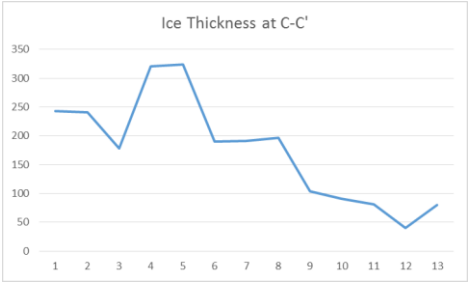

C-C’

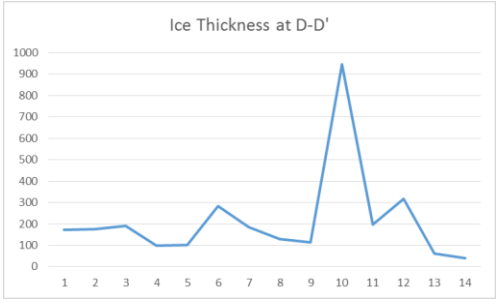

D-D’

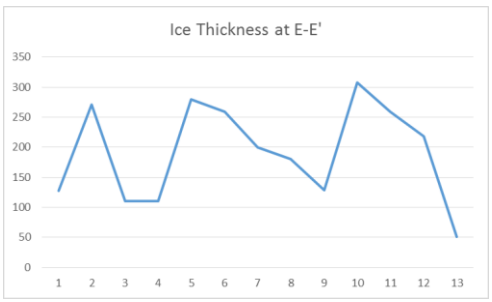

E-E’

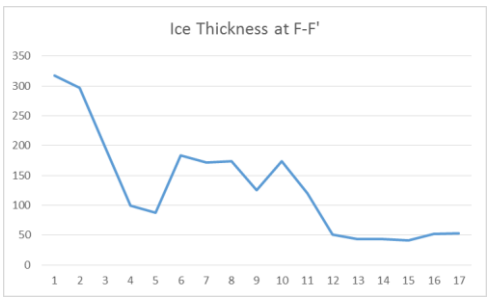

F-F’

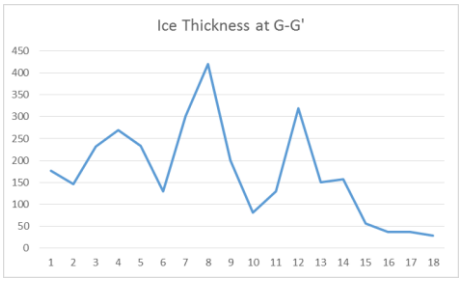

G-G’

Figure 5.11 Cross-Section Graphs Of The Main Trunk Of Gangotri Glacier; Y-Axis Represent Ice Thickness In meter And X-Axis Represent Point Interval At 100m Each

Shown above is the ice thickness variation over the main trunk of Gangotri glacier. AS can be seen the variation over the trunk varies from 50m to 412m over the stretch of the trunk. This is consistent with the depth seen over the other parts of the glacier and other glacier in the group as well. As can be seen profile of the depth islands over the glacier body wherein depth is not uniform over the whole cross section as is produced from GlabTop model and other slope based models. This is due to the interpolation carried out in these models. Also this can be due lateral moraines formed over the glacier body approximate to the low depth of the ice. This can also provide vital information of the physics involved in the glacier body.

Also as can be seen from Figure(5.19 and 5.20) the smoothness of the glacier bed is achieved in GlabTop and Slope Dependent models. Further analysis using Ground Penetrating Radar (GPR) measurement is required to truly asses the situation underground. As GPR was unavailable during field visit, Terrestrial Laser Scanner(TLS) and DGPS measurment were used to discern the height at snout of the Glacier.

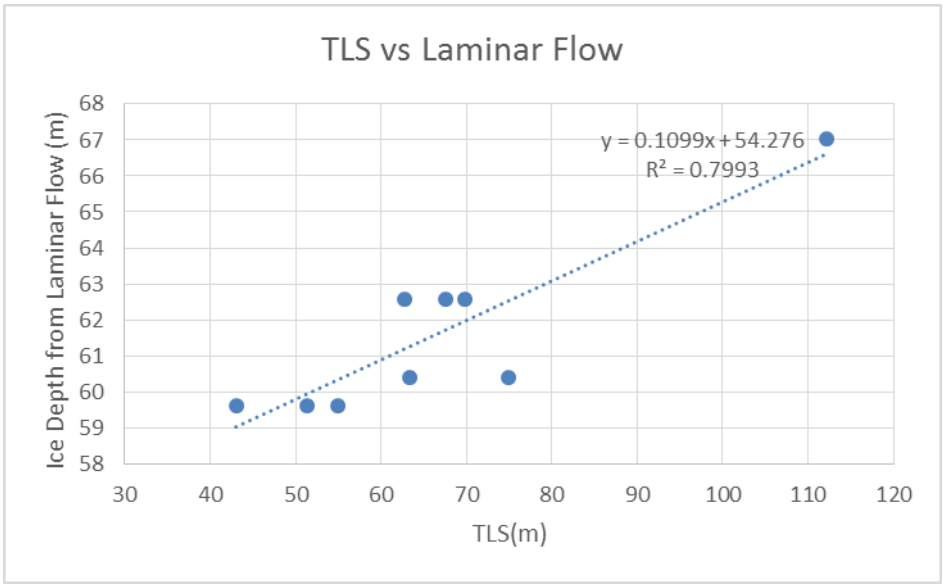

Figure 5.12 TLS vs Laminar flow Correlation

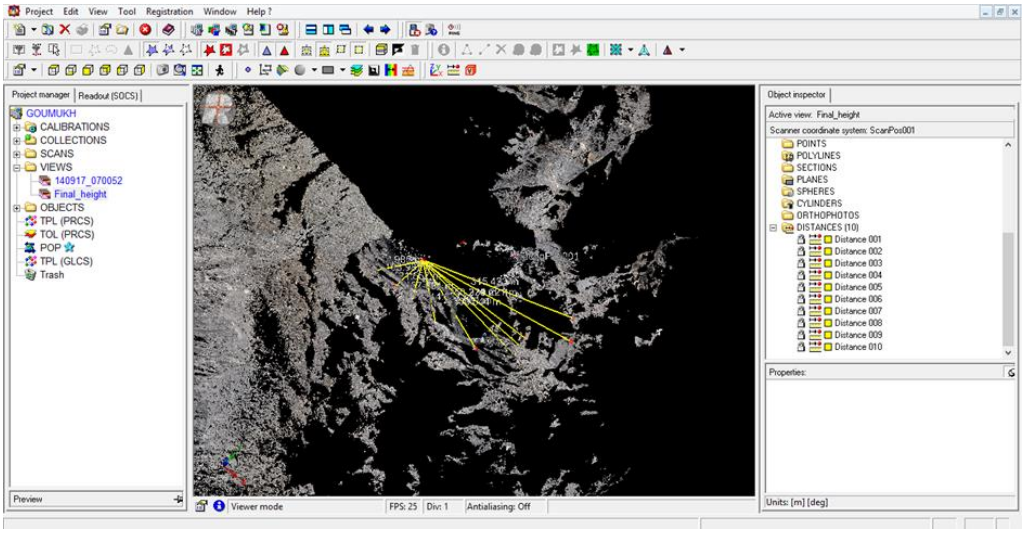

Figure 5.13 Nadir View of TLS Post processing (Note similar feature in Figure 5.16)

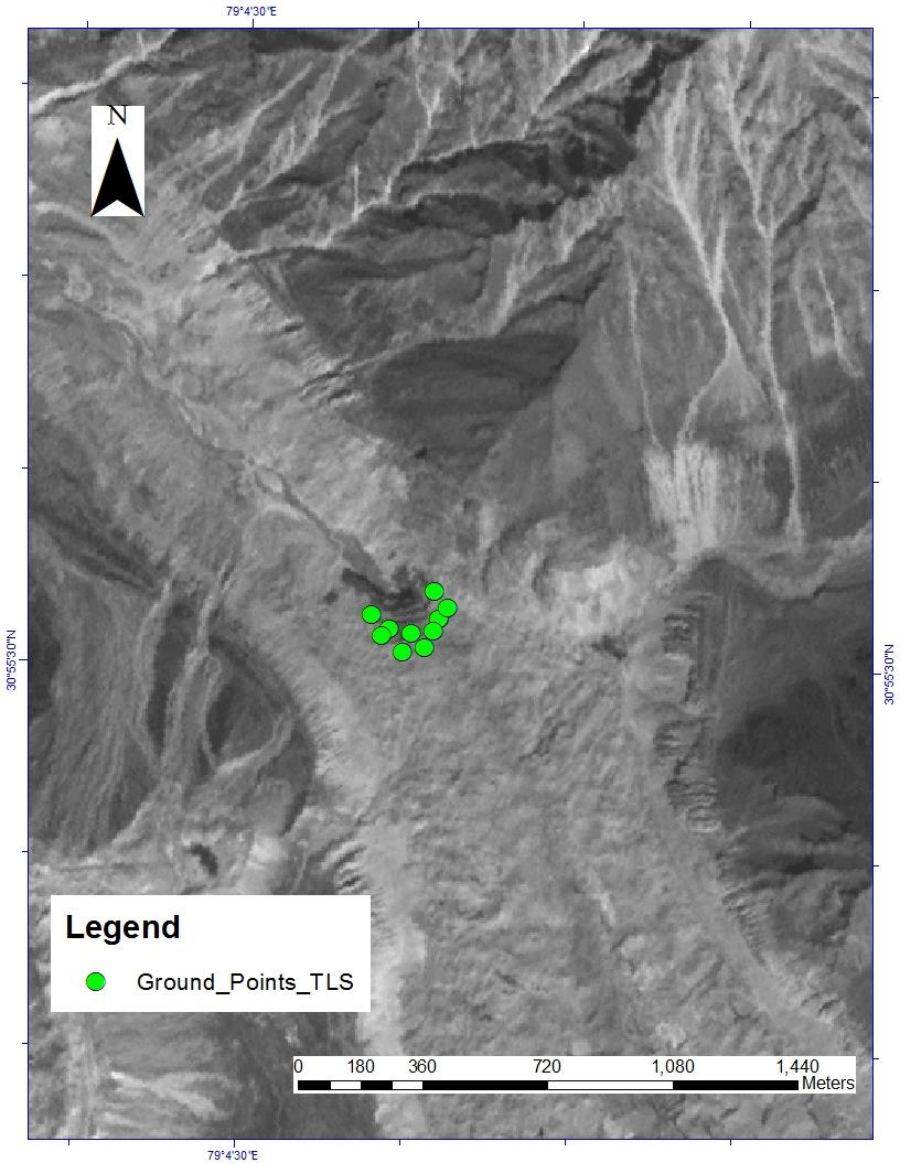

Figure 5.14 Points taken for Depth extraction from Laminar flow map; Note the feature match with Figure 5.13

The R^2 value (=0.79)is pretty high for a model with inheretent errors. This shows that the model is very accurate to model glacier heights and the error is low too. One problem is that we don't know the amount of layer submerged in the ground. This challenge can only be solved with the use of Ground Penetrating Radar. The accuracy achieved from the TLS is itself quantified at R^2=0.9987. Hence the model can be calibrated at snout for future studies using TLS. Also if TLS is used with the inbuilt GPS unit for accurate positioning, changes in glacier height can be observed on a seasonal basis.

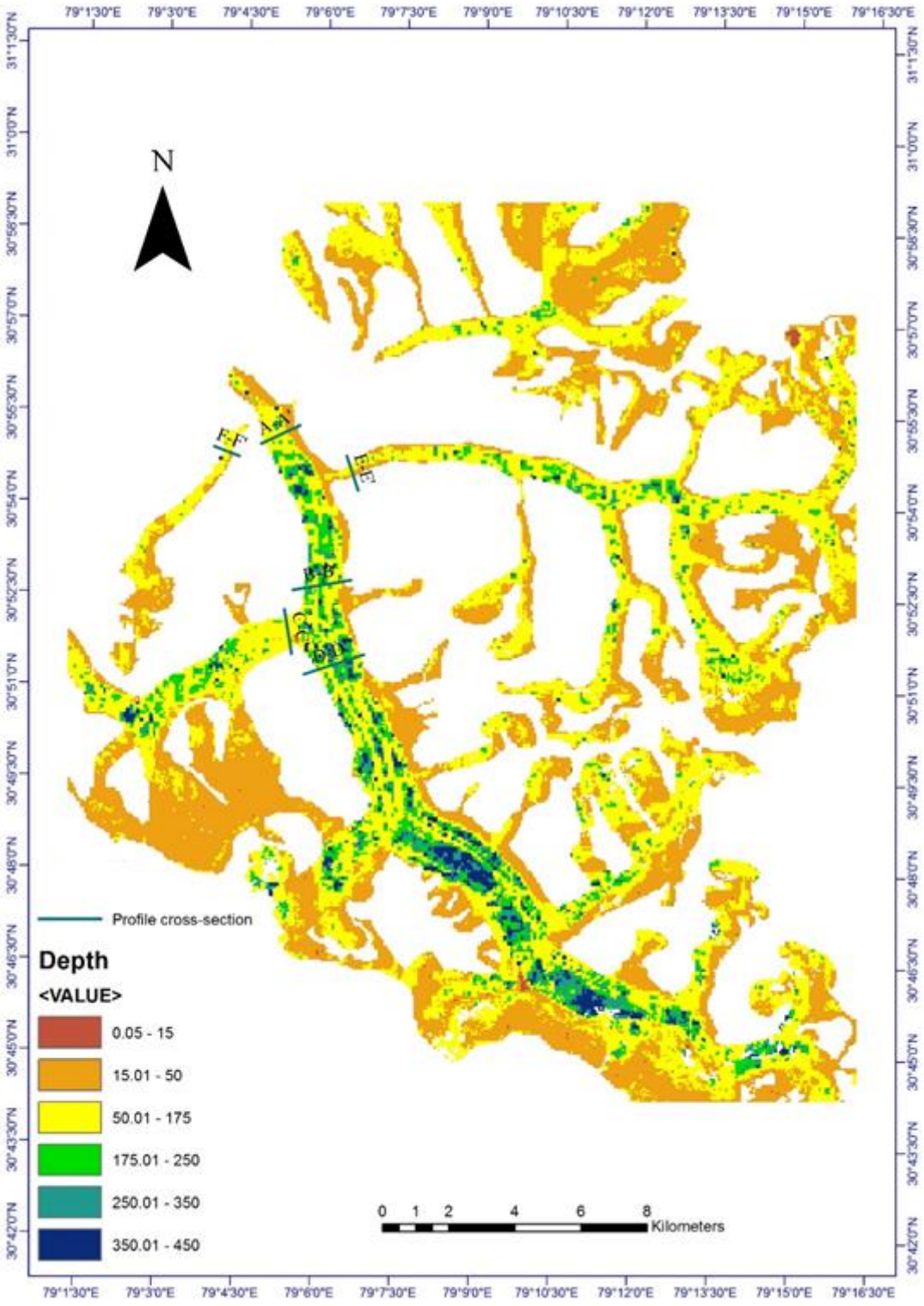

Figure 5.15 Average Ice Thickness of the Gangotri glacier for time interval 1992-2014

The velocity map for the entire time period is displayed in Figure 5.10. The various Cross-section profiles have been created where the depth is analysed and the variation in basal velocity is tested for the corresponding depth variation. As can be seen in the map, the depth forms a kind of dredging line in the bed. This can be due to the fact of the branch glacier

bringing its extra debris to the main glacier hence increasing the depth of the ice. As the depth is related to velocity (Figure 5.11), higher velocity means the mass-continuity equation is preserved in this physical process hence confirming the validity of the method.

Also the variation in the depth is low as compared to the variation in velocity. This may be due to the fact that the power with which the velocity is calculated is 4 (n+1) from Equation 4.11. Hence the velocity component does not greatly affect the depth in final calculation of the velocity. Also the variation in velocity by 5% changes the depth by ~5m and the variation in velocity by 10% changes the depth by ~17m. Hence showing an exponential growth for a linear input in the equation. Also a marked change from what is visible in Figure 5.10, the depth increases when the velocity increases. This is true in the sense that the velocity is directly proportional to the depth but the basal velocity is inversely proportional to depth calculation.

Figure 5.16 Profile cross-Section for different ratio of basal velocity(in terms of percentenge of surface velocity)

Note: Figure5.16 (A-F) x-axis represent the profile length (100m interval) from x-x’; y-axis represents ice thickness calculated from the model.

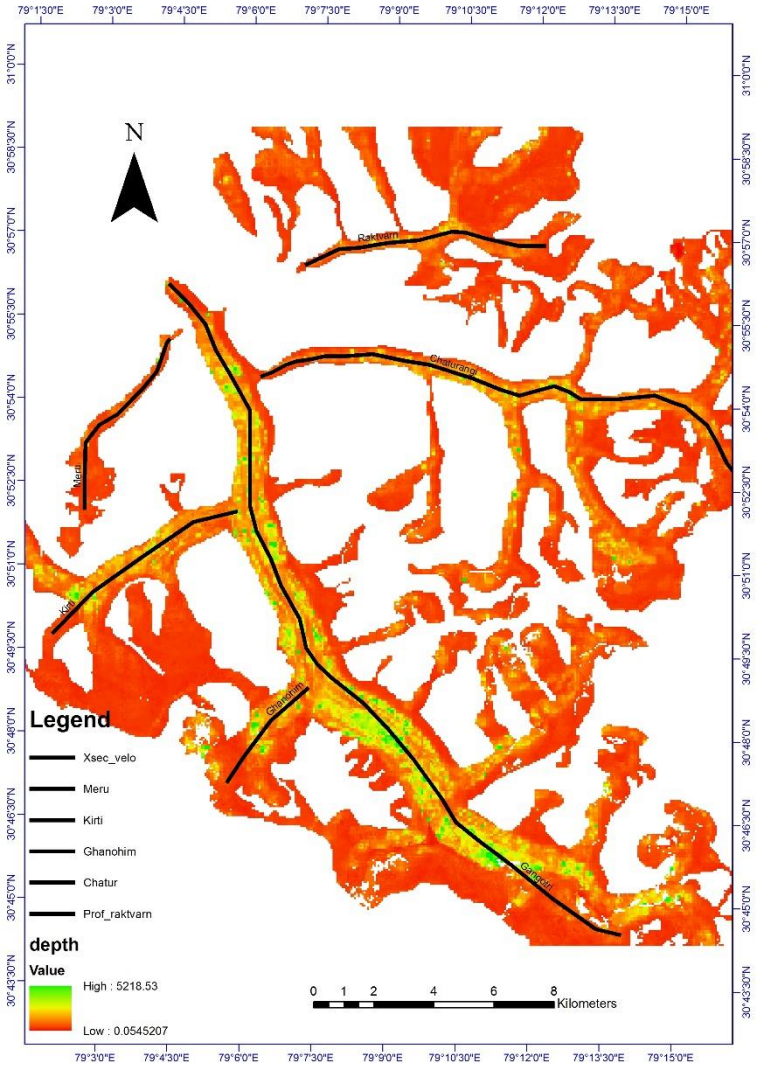

Figure 5.17 Longitudinal Profile Along Major Glaciers (Depth 2013-14)

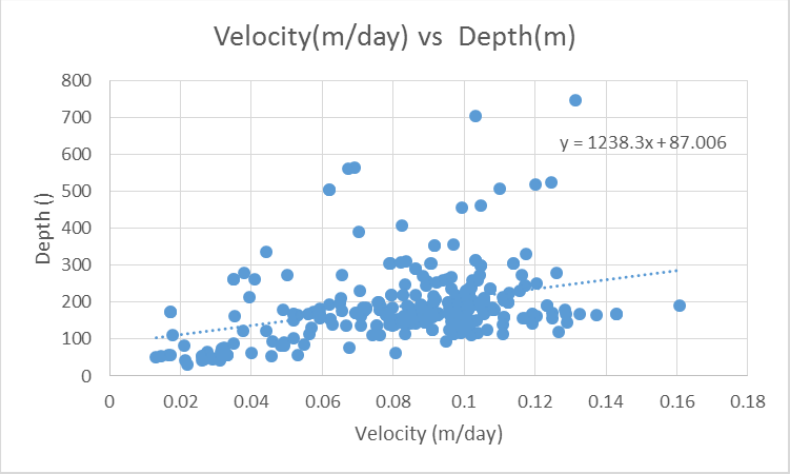

Figure 5.18 Depth vs Velocity graph (Notice the rising Trendline)

The results of profile section in Figure(5.12) have been shown in Appendix 1. The major conclusion of the profile analysis have shown that the variation in Lamiar flow model is very

huge where variation from 20m to 600m is easily visible. The same streach is linear for most of the profile cross-section in GlabTop and slope dependent models. This is due to the fact that both GlabTop and Slope Dependent models are a variation of each other. Also varying basal velocity and plotting it with depth along the profile reveal some interesting observation; major glacier profile show huge variation for the change in velocity but the same effect is less in smaller glacier. This may be due to smaller velocities associated with the small glacier.

5.4. Glacier Ice Thickness Using Slope and Glabtop Model

The Ice thickness derived from slope dependent equations (4.14), (4.15) & (4.16) is shown in Figure 5.8. The slope dependent approach works on the premise that all glaciers are alike up to a certain extent and hence topography would not be altered much. Hence we see a smooth almost planar topography of the bed in the figure. This also stem from the fact that

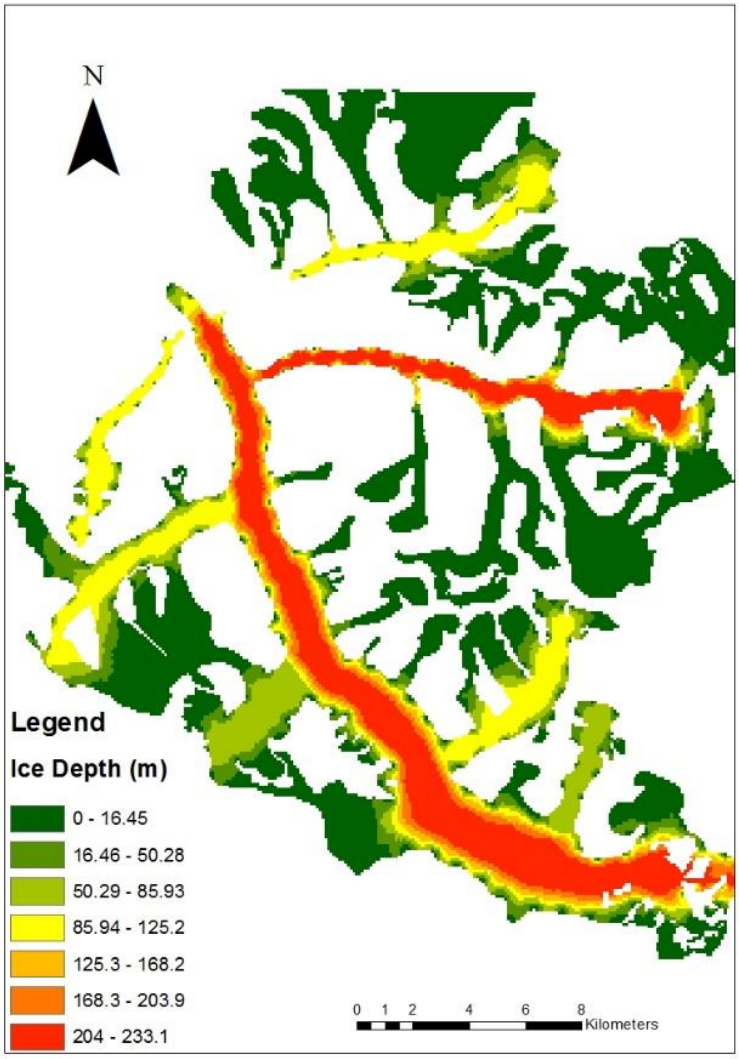

Figure 5.19 Ice Depth From Slope Dependent Equations

Equation (4.13) provided a multiple to be used to extrapolate the values calculated for the entire glacier bed. This criteria fits this glacier as the depth of the glacier is $<1/10^{th}$ of the glacier width over majority of the glacier area. Also since only the major branch lines were

digitized for this particular approach as the model works for individual glacier with no branching, the changes in the bed topography is very visible near the conjunction of main glacier and branching glacier. Also a mean depth for different branches was calculated and has been presented in the Table 5.5. The Ice depth is the most in the main trunk and Chaturangi glacier at 222.10m

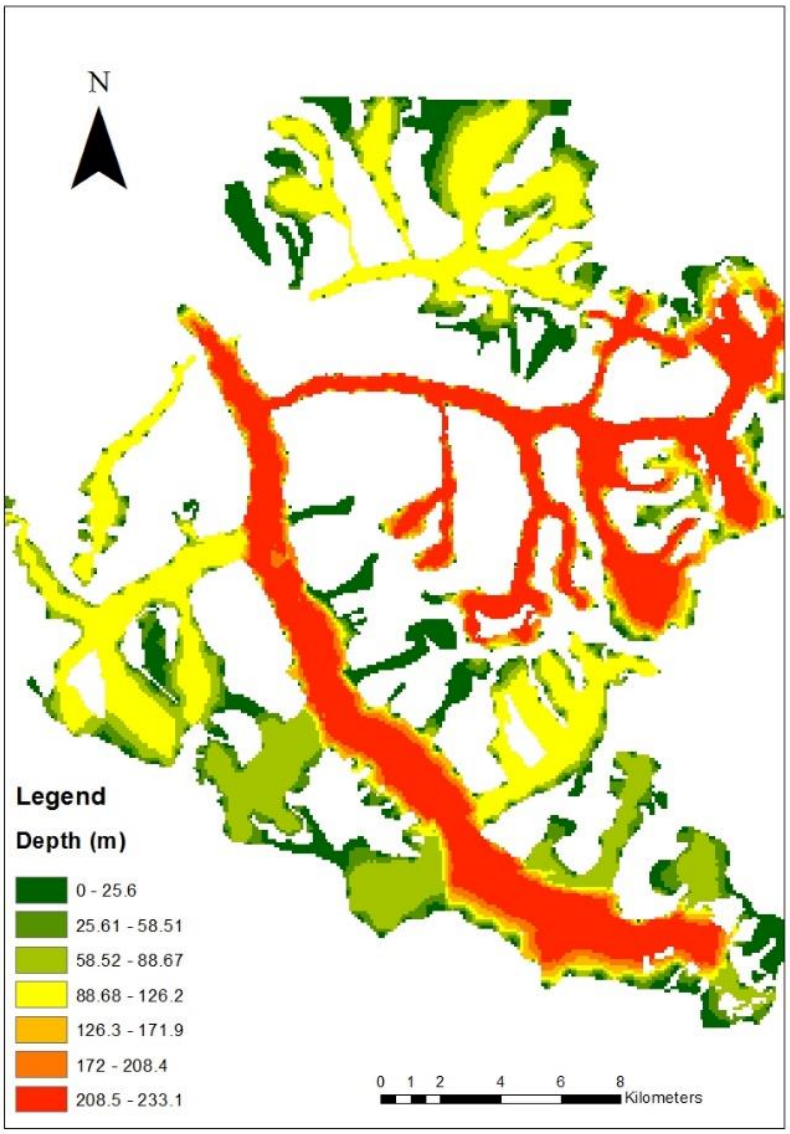

Figure 5.20 Ice depth from GlabTop Model Approach

233.10m respectively. These are also some of the largest spanning glaciers in the group. This supports the hypothesis that states the depth as directly proportional to its area. All other glacier branches are medium in depth (75.97m to 119.03m) with the average depth and volume calculated to be 172.88m and 46.7376km^3 for the whole glacier.

Table 5.6 Parameters Used For Slope Dependent Model and Associated Ice Depth

	Length (km)	ΔH(km)	Slope (rad)	τ	Ice depth (m)	Area Covered (km2)
Gangotri	30	3.2	0.10626	150	200.42	87.87
Raktvarn	10.27	2	0.19233	150	111.21	47.88
Chaturangi	15.18	1.2	0.07888	129.62	233.10	64.89
Swachand	6.81	1.15	0.16729	126.7413	107.87	16.11
Malandi	4.26	0.85	0.19694	104.9013	75.97	4.58
Meru	8.53	1.45	0.16837	140.7513	119.03	5.57
Kirti	9.01	2	0.21843	150	98.10	31.60
Ghanohim	4.03	0.6	0.14779	80.72	77.68	11.83

Here ΔH is altitude difference from lowest point to peak in a glacier and τ is basal stress.

GlabTop model (Paul and Linsbauer, 2012)uses the same technique as defined for slope dependent approach but depth calculation are done for height intervals. This means that the branch lines digitized are more intensive and conform to the hydrological structure of the glacier bed. Hence τ, basal sheer stress, is calculated for height interval of 500m each. This allows for more flexibility in calculating ice depth or bed topography of complex glacier system like Gangotri. Table 5.6 provides insight for model calculation of bed topography and associated parameters used.

Table 5.7 Parameters Used For GlabTop Model and Associated Ice Depth

	Length (km)	ΔH (km)	α(rad)	T	Ice depth (m)	Area Covered (km2)
Gangotri	30	3.2	0.10626	150	200.42	68.4
Raktvarn	10.27	2	0.19233	150	111.21	47.88
Swachand	15.18	1.2	0.07888	129.62	233.10	64.89
Swachand	6.81	1.15	0.16729	126.7413	107.87	16.11
Malandi	4.26	0.85	0.19694	104.9013	75.97	4.58
Meru	8.53	1.45	0.16837	140.7513	119.03	5.57
Kirti	9.01	2	0.21843	150	98.10	31.60
Ghanohim	4.03	0.6	0.14779	80.72	77.68	11.83
Gangotri2	4.7	1	0.20963	116.8	79.54	19.47

Here ΔH is altitude difference from lowest point to peak in a glacier and τ is basal stress.

As can be seen the previously neglected glacier branch is now incorporated for further analysis of glacier bed topography. This also shows the robustness of the model as well as the fast application over large glacier outlines. Ice depth varies from 222m to 75m in average over the entire glacier. The volume thus calculated is at 42.47 km^3 for the whole glacier. The basal stress for the points are calculated using Equation (4.1) and (4.22). This is calculated for just point data as opposed to whole glacier to point out the fact that the stress does not always form a direct relation with the depth and other factor may also be involved. Also basal

stress cannot be verified in field as equipment availability was an issue. This indirect approach point to further analysis of the relation between the two for all classes of glaciers.

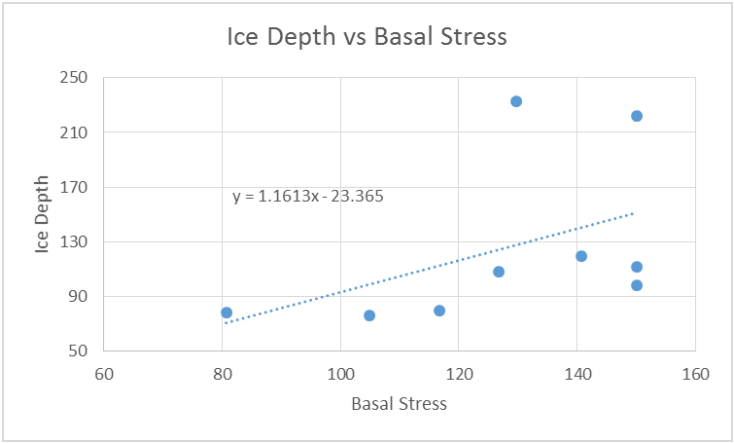

Figure 5.21 Trend line between Basal Stress and Ice Depth (Thickness) for GlabTop Model

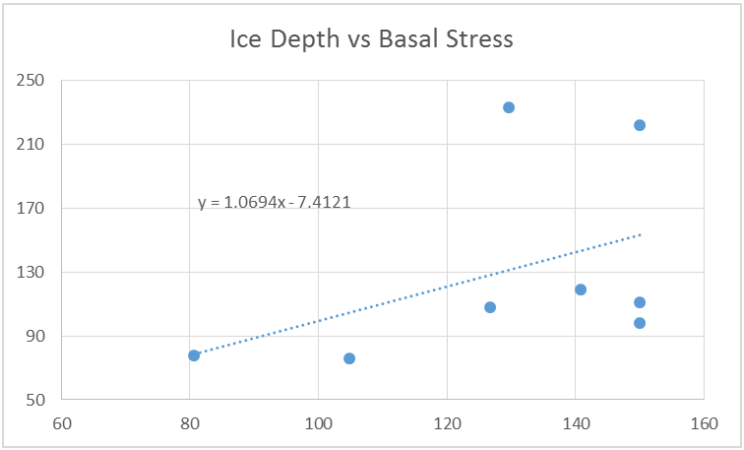

Figure 5.22 Trend line between Basal Stress and Ice Depth (Thickness) for slope dependent approach

Figure 5.19 & 5.20 shows the trend line for the basal stress and ice depth using two approaches mentioned earlier. The equation depicts the relation followed by the two parameters. Clearly an upward trend signifies and cement the direct relation between depth and stress. This stems from the fact that greater depth will lead to more mass over the area under consideration and hence more force. Also as the depth increases more ice layers will be sliding over one another thus increasing driving stress. Comparing the two approaches we can instantaneously see that GlabTop employs a greater multiple that slope dependent approach for its trend line suggesting more impact from depth calculation. Inversely slope dependent approach is slightly close knit to stress. The constant in the equation suggest that GlabTop will need greater Basal stress to account for flow in ice column than that required by slope dependent models.

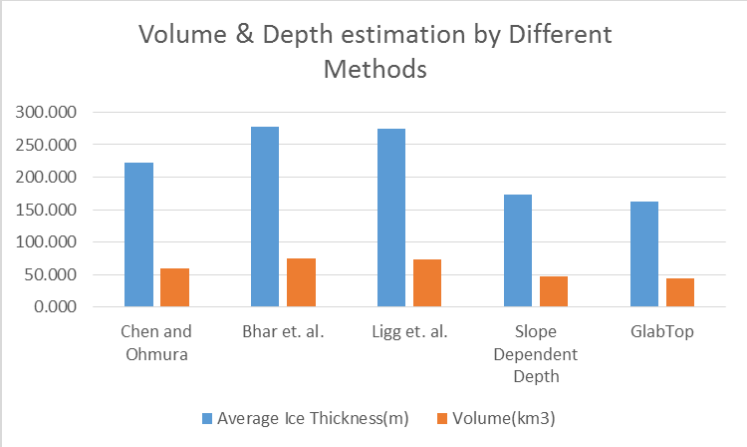

Figure 5.23 Comparative Listing Of Final Result From Different Approch Used In The Study

Finally a comparative list of the methods employed for ice depth is shown in Figure 5.21. As is clearly seen in the graph both GlabTop and slope dependent method are nearer to each other as expected. But other models using the old V-A (Volume-Area) scaling technique are constantly overestimating the mean glacier depth. When compared to velocity dependent Laminar flow based model, the mean depth drops to more than 20m at 92m. This in effect can be from the error induced from feature tracking, DEM related error, parameter induced errors, etc. Hence a more detailed note in this regard is needed.

New factors based on studying the depth in this thesis is suggested for Gangotri group of glaciers for further V-A analysis in future is suggested as c = 0.193 and γ = 1.35. This is shown in Figure 5.22 with the other methods used in the study. A fact that should be kept in mind is that the constant is based on single glacial observation and can vary from glacier to glacier in the same mountain range.

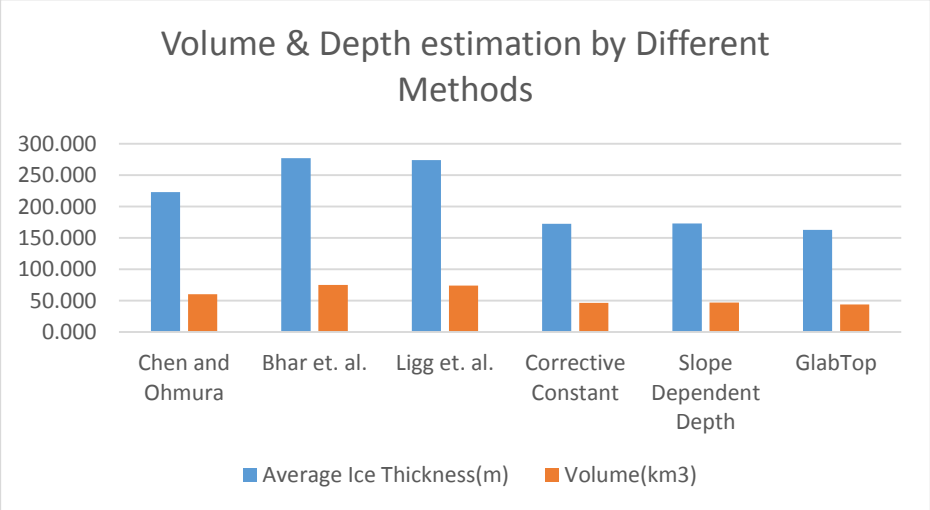

Figure 5.24 Comparative Listing Of Final Result from Corrective Constant Used in the Thesis

Note: Axis-y in Figure (5.21-5.22) represents numerical value for both average ice thickness (denoted by m) and average total volume calculated from the relation (denoted by km^3).

6. CONCLUSIONS AND RECOMMENDATIONS

6.1. Conclusion

Which error sources limit the quality of the movement map and how does this influence propagate in the feature tracking processing?

Many sources of error were identified during the study such as band spectral resolution, quantization levels, shadow pattern, ice coverage, mixed pixels, glacier delineation and band spatial resolution. These error will be present in the processing in varying degree; mixed pixel problem increases in medium resolution images and feature loss is a major problem in high resolution images. Also saturation of sensor leads to feature loss as evident in IRS 1C/1D sensors. These errors cannot be quantified as it depends on a lot of factors and need to be dealt separately for each sensor and topography case.

What are the error propagating parameters in the depth model used?

Depth models used have their own sets of error when dealing with inputs from different sources. This is evident from the formation of "depth islands" in the glacier when using laminar equation as model. This is attributed to local slope variations which cannot be properly eliminated using interpolation. Also the slope dependent models and the GlabTop model surely have digitization errors as these need manual input. Slope dependent models have abrupt changes in confluences of glacier branches this is an apparent error and rectified using interpolation. GlabTop approach uses the more hydro-logically correct approach but digitization errors will be present in this approach too.

What are the classes obtained using SAR (Synthetic Aperture Radar) techniques?

Various classes were obtained for the glacier using SAR data which was previously not possible from optical data. This provides a large avenue to automate the process of glacier classification. Although the classes identified varied with the technique used, it provides a technology demonstration for future studies where glacier classification can be carried out with SAR data. Verification of these types of classes is only possible through ground verification which was not possible due to time constrains. Hence visual verification was done which was found to be conclusive for the validity of the approach used.

6.2. Recommendation

A long term monitoring of glacier, in conjunction with ground data will give a better understanding of physical properties of glacier. Also Feature Tracking using Coarse Resolution imagery should be explored more for temperate glaciers.

Ground observation is very important for any study. A preliminary study with TLS is conducted but this opens up new avenue for ground truths; repeat TLS measurement from same position can be used to identify and track feature over time giving accurate results.

Most important is the vertical profiling of glacier, to understand and monitor internal as well as physical properties of glacier, which makes use of a GPR (Ground penetrating Radar). This should be explored more (especially in the lower frequency regions).

If weather data for decades are made available, models for ice sheet can be modified to run for glaciers in hilly region providing modelled outputs which can then be used to verify other remote sensing results and further improve upon the existing glacier model.

SAR decomposition techniques for glacier classification is a new topic and should be explored for further exploitation of this all-weather technique. A better field survey with decomposition from SAR imagery can then be used for development of model for automatic classification of glacier types. Further analysis of glacier in sub-seasonal interval should be conducted to extract changes in the glacier surface and infer its health accordingly.

References

Ahmad, S., Hasnain, S.I., Selvan, M.T., 2004. Morpho-metric characteristics of glaciers in the Indian Himalayas. Asian J. Water Environ. Pollut. 1, 109–118.

Anthwal, A., Joshi, V., Sharma, A., Anthwal, S., 2006. Retreat of Himalayan glaciers–indicator of climate change. Nat. Sci. 4, 53–59.

Bamber, J.L., Rivera, A., 2007. A review of remote sensing methods for glacier mass balance determination. Glob. Planet. Change 59, 138–148. doi:10.1016/j.gloplacha.2006.11.031

Barry, R.G., 2006. The status of research on glaciers and global glacier recession: a review. Prog. Phys. Geogr. 30, 285–306. doi:10.1191/0309133306pp478ra

Berthier, E., Arnaud, Y., Kumar, R., Ahmad, S., Wagnon, P., Chevallier, P., 2007. Remote sensing estimates of glacier mass balances in the Himachal Pradesh (Western Himalaya, India). Remote Sens. Environ. 108, 327–338. doi:10.1016/j.rse.2006.11.017

Berthier, E., Scambos, T.A., Shuman, C.A., 2012. Mass loss of Larsen B tributary glaciers (Antarctic Peninsula) unabated since 2002: UNABATED MASS LOSS OF LARSEN B GLACIERS. Geophys. Res. Lett. 39, n/a–n/a. doi:10.1029/2012GL051755

Berthier, E., Schiefer, E., Clarke, G.K.C., Menounos, B., Rémy, F., 2010. Contribution of Alaskan glaciers to sea-level rise derived from satellite imagery. Nat. Geosci. 3, 92–95. doi:10.1038/ngeo737

Berthier, E., Vadon, H., Baratoux, D., Arnaud, Y., Vincent, C., Feigl, K.L., Rémy, F., Legrésy, B., 2005. Surface motion of mountain glaciers derived from satellite optical imagery. Remote Sens. Environ. 95, 14–28. doi:10.1016/j.rse.2004.11.005

Bhambri, R., Bolch, T., 2009. Glacier mapping: a review with special reference to the Indian Himalayas. Prog. Phys. Geogr. 33, 672–704. doi:10.1177/0309133309348112

Bhambri, R., Bolch, T., Chaujar, R.K., 2012. Frontal recession of Gangotri Glacier, Garhwal Himalayas, from 1965 to 2006, measured through highresolution remote sensing data. Curr. Sci. 00113891 102.

Budillon, A., Pascazio, V., Schirinzi, G., 2008. Estimation of Radial Velocity of Moving Targets by Along-Track Interferometric SAR Systems. IEEE Geosci. Remote Sens. Lett. 5, 349–353. doi:10.1109/LGRS.2008.915937

Casey, K.A., Kääb, A., Benn, D.I., 2011. Characterization of glacier debris cover via in situ and optical remote sensing methods: a case study in the Khumbu Himalaya, Nepal. Cryosphere Discuss. 5, 499–564. doi:10.5194/tcd-5-499-2011

Clarke, G.K.C., Berthier, E., Schoof, C.G., Jarosch, A.H., 2009. Neural Networks Applied to Estimating Subglacial Topography and Glacier Volume. J. Clim. 22, 2146–2160. doi:10.1175/2008JCLI2572.1

Cuffey, K.M., Paterson, W.S.B., 2010. The Physics of Glaciers. Elsevier Science.

Eineder, M., Jaber, W.A., Floricioiu, D., Rott, H., Yague-Martinez, N., 2011. Glacier flow and topography measurements with TerraSar-X and TanDEM-X, in: Geoscience and Remote Sensing Symposium (IGARSS), 2011 IEEE International. IEEE, pp. 3835–3838.

Engeset, R.V., 2002. FIRN EDGE AND EQUILIBRIUM LINE DETECTION USING SATELLITE SAR, in: Proceedings of EARSeL-LISSIG-Workshop Observing Our Cryosphere from Space.

Fallourd, R., Harant, O., Trouvé, E., Nicolas, J.-M., Gay, M., Walpersdorf, A., Mugnier, J.-L., Serafini, J., Rosu, D., Bombrun, L., others, 2011. Monitoring temperate glacier movement by multi-temporal TerraSAR-X images and continuous GPS measurements. Sel. Top. Appl. Earth Obs. Remote Sens. IEEE J. Of 4, 372–386.

Fallourd, R., Harant, O., Trouvé, E., Nicolas, J.-M., Tupin, F., Gay, M., Vasile, G., Bombrun, L., Walpersdorf, A., Serafini, J., others, 2009. Monitoring temperate glaciers: combined use of multi-date TerraSAR-X images and continous GPS measurements, in: The Fifth International Workshop on the Analysis of Multi-Temporal Remote Sensing Images.

Gardelle, J., Arnaud, Y., Berthier, E., 2011. Contrasted evolution of glacial lakes along the Hindu Kush Himalaya mountain range between 1990 and 2009. Glob. Planet. Change 75, 47–55. doi:10.1016/j.gloplacha.2010.10.003

Haq, M.A., Jain, K., Menon, K.P.R., 2011. Change Monitoring of Gangotri Glacier Using Satellite Imagery, in: 12th ESRI India User Conference. pp. 6–8.

Heid, T., 2011. Deriving glacier surface velocities from repeat optical images. University of Oslo.

Huang, L., Li, Z., 2011. Comparison of SAR and optical data in deriving glacier velocity with feature tracking. Int. J. Remote Sens. 32, 2681–2698. doi:10.1080/01431161003720395

Hubbard, A., Willis, I., Sharp, M., Mair, D., Nienow, P., Hubbard, B., Blatter, H., 2000. Glacier mass-balance determination by remote sensing and high-resolution modelling. J. Glaciol. 46, 491–498.

Karimi, N., Farokhnia, A., Shishangosht, S., Elmi, M., Eftekhari, M., Ghalkhani, H., 2012. Elevation changes of Alamkouh glacier in Iran since 1955, based on remote sensing data. Int. J. Appl. Earth Obs. Geoinformation 19, 45–58. doi:10.1016/j.jag.2012.04.009

Kulkarni, A.V., 1992. Mass balance of Himalayan glaciers using AAR and ELA methods. J. Glaciol. 38, 101–104.

Li, H., Li, Z., Zhang, M., Li, W., 2011. An improved method based on shallow ice approximation to calculate ice thickness along flow-line and volume of mountain glaciers. J. Earth Sci. 22, 441–448. doi:10.1007/s12583-011-0198-1

Linsbauer, A., Paul, F., Haeberli, W., 2012. Modeling glacier thickness distribution and bed topography over entire mountain ranges with GlabTop: Application of a fast and robust approach. J. Geophys. Res. 117. doi:10.1029/2011JF002313

Malinverni, E.S., Croci, C., Sgroi, F., 2008. Glacier monitoring by remote sensing and GIS techniques in open source environment. EARSeL EProceedings 7, 120–132.

Negi, H.S., Thakur, N.K., Ganju, A., others, 2012. Monitoring of Gangotri glacier using remote sensing and ground observations. J. Earth Syst. Sci. 121, 855–866.

Paul, F., Linsbauer, A., 2012. Modeling of glacier bed topography from glacier outlines, central branch lines, and a DEM. Int. J. Geogr. Inf. Sci. 26, 1173–1190. doi:10.1080/13658816.2011.627859

Pellika, P., 2009. Remote Sensing of Glaciers. Taylor & Francis.

Shukla, A., Arora, M.K., Gupta, R.P., 2010. Synergistic approach for mapping debris-covered glaciers using optical–thermal remote sensing data with inputs from geomorphometric parameters. Remote Sens. Environ. 114, 1378–1387. doi:10.1016/j.rse.2010.01.015

Shuman, C.A., Berthier, E., Scambos, T.A., 2011. 2001–2009 elevation and mass losses in the Larsen A and B embayments, Antarctic Peninsula. J. Glaciol. 57, 737–754.

Strozzi, T., Luckman, A., Murray, T., Wegmuller, U., Werner, C.L., 2002. Glacier motion estimation using SAR offset-tracking procedures. IEEE Trans. Geosci. Remote Sens. 40, 2384–2391. doi:10.1109/TGRS.2002.805079

Trouvé, E., Pétillot, I., Bolon, P., Gay, M., Bombrun, L., Nicolas, J.-M., Tupin, F., Walpersdorf, A., Cotte, N., Hajnsek, I., others, 2008. Monitoring Alpine glacier activity by a combined use of TerraSAR-X images and continuous GPS measurements Â?` the ArgentiÃ?` re glacier experiment, in: Synthetic Aperture Radar (EUSAR), 2008 7th European Conference on. VDE, pp. 1–4.

Wagnon, P., Linda, A., Arnaud, Y., Kumar, R., Sharma, P., Vincent, C., Pottakkal, J.G., Berthier, E., Ramanathan, A., Hasnain, S.I., others, 2007. Four years of mass balance on Chhota Shigri Glacier, Himachal Pradesh, India, a new benchmark glacier in the western Himalaya. J. Glaciol. 53, 603–611.

Zemp, M., Hoelzle, M., Haeberli, W., 2009. Six decades of glacier mass-balance observations: a review of the worldwide monitoring network. Ann. Glaciol. 50, 101–111.

.

Appendix 1

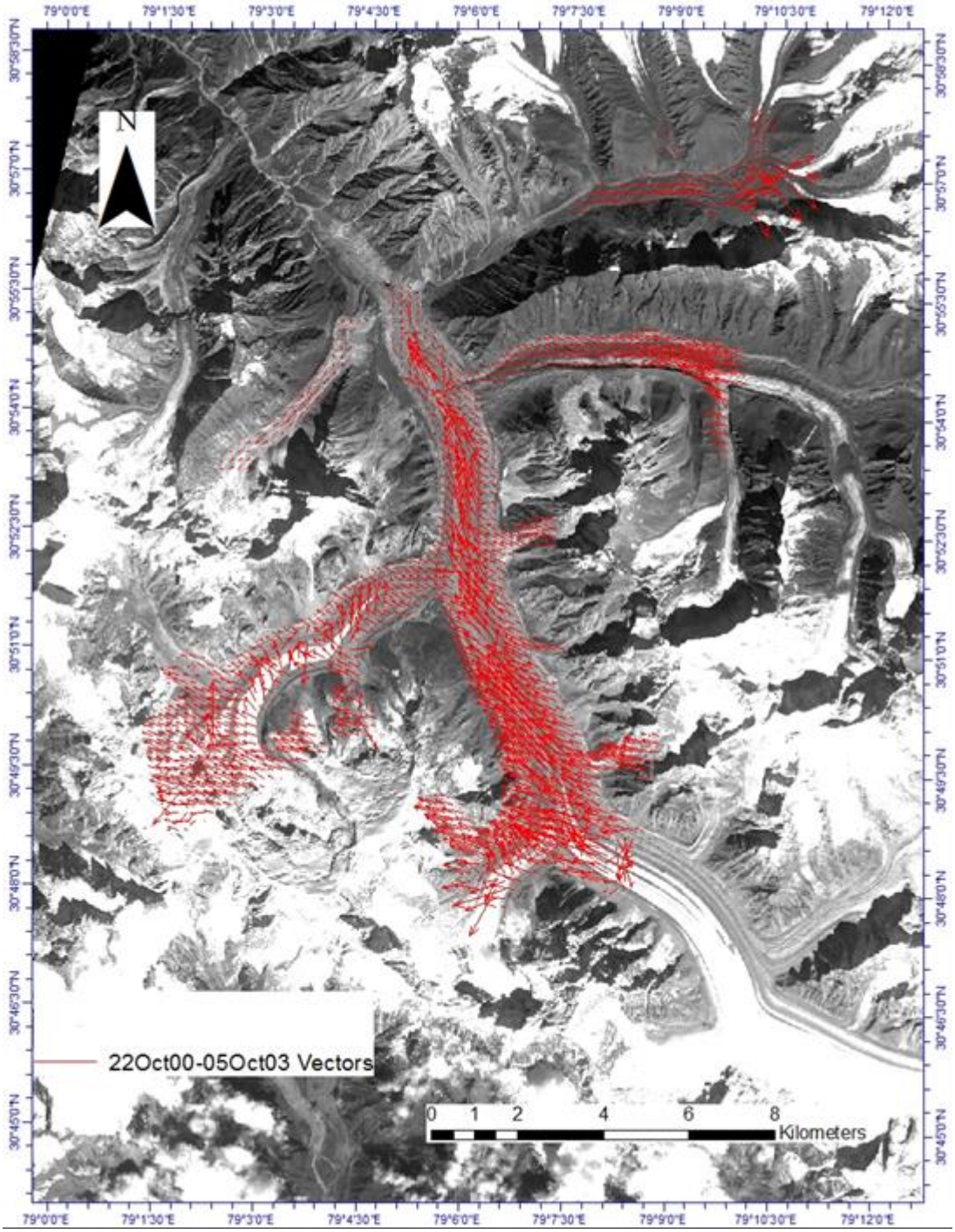

Figure A.1 Velocity Vector for 22Oct'00-05Oct'03

	Maximum	Minimum	Average
E-W Movement	325.6 m	1.53 m	3.16 m
N-S Movement	299.9 m	1.1 m	4.07 m
Error	1	0	0.178

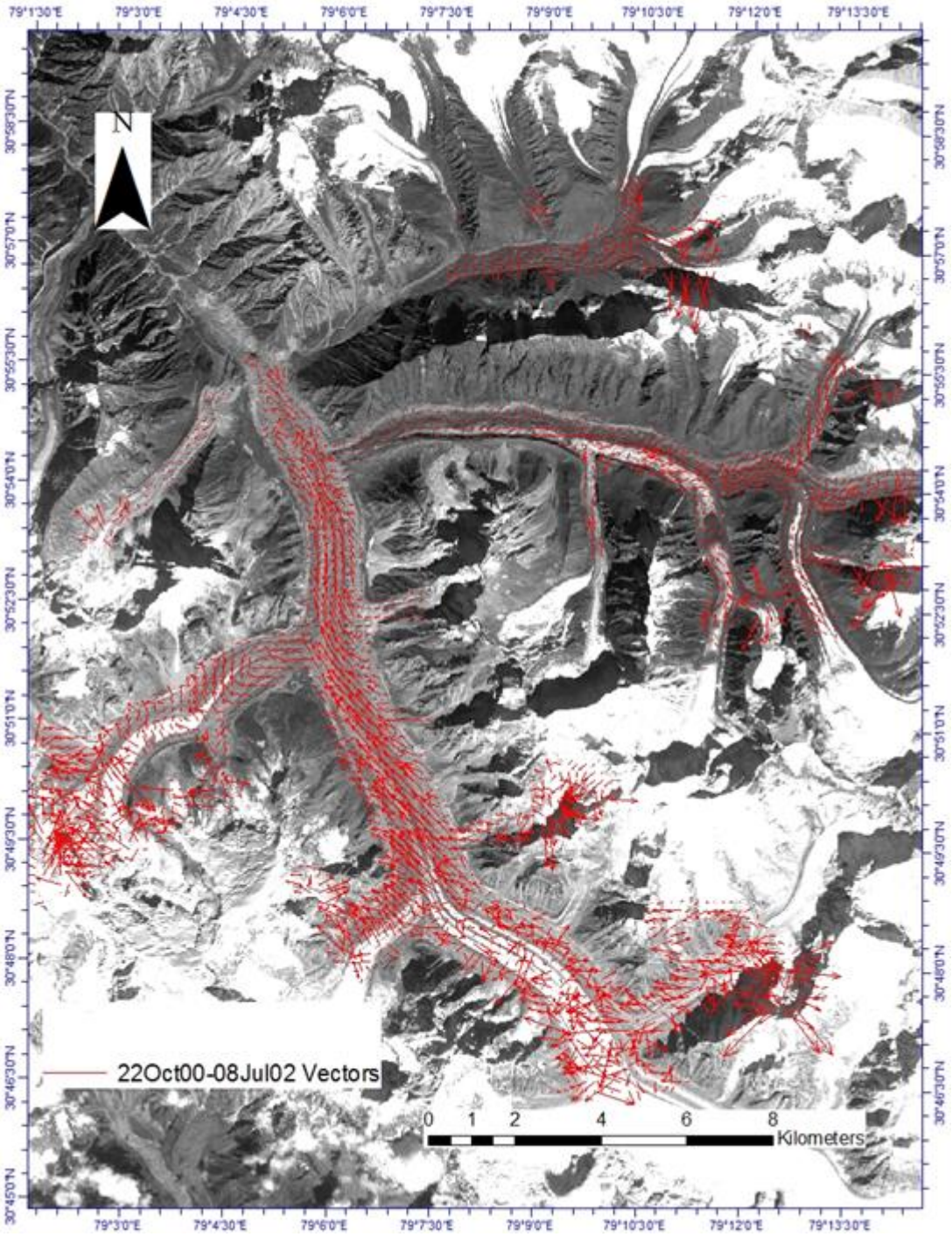

Figure A.2 Velocity Vector for 22Oct'00-08Jul'02

	Maximum	Minimum	Average
E-W Movement	328.9 m	1.01 m	4.39 m
N-S Movement	286.5 m	1.22 m	1.05 m
Error	1	0	0.224

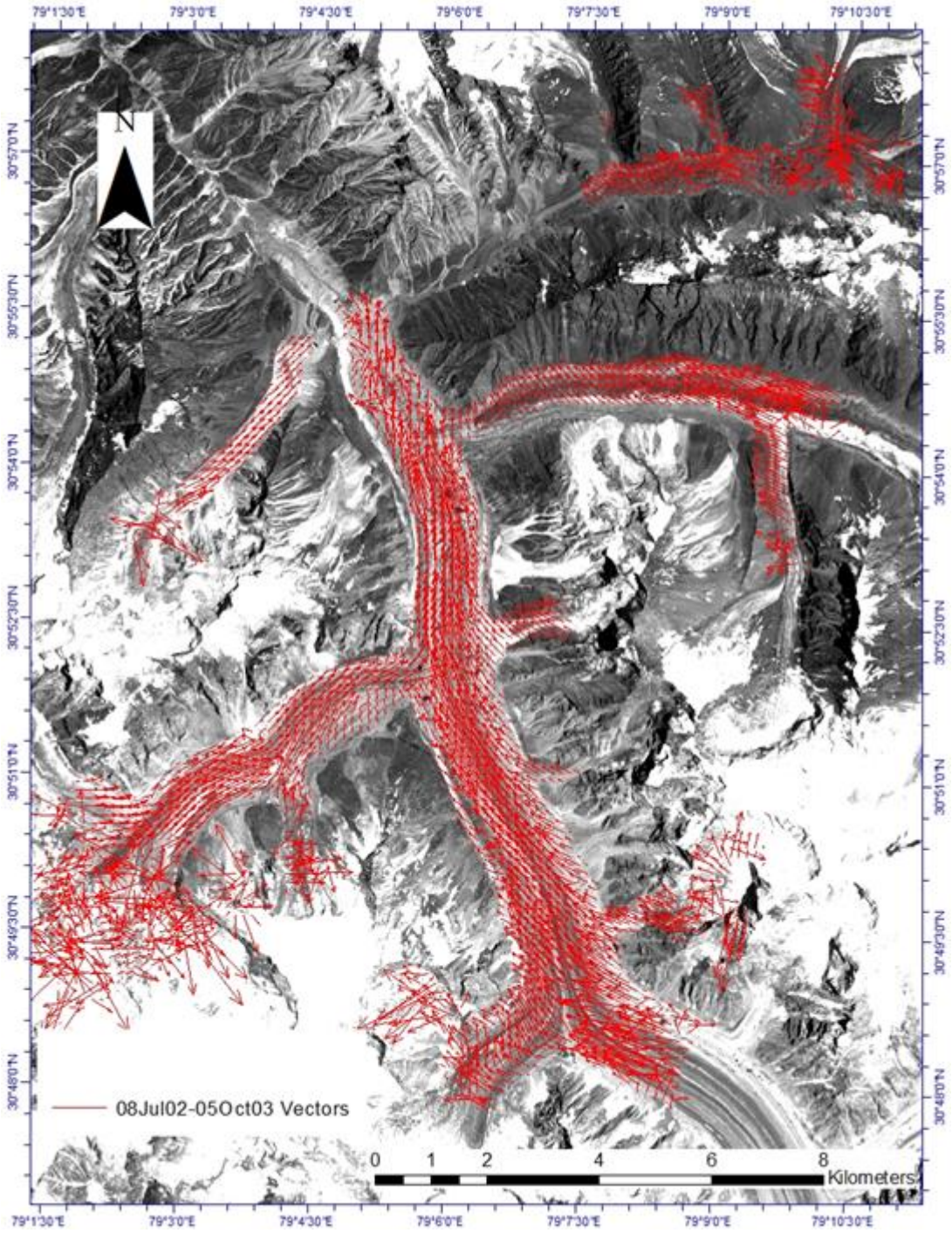

Figure A.3 Velocity Vector for 08Jul'02-05Oct'03

	Maximum	Minimum	Average
E-W Movement	329.9 m	1.04 m	3.1 m
N-S Movement	329.5	1.1 m	4.07 m
Error	1	0	0.178

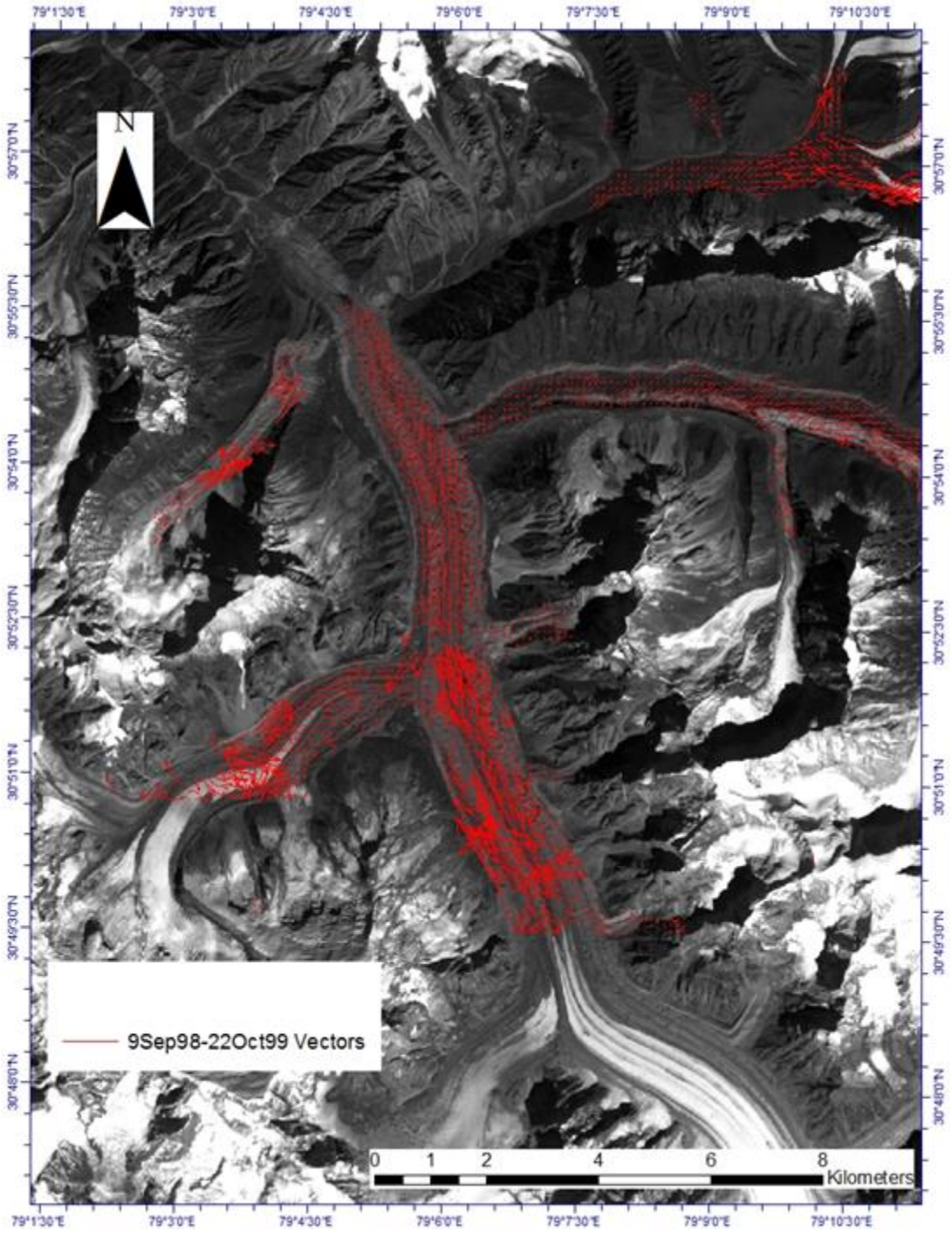

Figure A.4 Velocity Vector for 09Sep'98-22Oct'99

	Maximum	Minimum	Average
E-W Movement	360.5 m	1.02 m	9.9 m
N-S Movement	278.5 m	1.1 m	6.2 m
Error	1	0	0.192

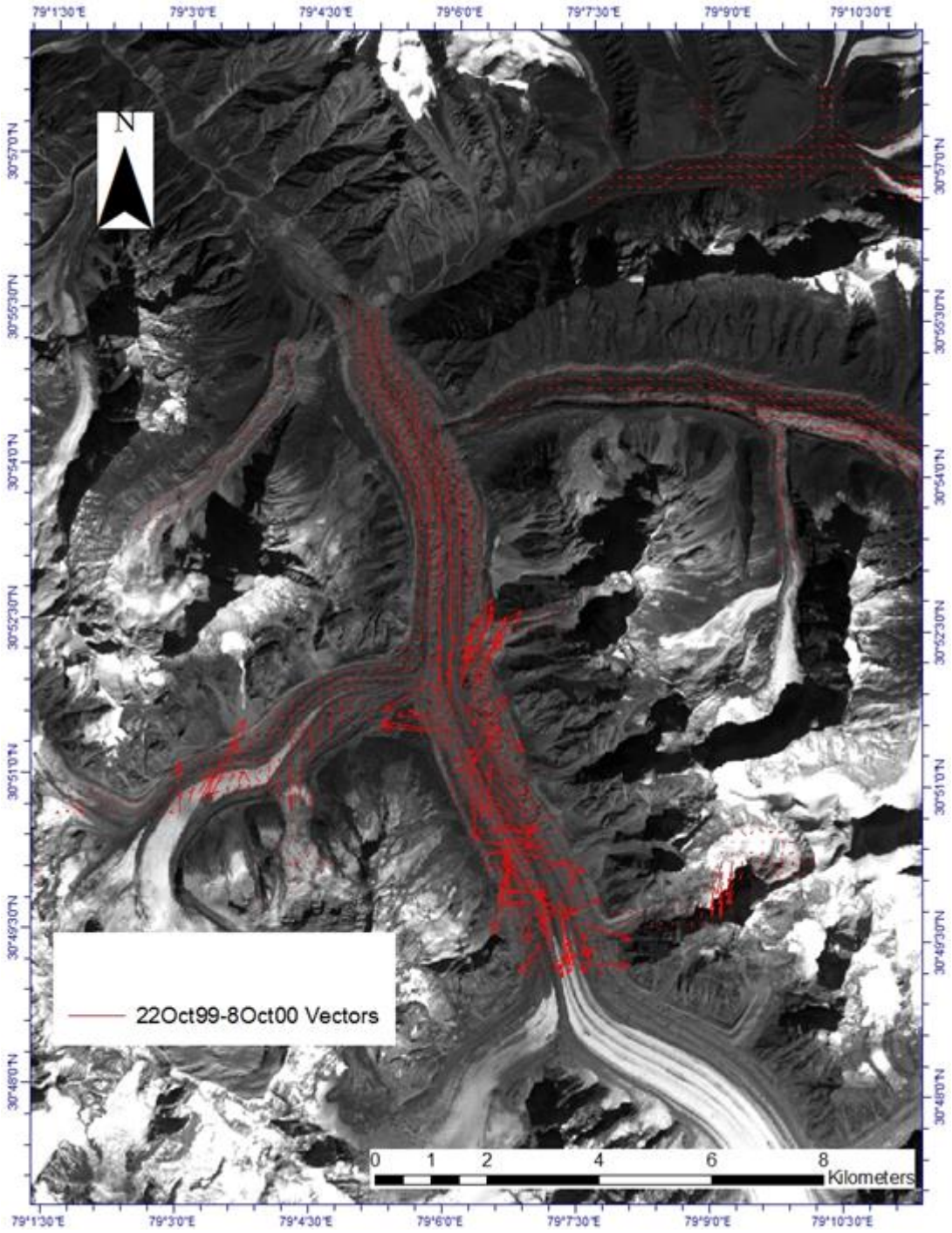

Figure A.5 Velocity Vector for 22Oct'99-08Oct'00

	Maximum	Minimum	Average
E-W Movement	310.8 m	1.8 m	4.8 m
N-S Movement	270.05 m	3.2 m	3.5 m
Error	1	0	0.3

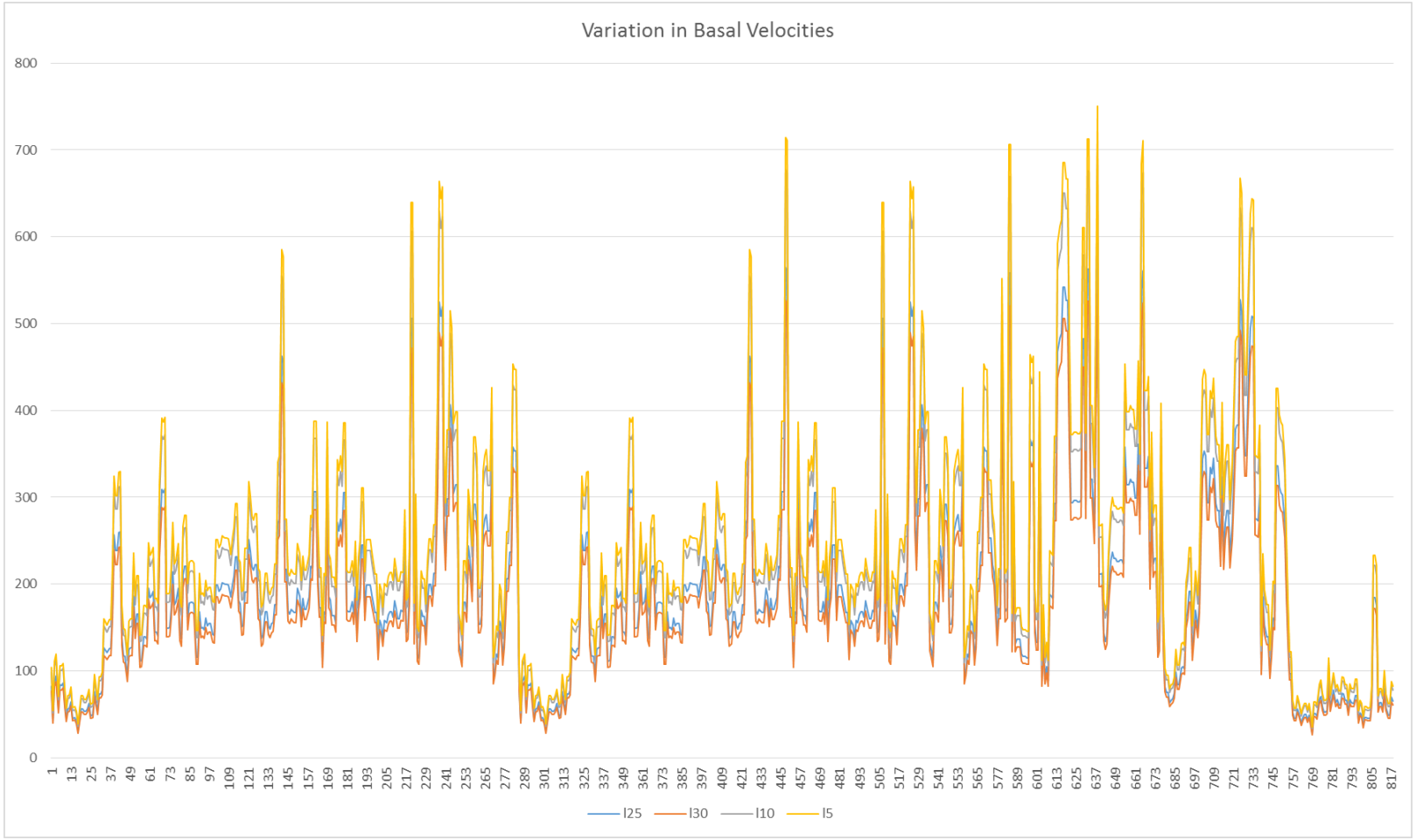

Figure A.6 Basal Velocity vs Depth in main Gangotri Glacier

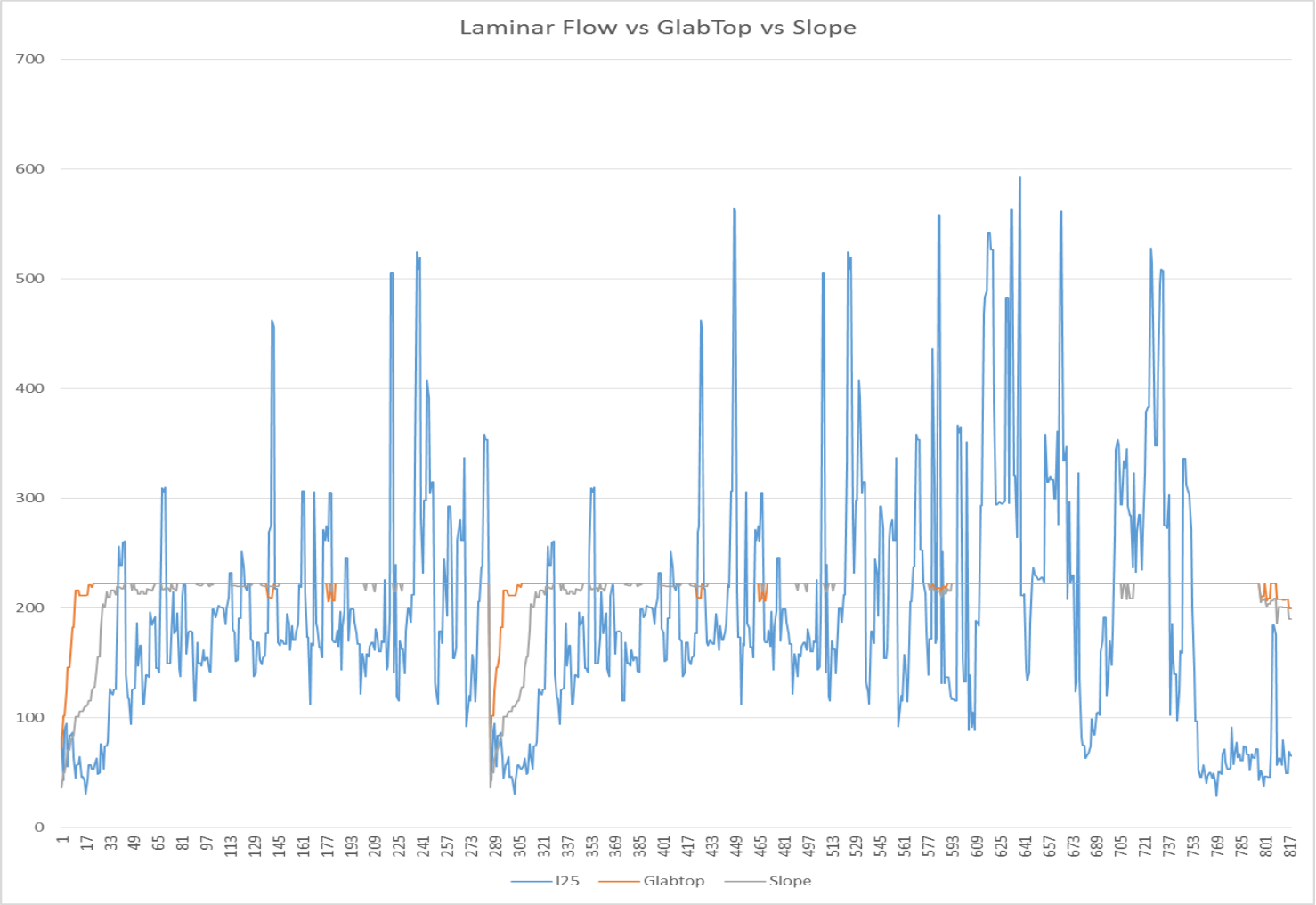

Figure A.7 Comparative Glacier Depth of Gangotri Glacier

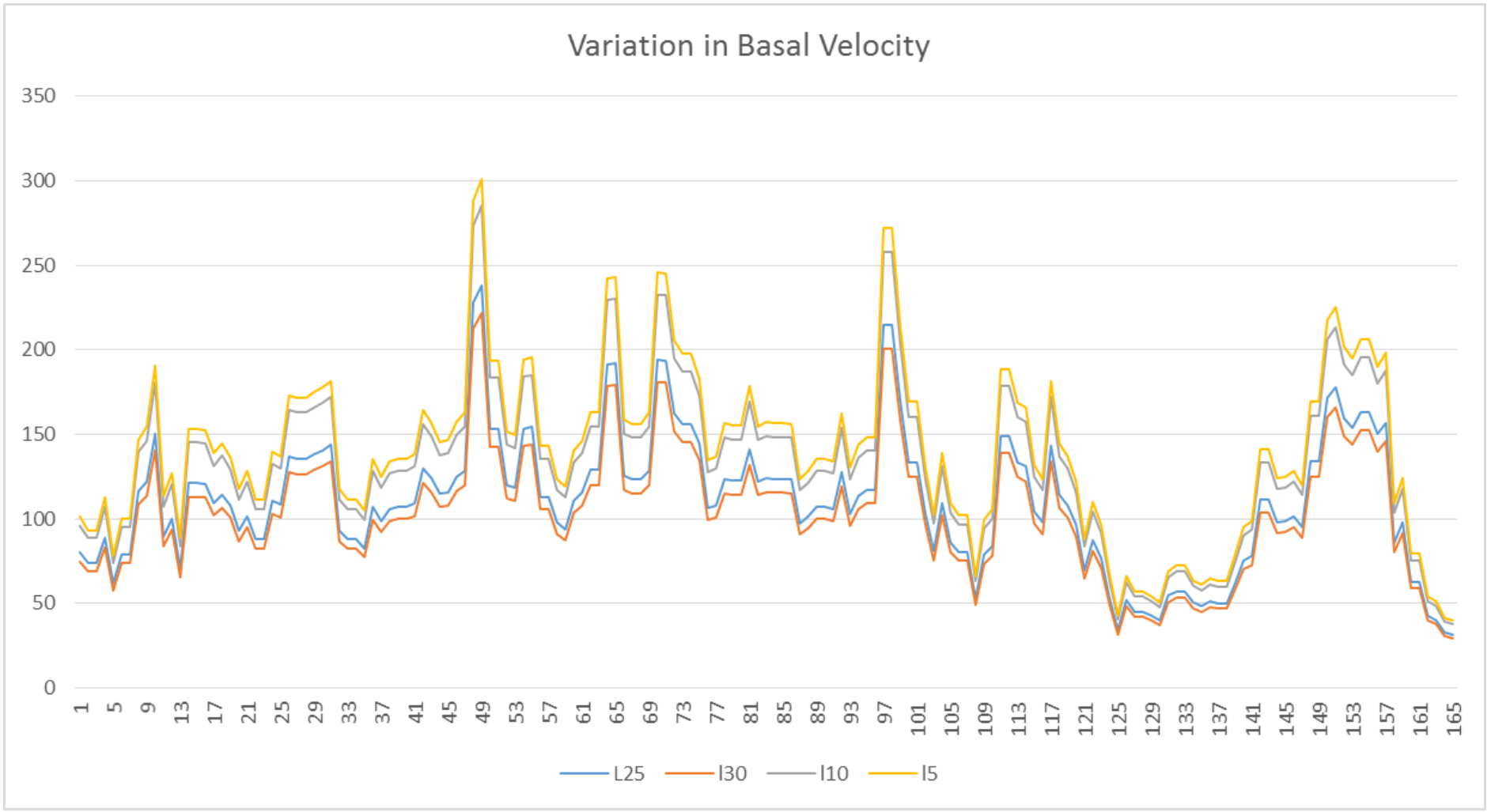

Figure A.8 Basal Veocity vs Deth in Raktvarn Glacier

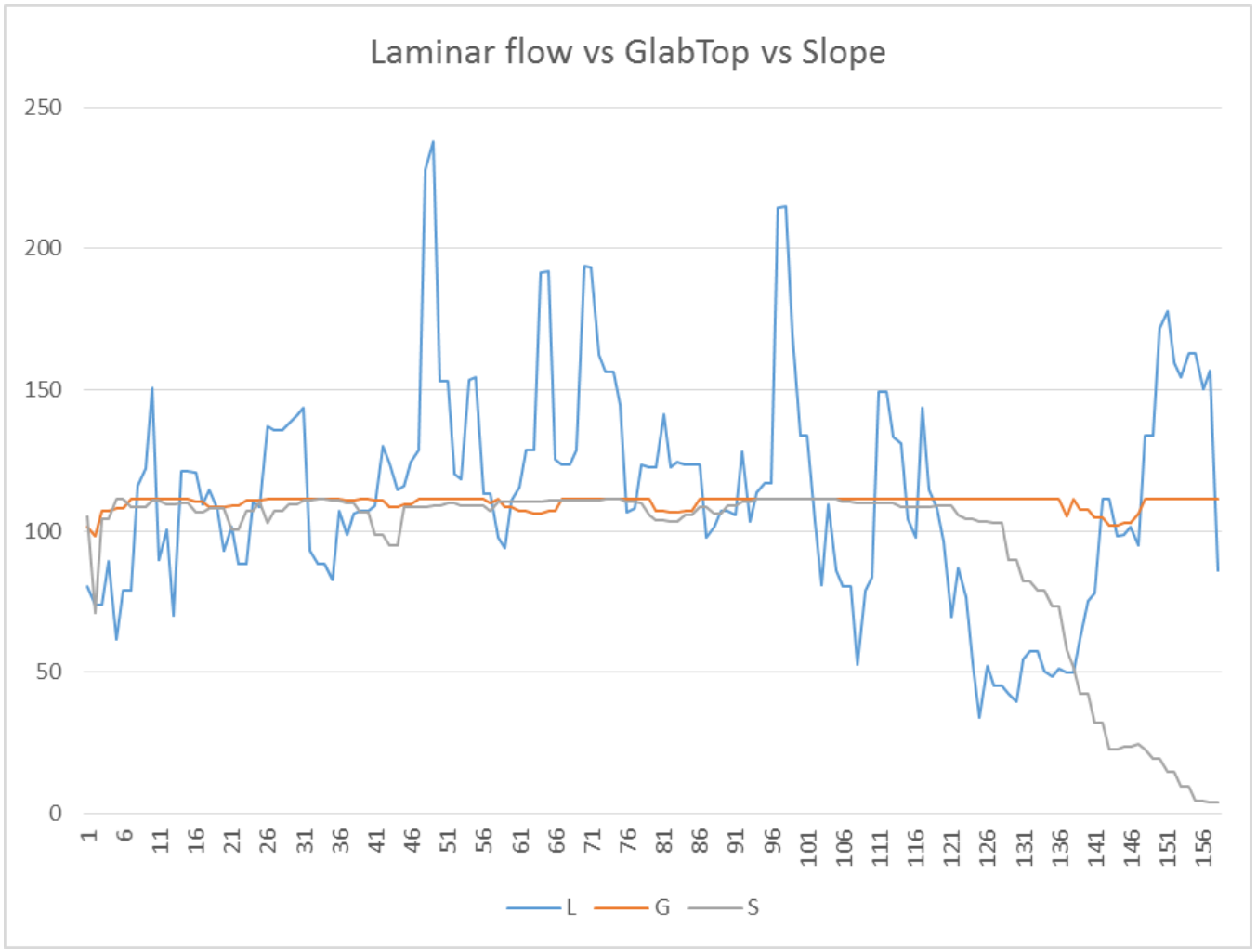

Figure A.9 Comparative Depth of Raktvarn Glacier

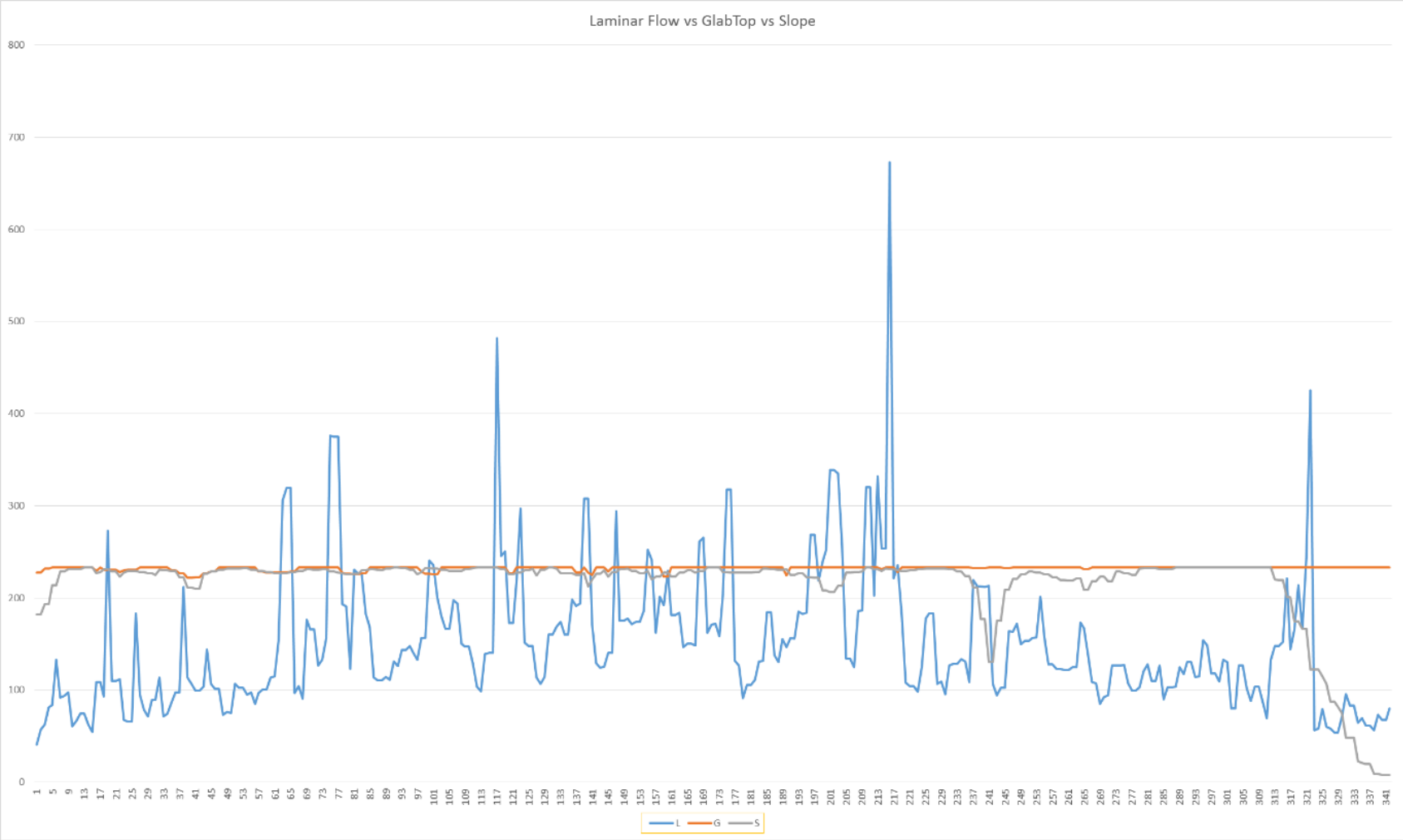

Figure A.10 Comparative Depth of Chaturangi Glacier

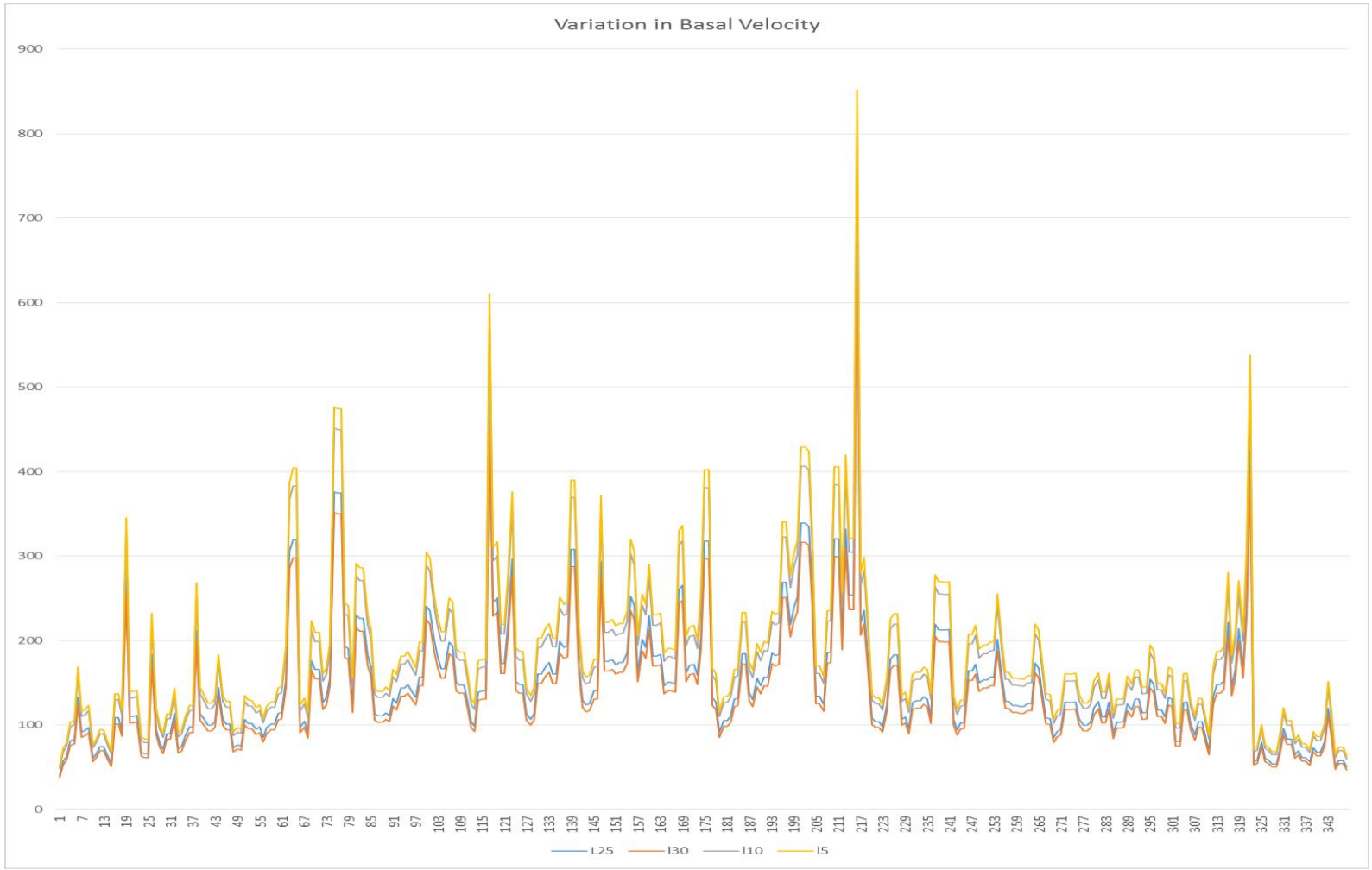

Figure A.11 Basal Velocity vs Depth in Chaturangi Glacier

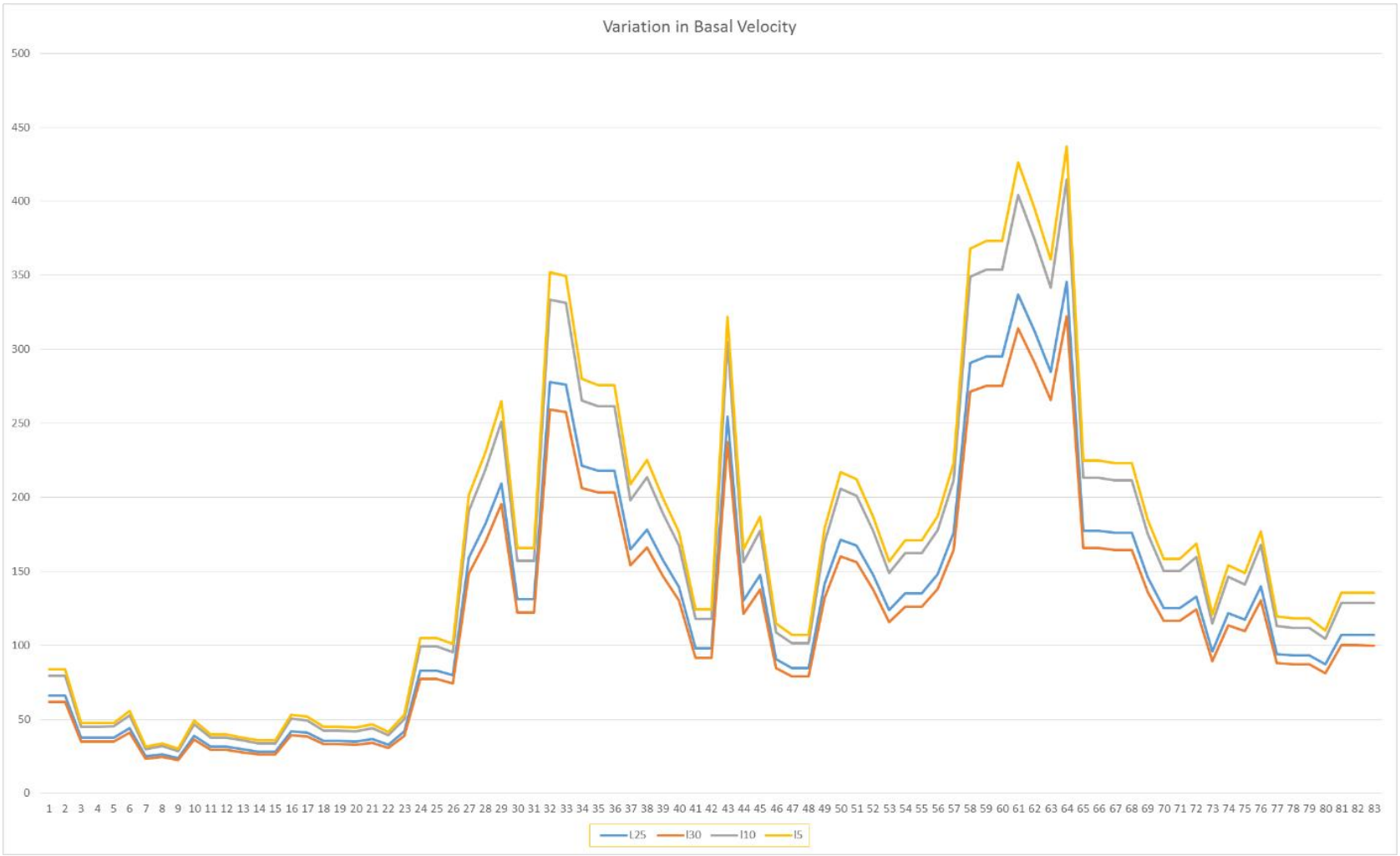

Figure A.12 Basal Velocity vs Depth in Ghanohim Glacier

Figure A.13 Comparative depth of Ghanohim glacier

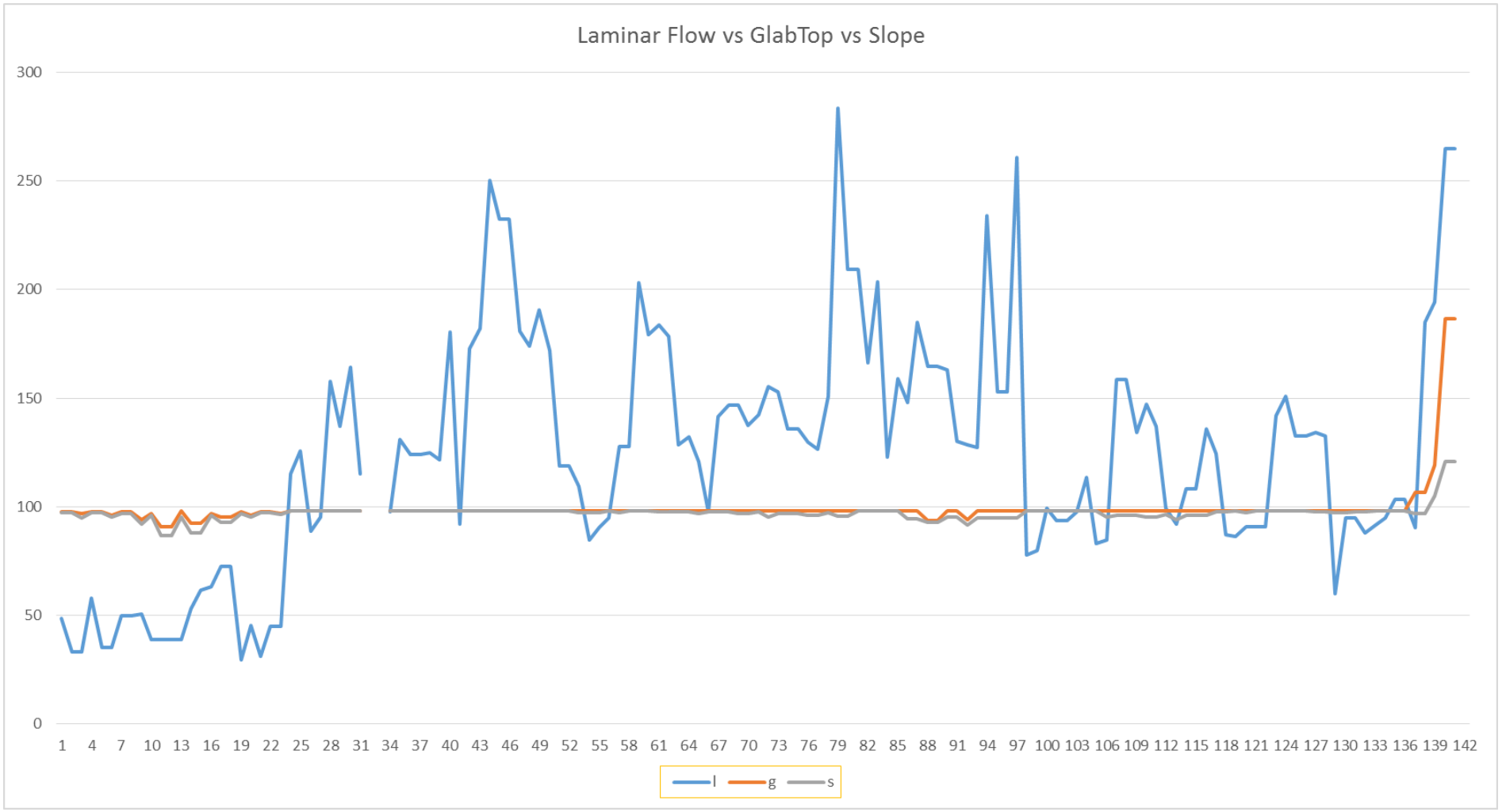

Figure A.14 Comparative Depth of Kirti Glacier

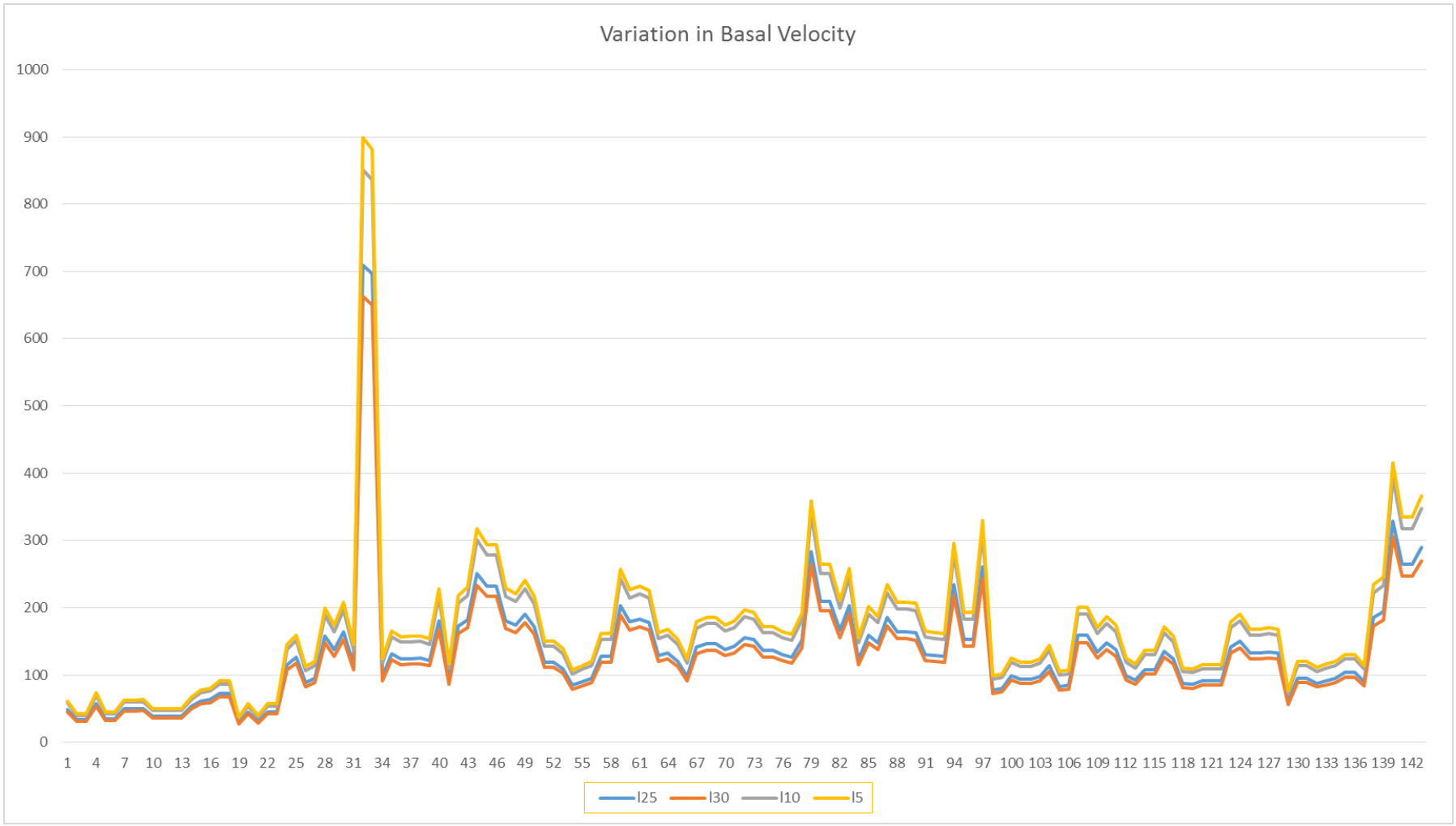

Figure A.15 Basal Velocity vs Depth in Kirti glacier

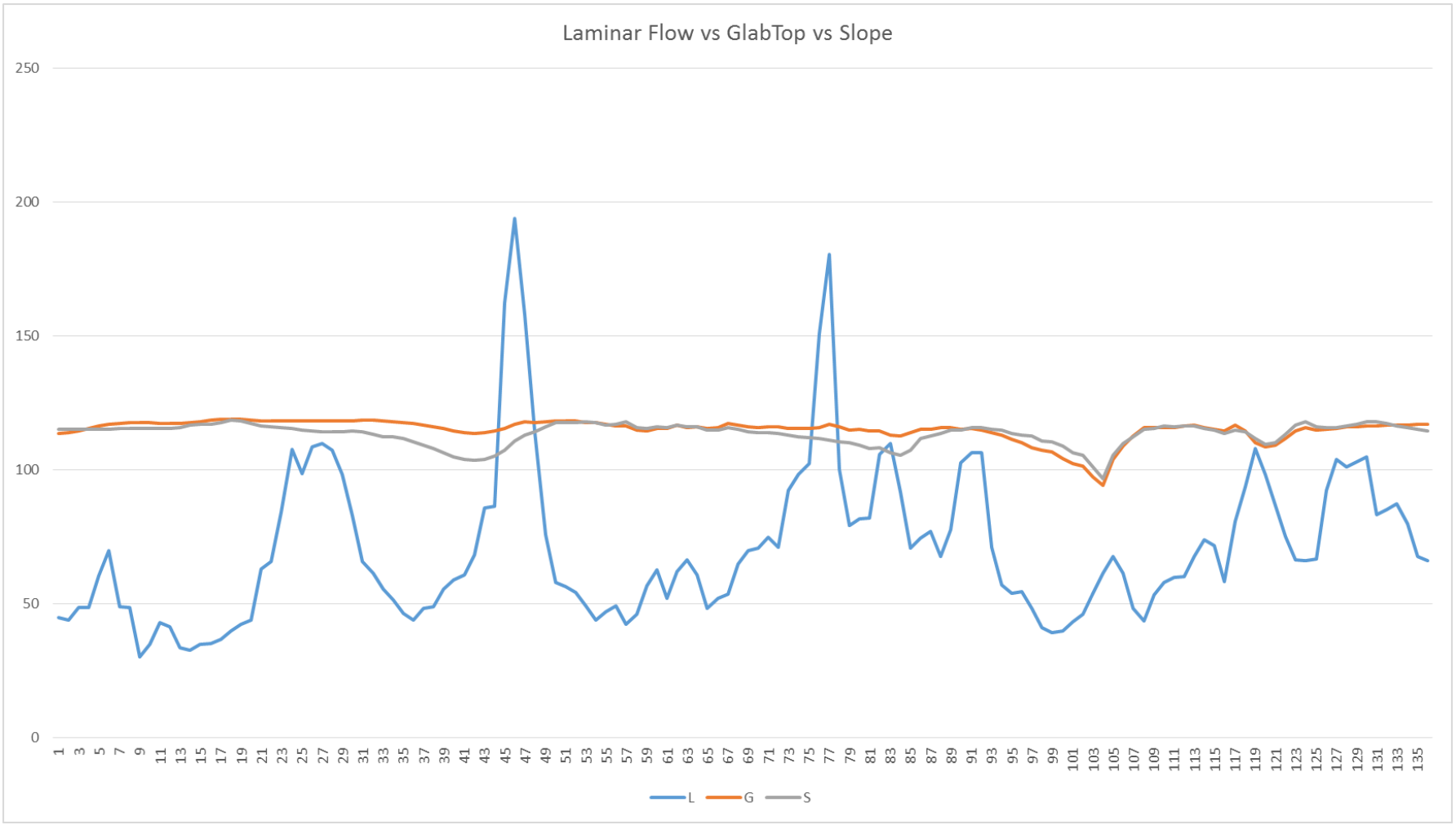

Figure A.16 Comparative Depth in Meru glacier

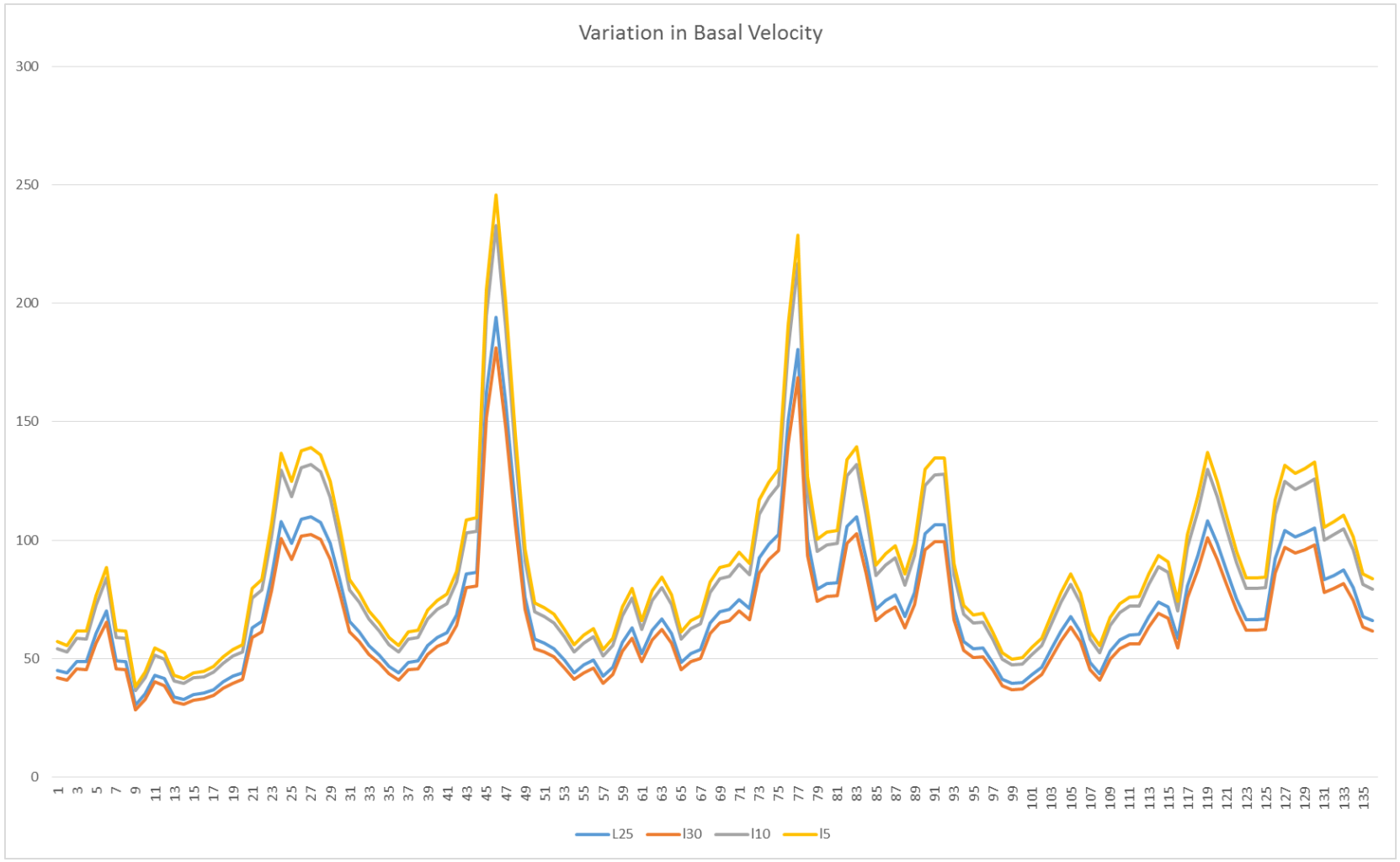

Figure A.17 Basal velocity vs Depth in Meru glacier